School of Civil and Mechanical Engineering

Improving Cooling Effectiveness in Air-Cooled Data Centres: Analysis and Assessment using Computational Fluid Dynamics

Faraj Jaber R Aljohani

This thesis is presented for the Degree of
Doctor of Philosophy
of
Curtin University

November 2018

Declaration

To the best of my knowledge and belief this thesis contains no material previously published by any other person except where due acknowledgment has been made. This thesis contains no material which has been accepted for the award of any other degree or diploma in any university.

Signature: …….

Date: ……...

Authored Publications Formed from Thesis

I Faraj Jaber R Aljohani contributed to the majority of the published papers work such as generating, presenting and analysing the results and the co-authors provided valuable guidance and review to the publications entitled:

1- F. J. Aljohani, A. J. C. King, R. Narayanaswamy "Comparison between k- ε RANS Model and SST k-ω SAS Model in Data Centre Simulations" In *20th Australasian Fluid Mechanics Conference*, Dec 5, 2016, Perth, Australia

2- F. J. Aljohani, A. J. C. King, R. Narayanaswamy "Evaluation of SAS Turbulence Modelling for Data Centre Simulations" submitted to *Applied thermal engineering* journal in 1/10/2018.

Signature of the candidate: ……

I, as a Co-Author, endorse that this level of contribution by the candidate indicated above is appropriate.

Dr. Andrew James King Signature: ……

Assoc. Prof. Ramesh Narayanaswamy Signature: ……

Acknowledgements

I would like to express my special appreciation and earnest thanks to my main supervisor Dr Andrew King, and my co-supervisor Assoc. Prof. Ramesh Narayanaswamy for their guidance, encouragement, and tremendous assistance throughout the research. Moreover, I would like to thank The National eResearch Collaboration Tools and Resources project (Nectar) and the Pawsey Supercomputing Centre for providing me access to their resources to conduct my research. I am also grateful to the Saudi Arabian Cultural Mission in Australia for their financial support and their continuous dedication to complete this work.

Finally, I take privilege to acknowledge and thank my family. My mother and my wife for their continued encouragement and support and for their countless sacrifices to complete this work. Also, my children Jawan, Miral and Omar, they inspired me through the hard times to relieve stress.

Abstract

Data centres are a corner stone to the modern technology revolution. They manage, organise and operate the Information Technology (IT) equipment. Their design requires efficient operation with close to zero downtime. The increasing demand in digital services resulting from high power computing increases data centres' electrical power consumption of which a significant portion is consumed in cooling down the IT equipment. Consequently, improving cooling system effectiveness is a necessity to reduce the power consumption and to achieve low downtime operation. Computational Fluid dynamics (CFD) is used widely in data centre design studies to enhance their cooling effectiveness. The most common cooling technique used in today's data centres is air cooling with raised floor data centre infrastructure. Hence, improving cooling techniques for this infrastructure can be adapted by the majority of today's data centres.

This thesis proposes using a turbulence model that can overcome the limitations of the current turbulence model used data centre simulations. Besides, it addresses the problems of thermal inefficiencies and effective use of cooling resources. The thesis validates the numerical simulations by comparing them with vented enclosure experiment and the validity of using OpenFOAM solver for buoyant driven flows was validated against a natural convection of air in a square cavity study. The limitations of using k-ε RANS turbulence model for data centre numerical simulations for three different air distribution systems for raised floor data centre were investigated and the SST k-ω SAS (Scale Adaptive Simulations) turbulence model was suggested to be used for the first time. Blade servers were integrated with 1U servers in a single rack with seven different rack configurations to figure out the best possible configuration with respect to the cooling effectiveness. Rack level thermal analysis was considered by installing a sub-cooler at the top of the racks which was proposed with the raised floor infrastructure for the first time.

The results showed that the k-ε RANS model for the room return vent infrastructure can not detect the hot air infiltration for the racks at the end of the aisles; whereas, with regards to the hot air infiltration form the middle racks this model showed good agreement with the SST k-ω SAS. Unlike, the ceiling return vent infrastructure where both models showed acceptable agreement for hot air infiltration form both the end and middle racks.

It was also found both the hot air recirculation and temperature distribution within the data centre room heavily rely on the power profile across the rack where the best possible server arrangement was found when the blade servers clustered at the top of the rack cabinet which resulted in the highest return air temperature with assistance of buoyancy forces by preventing the hot air from being infiltrated into cold aisles. The sub-cooler demonstrated promising performance by enhancing the cooling effectiveness considerably with 85% of the cooling capacity load that needed by the data centre compared with 100% without the sub-cooler.

Table of Contents

List of Figures

List of Tables

List of Abbreviations

Nomenclature

HCSCR	Hard Floor CRAC Supply CRAC Flooded Return
HCSLR	Hard Floor CRAC Supply Locally Ducted Return
HCSFR	Hard Floor CRAC Supply Fully Ducted Return
HLSCR	Hard Floor Locally Ducted Supply CRAC Flooded Return
HLSLR	Hard Floor Locally Ducted Supply Locally Ducted Return
HLSFR	Hard Floor Locally Ducted Supply Fully Ducted Return
RLSCR	Raised Floor Locally Ducted Supply CRAC Flooded Return
RLSLR	Raised Floor Locally Ducted Supply Locally Ducted Return
RLSFR	Raised Floor Locally Ducted Supply Fully Ducted Return
RFSCR	Raised Floor Fully Ducted Supply CRAC Flooded Return
RFSLR	Raised Floor Fully Ducted Supply Locally Ducted Return
RFSFR	Raised Floor Fully Ducted Supply Fully Ducted Return
Re	Reynolds Number
Ra	Rayleigh number
Gr	Grashof Number
Pr	Prandtl number
C_p	Specific Heat

*$_*$L	Linear Characteristic Length
k	Thermal Conductivity
T	Temperature
T_{ref}	Reference Temperature
T_{in}^{r}	Rack Inlet Temperature
T_{out}^{r}	Rack Outlet Temperature
$T_{CRAC-out}$	Outlet Temperature of Computer Room Air Conditioning
U	Velocity
u_*	Friction Velocity
P	Pressure
P_{total}	Total Pressure
P0	Static Pressure
D	Diameter
D_h	Hydraulic Diameter
u'	Fluctuating Velocity in x-direction
v'	Fluctuating Velocity in y-direction
w'	Fluctuating Velocity in z-direction
$L_{vk,3D}$	Von Karman Length Scale
I	Turbulence Intensity

y^+	Non-Dimensional Distance
k	Turbulent Kinetic Energy
k_{res}	Resolved Kinetic Energy
k_{SGS}	Sub-Grid Scale Kinetic Energy
k_{tot}	Total Kinetic Energy
$\dot{m}$	Mass Flow Rate
Q	Enthalpy Rise
K	Empirical Factor of Flow Resistance
F	Fractional Open Area
P_f	Fan Power
P_{ft}	Total Fan Power

Greek Symbols

μ	Fluid Viscosity
ν	kinematic viscosity
ρ	Fluid Density
Γ_t	Turbulent Diffusivity
τ_{ij}	Reynolds Stress Tensor
μ_t	Turbulent Eddy Viscosity

ε	Rate of Dissipation of the Turbulence Kinetic Energy
ω	Specific Rate of Dissipation of the Turbulence Kinetic Energy
σ	Empirical Constant
β	Empirical Constant
E	Rate of Deformation
S	Mean Rate Strain Tensor
τ_w	Wall Shear Stress
μ_f	Fan Efficiency

Chapter 1: Introduction

1.1. Background

Data centres are large facilities that contain computing equipment used in the Information and Communications industry to process, store and transmit information [1]. Data centres are considered a corner stone of modern society, supporting activities such as banking, social networking, teaching and learning. Therefore, continuous operation with minimal downtime should be guaranteed. This requires two important things, reliable power and reliable cooling.

A typical data centre design consists of a raised floor with air return through the room. During operation IT servers convert the electrical power into heat which is removed by recirculating cold air out of the Computer Room Air Conditioning (CRAC) units. The cooling capacity of the CRAC units should be sized to remove the heat load of the server racks. Typically, CRAC units cool air to 10 ºC to 17 ºC using chilled water or refrigerant. Data centres are frequently designed in a cold/hot aisle arrangement. The cold aisle receives the cold air provided by the CRACs through the vent tiles, then the server racks draw this cold air to remove the heat dissipated by the servers. After that, the hot aisle receives the hot air exhausted by the sever fans before being ducted to the CRAC units' inlets.

Figure 1 shows the air distribution within the room return air infrastructure. The figure highlights the main problems that have been identified in a typical data centre, hot air recirculation and cold air bypass. The hot air recirculation will result in a significant difference in the inlet temperature between the upper and the lower part of the server racks. Whereas, the cold air bypass affects the cooling process efficiency by reducing the cold air received by the servers. Another important inefficiency due to the cold air bypass is the possibility of mixing the cold air and hot air streams in the upper part of the data centre room. This may not be avoidable especially with longer path of exhaust air [2]. The focus in this thesis will be on a raised floor layout with room and ceiling air return. This layout is the most common in current data centres [3].

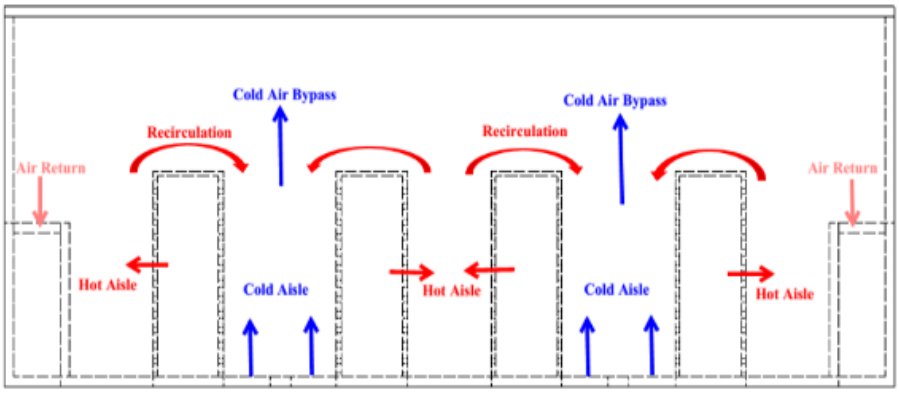

Figure 1: Typical data centre air distribution with room return infrastructure.

There has been continuous development in many aspects of data centre in previous research. However, most of this work has concentrated on developing performance parameters based on Computational Fluid Dynamics (CFD) modelling of different data centre configurations in order to optimize cooling efficiency [4]. CFD simulations are used to visualize the air and thermal distribution throughout the data centre's rooms. It has the ability to give a detailed insight and accurate values for the rack and CRAC inlet and outlet temperatures. However, to determine the cooling efficiency from CFD simulations may be challenging as CFD simulations give qualitative description for the thermal distribution which are not be used to construct numerical data regarding the data centre thermal performance. Hence, there is a necessity for proposing dimensionless indices to give a quantitative analysis to construct numerical data as yardsticks to interpret those measured temperatures Herrlin [5]. Typically, thermal indices interpret the CFD simulation and can identify various options to enhance the cooling efficiency.

The k-ε turbulence model, which is classified as a Reynolds Averaged Navier-Stokes (RANS) equations turbulence model, is widely used in data centre numerical simulations [6]. Despite the fact that some work states that the k-ε turbulence model is the best choice for data centre numerical simulation, the discrepancy between the numerical and the experimental results are significantly large especially in the cold and hot aisles [7, 8]. Moreover, no clear attempt has been made to compare the k-ε RANS model results with experimental data from the critical regions within the data centre room, namely the

hot and cold aisles, in all the published research literature so far recommending the k-ε RANS model. Therefore, in this thesis, simulations using the k-ε RANS model were carried out and compared with the more detailed turbulence model, the k-ω SST SAS (Scale Adaptive Simulation) model, which is classified as a Large Eddy Simulation (LES) turbulence model, to identify any limitations of the k-ε RANS modelling.

In general, the main drawback of the k-ε RANS model is the way of calculating the turbulent viscosity, which does not directly relate the turbulent viscosity to the Reynold stresses as the turbulence is considered isotropic. Hence, this turbulence model might be affected to behave poorly in data centre numerical simulations. Nevertheless, there is no evidence in the literature that the k-ε RANS model has been compared against other turbulence models to verify its accuracy in the data centre numerical simulations. Because of the limitations of the k-ε RANS model, it may not be able to predict precisely how the hot air infiltrated into the cold aisle and also how the cold air escapes from the cold aisle prior to entering the servers. The k-ω SST SAS model, on the other hand, is a hybrid model, using a RANS model near the wall and like a LES solution away from the wall generating DES like simulation results. Although, this model is much more computationally intensive than the k-ε RANS model, it allows large transient turbulent structures to be captured.

RANS models have the advantage of being computationally inexpensive compared to LES models while giving accurate results for the mean velocity, pressure and temperature in many industrial applications with fully turbulent flows. However, they behave poorly in cases of high stream line curvature, severe pressure gradients, flow separation and strongly buoyant flows. All these features might be present in the data centre due to the complex interactions between different air streams and high temperature differences. Therefore, in this thesis the k-ω SST SAS (as LES-like model) model will be used to capture these complex interactions inside the data centre room.

One of the most important issues concerning data centres is the energy consumption where one large data centre may consume around 10-20 MW of electricity. Also, it has been found that the energy consumption of a data centre has doubled every four years over the last decade [9]. Therefore, the consequences of very high usage of

electricity and the methods of heat dissipation are the main concerns for data centre designers. In fact, this highlights the importance of cooling process efficiency in data centres as the cooling system for a data centre may consume around 50% of the total energy [10]. The cooling process is not only important to save energy but also to guarantee continuous and reliable operation as any interruption may cause serious implications in computing operations at all levels. Apart from small number of research papers which conducted rack thermal analyses and their effect on the data centre thermal performance, the majority of published papers concentrate on the enhancement of thermal performance and energy usage of data centre at the room level and exclude rack level thermal analysis [11]. Therefore, this thesis will study these effects on the rack level thermal performance. As the heat density inside the data centre room is continuously increasing, unconventional solutions should be proposed to overcome these problems.

1.2. Thesis Aims and Objectives

This thesis will focus on air cooled raised floor data centres. The objectives of this work are:

1. To identify any limitation of the k-ε RANS turbulence model for data centre numerical simulations by comparing its results with the k-ω SST SAS turbulence model.
2. To identify the best air-cooled servers' arrangement with different heat generation rates in a single data processing cabinet and study the effects of the buoyancy forces on the air movement inside the data centre room.
3. To optimise a novel rack-level sub-cooler to enhance both the cooling effectiveness and energy usage. The sub-cooler is proposed for the first time in this thesis.

1.3. Significance

The contributions of this thesis are significant because of the following reasons. The first is that it identifies and addresses a valid concern regarding the current data centre modelling technique.

The majority of published data centres' studies use the k-ε RANS turbulence model, in this thesis the limitations of using this model have been explored and overcome by suggesting a more robust technique using the k-ω SST SAS turbulence model. Using this approach and the k-ω SST SAS turbulence model, future studies will give better prediction of a data centre's thermal performance and airflow distribution.

The second contribution is that it allows increasing the volumetric heat generation rates for a given room size. This was achieved by optimising the server arrangement within a single rack to allow more heat output and computation maintaining acceptable cooling effectiveness. This thesis presents the best possible servers arrangement in a single processing cabinet to give high cooling effectiveness at the room level cooling.

The third major contribution of this thesis is the proposal of a new technique for enhancing cooling in data centres. This new technique uses rack level sub-cooler installed at the top of a rack and integrated with the perforated tile air supply. By installing these devices not only can better cooling efficiency be achieved but also energy usage can be improved significantly due to the better use of available cooling resources.

1.4. Thesis Organisation

The remainder of this thesis is arranged as follows:

Chapter 2: This chapter presents a review of the literature concerning data centre cooling with a general introduction to their layout and the methods of cooling. At the end of this chapter the research gaps are identified for exploration in the subsequent chapters.

Chapter 3: This chapter presents specific background about CFD and the relevant governing equations for fluid flow and heat transfer. The proposed simulation method and boundary conditions for the numerical simulations are presented. Next, details of the modified OpenFOAM solver incorporating the k-ω SST SAS model with buoyancy is presented. The final part of this chapter presents the mesh sensitivity study for both the RANS and SAS turbulence simulations.

Chapter 4: The first objective of this study is addressed in this chapter by considering the three most common air distribution systems in which the limitations of using the k-ε RANS turbulence model are identified. This chapter also validates the solvers used in this research by comparison with experiments and simulations.

Chapter 5: This chapter investigates the effect of air cooled server arrangement with different heat generation rates in a single data processing cabinet and the resultant effects on the air movement inside the data centre room. This chapter also presents additional validation of the modified solver by comparing its results against the bench mark numerical solution for natural convection of air in a square cavity.

Chapter 6: This chapter presents an optimised design of a rack integrated sub-cooler. The sub-cooler is located at the top of the rack and integrated with the perforated tile air supply. This cooling supply arrangement is presented for the first time in this thesis.

Chapter 7: This chapter concludes the thesis and presents some suggestions for future work based on the preceding chapters. Additionally, the research limitations and their potential impact on the results are discussed.

Chapter 2: Literature Review

2.1. Introduction

In this chapter, the data centre configurations and cooling solutions will be reviewed. In addition, the latest enhancement techniques in data centre cooling will be reviewed. Cooling energy in data centres consumes a substantial portion of the total energy of data centres. The cooling techniques of the data centres can be air or liquid cooling. Sundaram and Ramalingam [12] stated that the simplest cooling principle method for most electronic systems is air cooling. Therefore, in this chapter, the air cooling techniques will be reviewed.

2.2. Data Centre

Recent advancements in computing hardware have resulted in rapid growth computing thus data centres have become indispensable facilities in the world. According to Cho and Kim [13] data centres are defined as "facilities that house IT servers and data storage systems". The main components of a data centre, as shown in Figure 2, are:

- Computer Room Air Conditioning units (CRACs): They control and maintain the temperature, humidity and air distribution at acceptable conditions in the data centre environment.
- Raised Floor: It is the unoccupied space under the server racks to be used in the mechanical and electrical services passage and to supply the cold air through.
- Server Racks: The cooling system is designed primarily to meet the heat dissipation of the servers to maintain them at acceptable temperature.

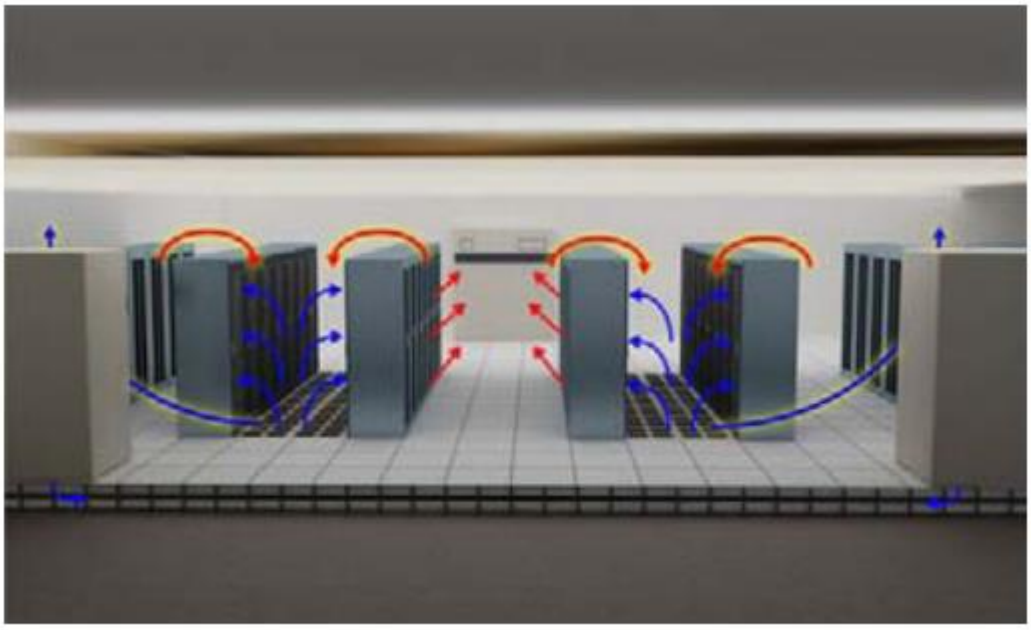

Figure 2: Typical raised floor hot aisle/cold aisle data centre [14].

2.3. Data Centre Cooling Energy Consumption

The energy consumption by data centres is almost 50 times more than the energy consumed by general buildings with constant energy demand throughout the year unlike the general buildings [15]. One large data centre may consume around 10-20 MW of energy, and in the last decade the electricity consumption has doubled every four years [9]. According to some estimations, data centres consumed about 100 billion kWh of electricity in 2016 [16]. In fact, this gives rise to the importance of the cooling process efficiency in data centres as the cooling system for a data centre may consume around 50% of the total energy consumed by a data centre, as demonstrated by Figure 3 [10, 17]. The increasing demand of internet and clouding services such as Facebook and Google participating in the large growth of the data centres and hence more energy consumed to meet the increasing demand [18].

The efficiency of energy use in data centre is essential in modern data centres as it will impact many aspects such as energy cost, performance and environment as the IT currently accounts for 2% of carbon emissions and expected to increase 50% in 2020 [19].

The consequences of very high usage of electricity and the methods of the heat dissipation are main concerns for data centres customers.

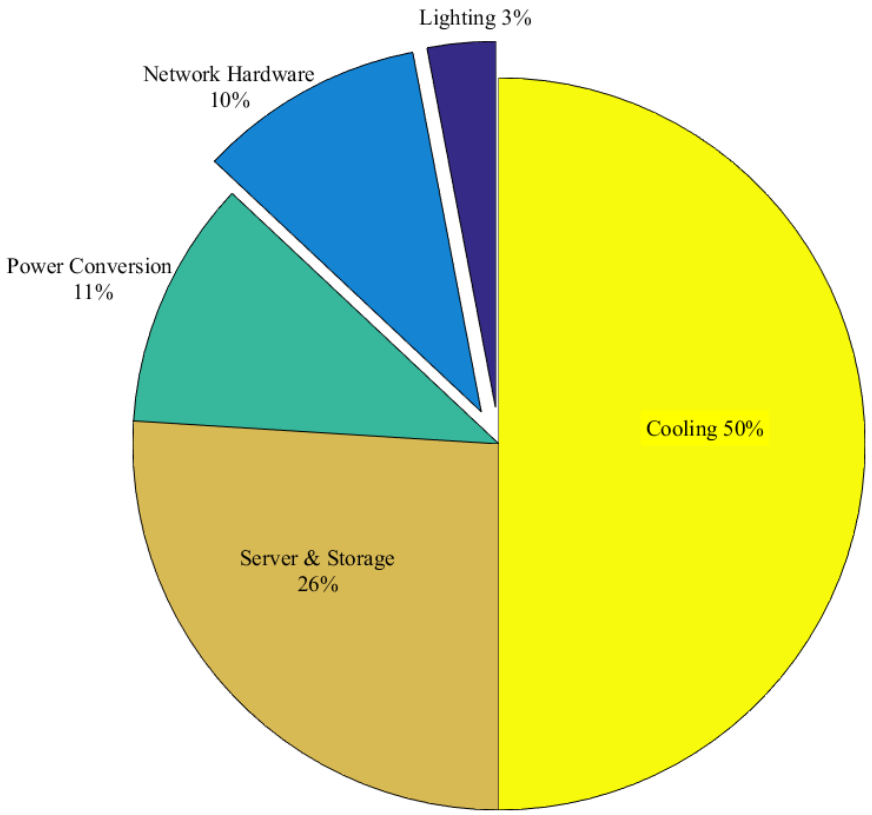

Figure 3: The energy consumption by different components of a data centre, adapted from [10].

2.4. Data Centre Cooling Energy Optimisation

Many techniques have been applied to data centres to save cooling system energy use. For example, the cold aisle hot aisle approach is widely applied in the current data centres as one of the most approaches used [20], increasing the IT equipment allowable temperature [21] and using the free cooling technique by using the outside cold air and water in the cold seasons [22, 23]. In addition, Choo, et al. [24] proposed optimisation of thermo-fluid flow for medium size data centres to remove the redundant CRACs, increase the CRACs inlet temperature, implement containment for the cold aisle and to use outdoor air cooling. The conventional refrigerant cycle has been replaced by David, et al. [25] by developing less chiller cooling which may save up to 90% of the energy consumed by the

chiller. There are many techniques have been utilised to save the energy of the data centre cooling system especially by exploiting the weather conditions. However, there is no enough evidence that the thermal analysis of different data centre components such as the racks attracted attention to be investigated. Also, there is enough indication that the effect of the server arrangement with different heat generation has been studied to explore the best arrangement for best data centre thermal performance.

2.5. Data Centre Thermal Guidelines

To keep data centre in acceptable working conditions, IT equipment operators should meet recommended guidelines. ASHRAE TC9.9 released one of the most used thermal guidelines for data processing environments. The IT server inlet dry bulb temperature recommended range for ASHRAE TC9.9 is between 18 and 27 ºC and the range of acceptable humidity is between 20% and 80% as shown in Table 1. The temperature range at the inlet of the IT server is identified to both save energy and in the same time keeping the equipment in save operating conditions. The subscripts a-e definitions can be found in [27]. On the other hand, the proper quantity of humidity in the air entering the IT servers is essential to maximise the performance and availability of computing equipment [26]. Figure 4 shows the psychometric chart of four envelops for acceptable ranges of temperature and humidity for data centres; however, any of these envelops can be used for data centres [27].

Table 1: ASHRAE 2008 Thermal Guidelines [27].

Class	Equipment Environment Specifications									
	Product Operation [a, b]							Product Power Off [b, c]		
	Dry Bulb Temperature (°C)		Humidity Range, Non Condensing		Maximum Dew Point (°C)	Maximum Elevation (m)	Maximum Rate of Change (°C/h)	Dry-Bulb Temperature (°C)	Relative Humidity (%)	Maximum Dew Point (°C)
	Allowable	Recommended	Allowable (% RH)	Recommended						
1	15 to 32 [d]	18 to 27 [e]	20 to 80	5.5°C DP to 60% RH and 15°C DP	17	3050	5/20 [f]	5 to 45	8 to 80	27
2	10 to 35 [d]	18 to 27 [e]	20 to 80	5.5°C DP to 60% RH and 15°C DP	21	3050	5/20 [f]	5 to 45	8 to 80	27
3	5 to 35 [d, g]	NA	8 to 80	NA	28	3050	NA	5 to 45	8 to 80	29
4	5 to 40 [d, g]	NA	8 to 80	NA	28	3050	NA	5 to 45	8 to 80	29

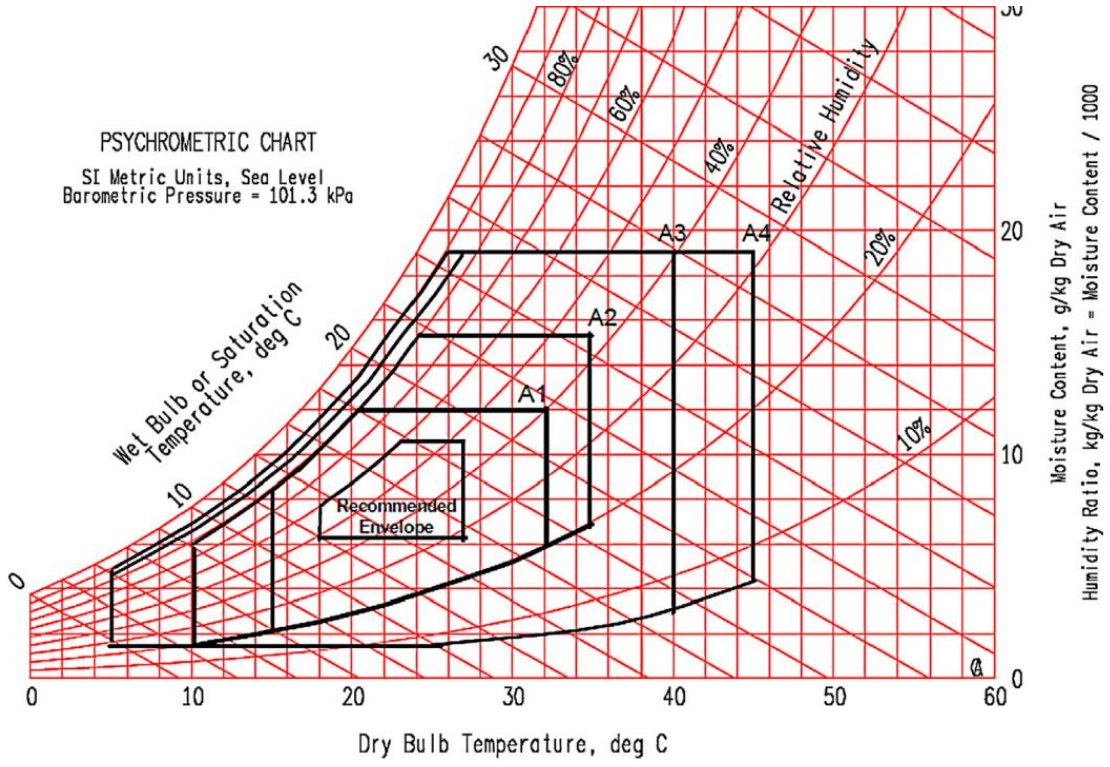

Figure 4: ASHRAE environmental classes for data centres [27].

2.6. Air Distribution System

The data centre air distribution system mainly designed to achieve an efficient air cooling to the IT servers. According to Cho, et al. [3] in data centres, there are in total 13 possible combinations of air distribution systems based on 12 types for supply ad return systems as Figure 5 shows, and one for the hard floor or raised floor systems. However, only six types may be used by excluding the direct connection methods of supply and return air due to using of the rack mounted servers in large data centres. The main function of the air distribution system is to prevent overheating of the server racks [13].

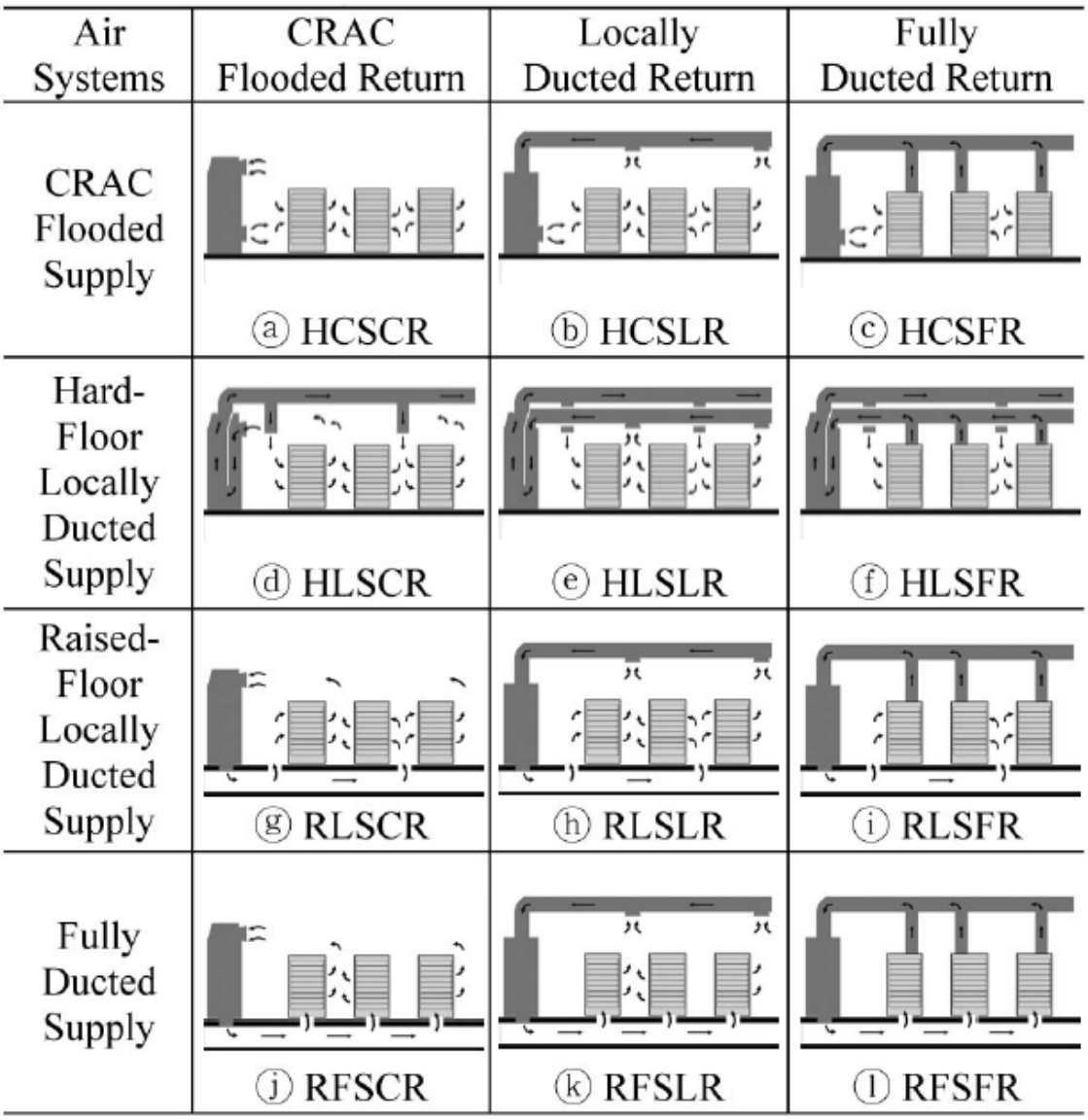

Figure 5: Twelve types of air distribution systems [3].

The air distribution system consists of cold air supply system and hot air return system. The supply system supplies the chilled air to the server racks from the CRAC units. Whereas, return system draws the exhaust air from the server racks to the CRAC units to eliminate the heat dissipated by the IT servers. Cho, et al. [28] conducted an important study to figure out the best air distribution system among many candidates, and the most important conclusions have been found are:

- The overhead supply local return is appropriate overall but because the chilled air is supplied by overhead ducts the lower part of the server racks may not receive enough cold air and hence there will be starving servers near the bottom of the racks.
- Generally, the most effective air distribution system is the underfloor distribution system if the occurrence of exhaust air recirculating to the upper part of the servers is prevented.
- The flooded supply method causes unstable air and temperature distribution throughout the data centre and it is the best choice for only small data centres.

Srinarayana, et al. [29] argued that the best air distribution system is the overhead of cold air supply because it gave a uniform cold airflow at the inlet of the server racks unlike the under-floor air supply which led to hot spots at the upper part of the cold aisle. Herrlin [5] mentioned that the main difference between the overhead and under floor cold air supply is that the gravity-assisted mixing for the overhead supply will promote more mixing in the aisles. Cho, et al. [3] stated that; although, the raised floor data centre is the most common air distribution system used among the others, there are some drawbacks including cost, design time, earth quack susceptibility, safety hazard, security, reliability and some other problems. Another problematic may happen because of suing raised floor data centre is the perforated tile airflow non-uniformity which may cause excessive or insufficient for cooling of the server racks [30]. Srinarayana, et al. [29] stated that the worst scenario was the flooded supply and return air distribution system as it allowed for heavily mixing of the cold and hot air streams within the data centre room.

The effect of the air distribution systems on the temperature difference between the inlet and outlet server's temperature were explored by Rambo and Joshi [31]. They found

that the raised floor plenum with both room return and overhead return are the most efficient air distribution systems regardless the fact that the overhead return led to higher rack temperatures throughout the data centre room compared with the room return. Also, they found that the overhead supply led to the lowest rack temperature but it suffered from the end effect. In general, they argued that if the end effect of the overhead supply could be overcome e.g. by putting the lower power equipment at the end of the racks, it was the best choice among all air distribution systems.

2.7. Raised Floor Data centre

Regardless of the raised floor data centre drawbacks, it is the dominant air distribution system in the current data centre by amount around of 80% of all current data centres [3].The most important aspects of raised floor data centres design are the sizing of the perforated tiles for supplying of the chilled cold air, sizing of the underfloor plenum, and placement of server racks and CRAC units [32]. According to Schmidt, et al. [33] and Roger Schmidt [34] the airflow distribution through the perforated tiles mainly governed by the underfloor plenum space, flow obstructions under the plenum such as pipes and cables, locations of the modular AC units as well as their flow rates, perforated tiles layouts, and the tile open area. Pressure variation of the plenum under the perforated tiles and the perforated tile frictional resistance predominantly govern data centre flow rates; hence, controlling cooling flow rates could be achieved by monitoring the plenum pressure variation and the tile opening percentage [35]. These factors have resulted in a complex flow in the underfloor plenum which controls the airflow through the perforated tiles.

2.7.1. Raised Floor Plenum

The raised floor plenum is the unoccupied space under the server racks to be used in the mechanical and electrical services passage and also to supply the cold air to the data centre room. Schmidt, et al. [33] conducted a parametric study to investigate the effect of the raised floor plenum height and the tile open area on the airflow flow through the vent tiles. They found that when the pressure drop across the perforated tiles was comparable to the horizontal pressure variations in the raised floor plenum, the airflow rates through

the tiles were not uninform. It was also noticed that the height of the raised floor plenum strongly influenced both the pressure distribution and the horizontal velocity variations. Once the height of the raised floor increased, the pressure and horizontal variations non-uniformity diminished which led in turn to uniform airflow rates through the vent tiles as shown in Figure 6.

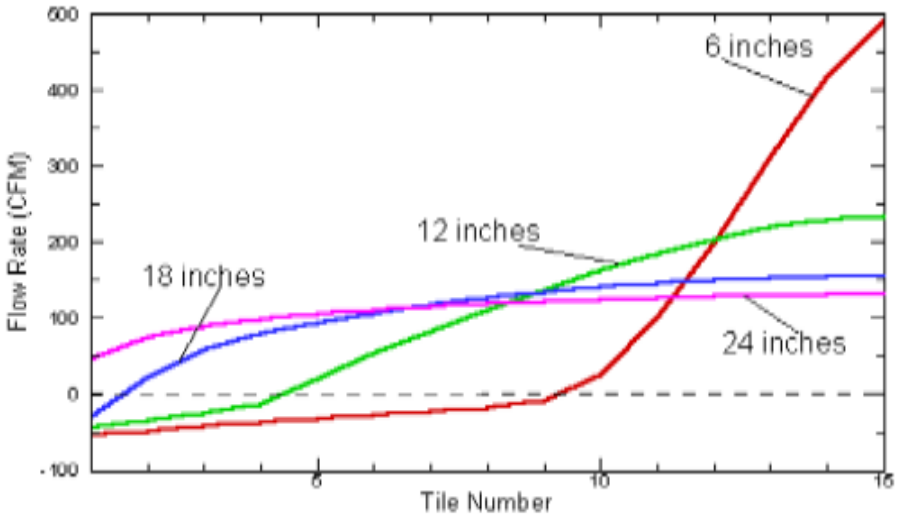

Figure 6: Effect of raised floor height on airflow rates through the perforated tiles [33].

Similar study was conducted by Karki, et al. [36] to illustrate the effect of varying the raised floor plenum height where they studied the basic configuration of a raised floor data centre with different plenum heights. The plenum height which was studied varied from 6 in to 30 inches. This study illustrated that the least flow rates uniformity was at the height of 6 inch, and as the plenum height increases the non-uniformity diminishes. Also, there was a reverse flow when the plenum height was at 6 inches; whereas, at 30 inch there was no reverse flow. With respect to the pressure variation it was found that it diminishes as the plenum height increases where at 6 inch the pressure variation was significant with negative pressure near the chilled air inlets, CRACs outlets. This result is completely consistent with Schmidt, et al. [33] result.

Though, the raised floor plenum could be designed to influence the uniformity of pressure variation and airflow distribution, changing the plenum height for an existing

data centre may not be feasible [36]. This problem may appear when more quantity of airflow is needed with the increasing of the cooling demand. As a result, one of the feasible solutions is to use different tiles with different open areas at different locations which will be discussed in details in the Perforated Tiles section. Moreover, Bhopte, et al. [37] reported that if the plenum height is small, near 12 inch, there will horizontal pressure variations in the plenum and hence there will be non-uniform airflows through the tiles. The inlet temperature of the server racks will not have sufficient amount of chilled air and hence will start to draw the air from the hot aisle and their inlet temperatures may exceed the recommended range. Depending on the same study it could be said that increasing of the plenum height could be beneficial up to a certain limit where after this limit there was noticeable increasing in the inlet temperature of the server racks. This can have attributed to highly fluctuating and complex airflow recirculation pattern in the data centre room.

2.7.2. Perforated Tiles

The server racks cooling requirements must be met by the cooling air flow rates through the perforated tiles [38]. To get the best possible utilization of the perforated tiles, designers and data centre managers should be able to modify the airflow rates through the tiles according to their demand [36]. Kang, et al. [32] carried out their study, CFD analysis, to investigate the effect of percentage open area of the perforated tiles on the airflow distribution through the perforated tiles and to provide detailed prediction of the flow distribution under the raised floor plenum. It was found that for 25% open area the flow experienced high resistance through the tiles; as a result, the pressure drop through the tiles was significantly high compared to the horizontal pressure variation in the raised floor plenum which has resulted in a uniform velocity over all the tiles. This behaviour is as same as the behaviour of uniformly pressurized raised floor plenum. However, with 60% open area the resistance from the tiles diminished, thereby the flow inertia became important and this led to some variations in exit velocity over the tiles.

Karki, et al. [36] stated that the tiles flow rates mainly depend on the pressure drop across the perforated tiles, which is the difference between the raised floor plenum pressure and the ambient pressure above the raised floor. Typically, the pressure variation

in the data centre room located above the raised floor are negligible compared to the pressure variations in the raised floor plenum. Therefore, the ambient pressure above the raised floor is assumed to be uniform relative to the raised floor plenum pressure. The perforated tiles flow rates, thus, mainly depend on the pressure levels in the raised floor plenum, and the horizontal pressure variations in the plenum are responsible for the non-uniformity in the flow rates through the perforated tiles. To avoid the airflow non-uniformity, the area of the perforated tile should be less than the area that available for the horizontal flow in the raised floor plenum [36].

Figure 7 (a) shows clearly that once the open area of the perforated tiles was reduced, the pressure drop across the tiles became high and at some point became much larger than the horizontal pressure variations in the raised floor plenum [38], [33]. If this is the case, the entire raised floor plenum could be considered as a uniformly pressurized and the airflow rates through the perforated tiles will be nearly equal as shown in Figure 7 (b). Another study for the effect of the perforated tiles open areas was conducted by Karki, et al. [36] . To illustrate their ideas, they studied a range of perforated tiles open areas, the tiles open areas were varied from 10% to 40% where all the tiles have the same open area. The flow uniformity diminished as the tiles open area increasing. Another important note was that the reverse flow near the CRACs units might be decreased with the decreasing of the tiles open area. It was found that there was no reverse flow for 10% and 15% tile area as Figure 7 (b) clarifies. Although, the small tile open area could result in a uniform flow, there is a major drawback for decreasing the tile open area where at some limit the plenum pressure becomes very high and a major proportion of the chilled air will escape through the pipes and cables openings because the flow resistance at the pipes and cables openings is comparable with the flow resistance at the perforated tiles. Also, another drawback for small tile open area is that more pressure in the plenum will increase the static pressure within the raised floor plenum which should be overcome by the CRACs units' blowers.

The perforated tiles are commonly characterized by their open area which in most cases is 25% [38]. This is can attributed to that the 25% open area is known to have a better airflow uniformity compared to that of higher percentage openings [29]. The

perforated tiles resist the flow and this can be estimated by the correlation of pressure-drop, for such case it can be expressed as $\Delta P = K(\frac{1}{2}\ \rho\ V^2)$. Where the V is the velocity of cold air entering the perforated tile, ρ is the cold air density and K is the flow resistance factor. The empirical factor of the flow resistance is based on measurements which can be expressed by $K = \frac{1}{F^2}\ [\ 1 + 0.5(1 - F)^{0.75} + 1.414(1 - F)^{0.375}]$. Where F is the fractional open area for the perforated tile. For this fractional open area 25%, the value of K is $K = 42.8$. Figure 7 (a) illustrates the pressure drop for a 25% open tile at different airflow rates.

It is clear from the above table that the pressure drop in the perforated tile with 25% openings, at airflow rate per tile 0.25-meter cube per second is near 12 Pa. The CRAC unit's airflow experiencing an internal static pressure by the filters and the cooling coils by amount of 250 to 500 Pa, and external static pressure by the impingement of the exhausted air on the plenum floor and turning the air on the subfloor by amount of 100 to 200 Pa. It is clear that the pressure drop in the perforated tiles is a small fraction compared with the other pressure drops. Thus, regardless of the tile openings, layouts and numbers, the CRAC units normally give almost the same amount of cold air [38].

For an existing data centre it may not be possible to adjust the under floor plenum height [33]. Also, if the perforated tile open area is decreased it may cause loss significant portion of chilled air through pipes and cables openings. Therefore, one of the feasible solutions is to use different tiles with different open areas at different locations. For example, the opening areas of the tiles above high pressure locations could be reduced and vice versa. Figure 7 (c) shows the airflow rates through uniform and variable tile open areas.

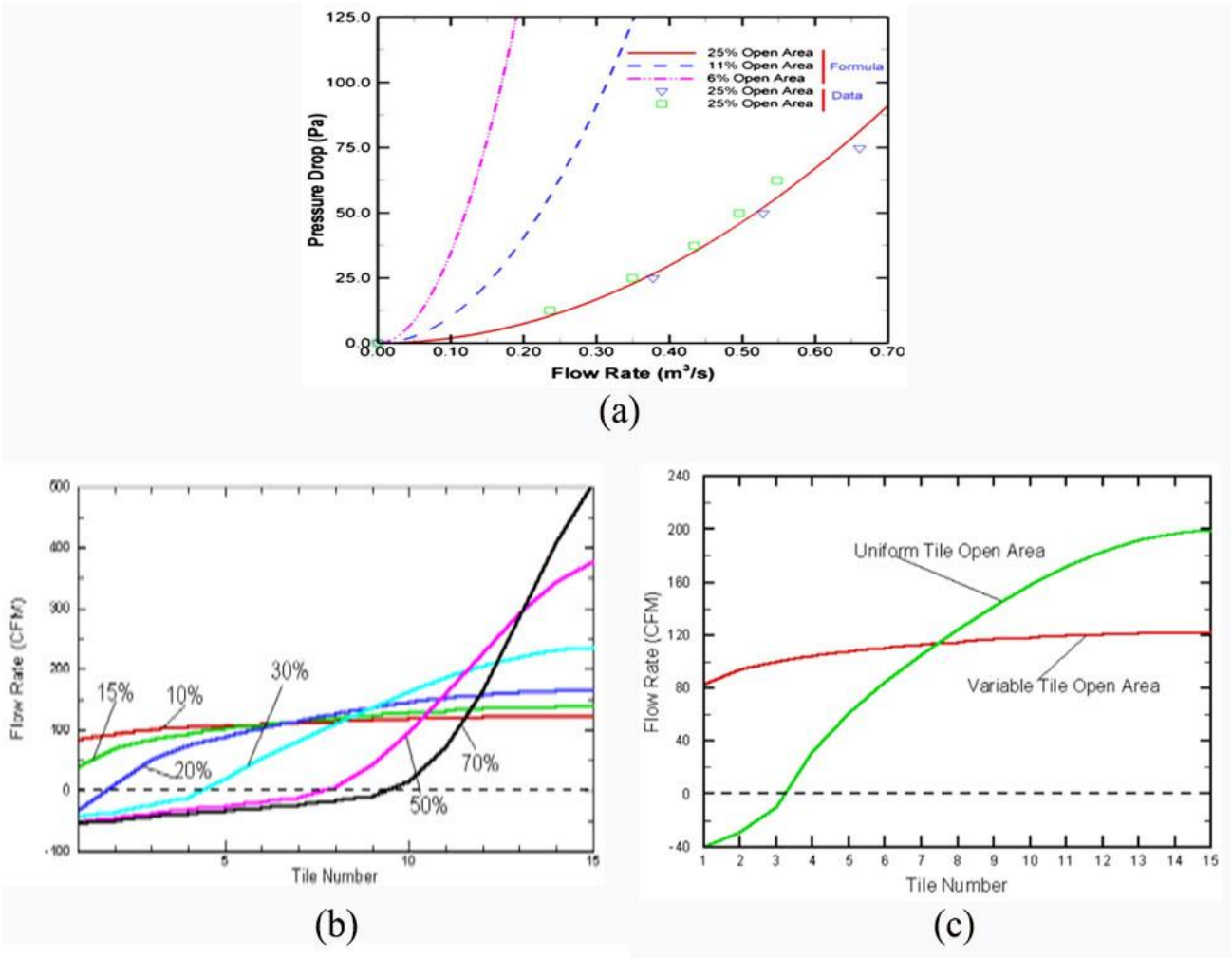

Figure 7: (a) Pressure drop as a function of the airflow rate for different perforated tiles opening percentage [38], (b) Effect of tile open area on airflow rates through tiles [33], (c) Flow rates through tiles for a variable tile open area arrangement [33].

Karki, et al. [36] used different tile areas for different region; for example, they use the largest open area near the CRACs units, the least pressure, and the tile open area decreases towards the opposite wall, the highest pressure. This configuration led to more flowrates near the CRACs units and less flowrates at the opposite wall, leading to more uniform flow rates through the perforated tiles along the raised floor. It was found that this configuration gives more uniform flow rates compared with 25% open area. This configuration can give more space utilization near the CRACs units by preventing any reverse flow.

2.7.3. Under-Floor Partitions

"Under-floor partitions act as flow obstructions and can have significant effect on the pressure distribution in the plenum" [36]. A high-pressure region is created on the upstream of the partition face when the air impinges a partition, and a low-pressure region is created on the downstream face. In fact, any desirable pressure and flow distribution could be achieved by using perforated partitions with suitable open areas and placing them in at suitable locations. Under flow partitions can also be used as 'flow guides', which can create channels within the raised floor plenum to direct the flow into specified regions. For instance, Karki, et al. [36] used inclined solid partition as shown in Figure 8 (b), which works as a converging channel where its area decreasing as the air moves away from the CRAC unit. Without the inclined partition the pressure will increase and the velocity will decrease as the air moves away from the CRAC unit. Within the inclined partition the horizontal velocity remains almost constant and the reduction in the area compensates for the reduced airflow rates. Because of the constant pressure under the perforated tiles, the flow rate though the perforated tiles were almost uniform as shown in Figure 9.

In the same study Karki, et al. [36] considered another configuration consists of two perforated partitions as shown in Figure 8 (a). The plenum is divided into three sections; and each of the partition has different open area. In this configuration, the pressure increases as the air moves away from the CRAC unit; however, unlike the basic configuration the pressure levels across the partitions depend on the partitions open area.

Therefore, the perforated partitions may provide unlimited flexibility to control the pressure and airflow distributions within the raised floor data centre.

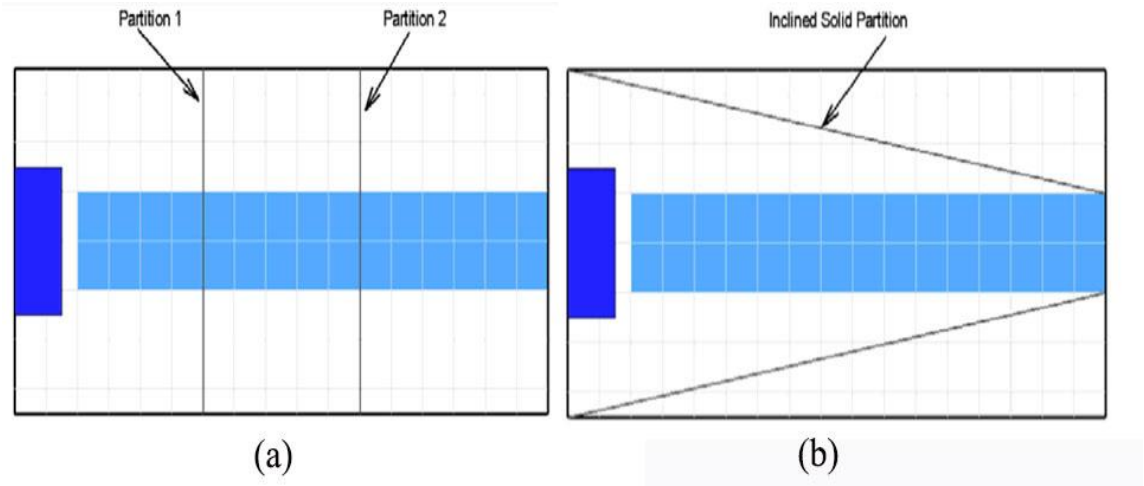

Figure 8: Under floor partitions: (a) Configuration with perforated partition, (b) Configuration with inclined partition [36].

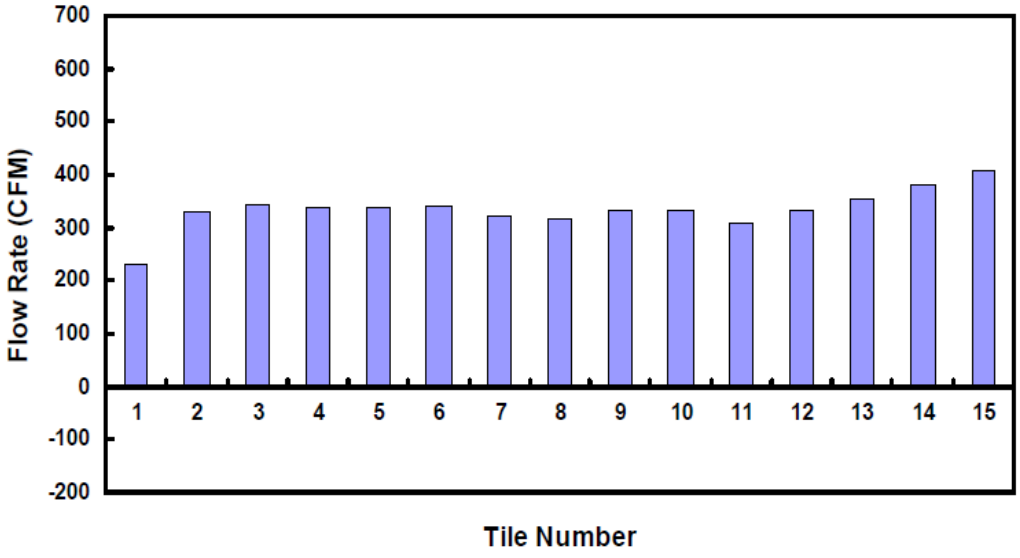

Figure 9: Airflow distribution for the layout with inclined partitions [36].

2.8. Server Racks Layout

The cold and hot aisles arrangement, as shown in Figure 10, was proposed by Sullivan [39] and has become a dominant arrangement in data centres. This arrangement of the server racks is to eliminate the possibility of that the exhaust air is drawn by the inlet of any other server racks [38]. The perforated tiles are placed in the cold aisle to pump the cold air directly into the servers to remove the heating load dissipated. The servers exhaust the hot air within the hot aisle then the air distribution system will exhaust the hot air into the CRAC units without entering the cold aisle. This arrangement separates the cold and air streams to increase the cooling effectiveness and to save energy.

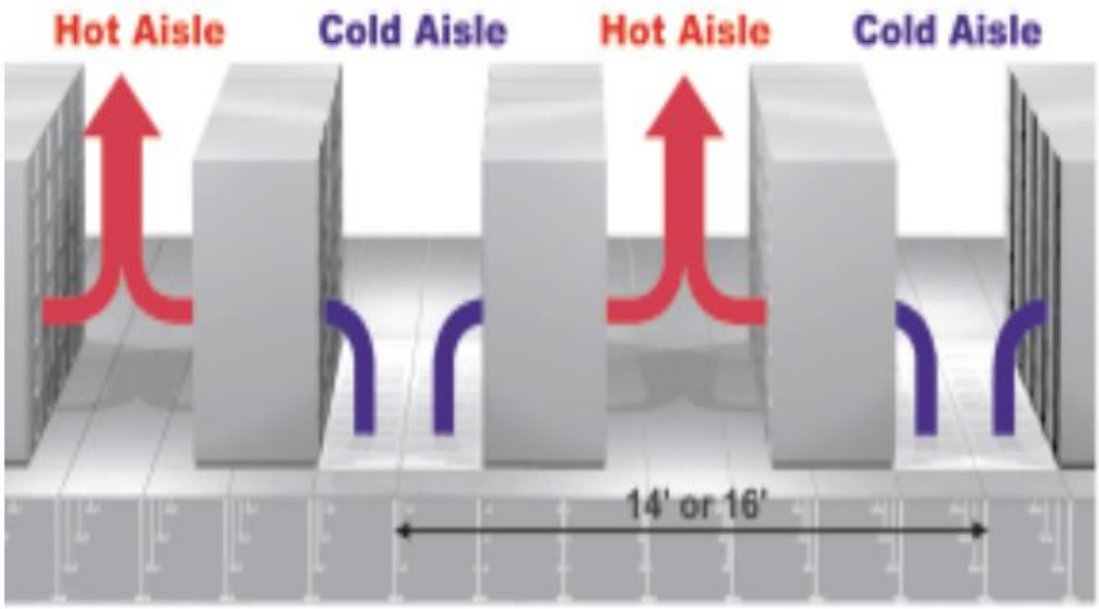

Figure 10: Cold and hot aisles arrangement [39].

The effect of the geometric asymmetry of the servers on the CRAC units heat removal was investigated by Patel, et al. [40]. Their hypothesis in this study is that even with minor perturbation of for the server racks, the CRAC units provision will be negatively affected compared to symmetric distribution for the server racks within the data centre. The comparison of the symmetric racks distributions with the asymmetric

racks distribution showed that with the symmetric distribution, the temperature pattern within the data centre was uniform and this can be attributed to the uniform airflow patterns. Whereas, asymmetric distribution of the racks disturbs the airflow patterns which in turn causes pressure drop in the aisles and creates positive pressure gradient at the end of the aisles. Consequently, this will force hot air recirculation in the room creating hot spots in the data centre. Rambo and Joshi [41] introduced energy metrics to quantitatively evaluate electronic thermal management solutions and for developing guidelines for optimal servers' arrangement in a single rack. Their study didn't consider the room level evaluations, instead it considered systems level electronics cooling only. They investigated three arrangements of placement the high-powered blade servers (1) near the bottom, (2) near the top and (3) spread out as much as possible. The best thermal performance among these three arrangements is spreading out the high-powered blade servers as possible. The next best choice is to spread the servers near the top. The worst thermal performance choice is to cluster server components near the middle. Additionally, Fakhim, et al. [42] found that the best server arrangement within the rack is to put double servers with double voids to have the best inlet thermal conditions.

2.9. Server Racks Heating Load

Schmidt and Cruz [43] studied the effect of the racks heating load on the servers' inlet temperature by comparing 4 kW, 8 kW and 12 kW with each other. Surprisingly it was found that by increasing heating load of the racks, the inlet temperature of the servers' decreases. The highest inlet temperature was for the 4 kW rack; however, 8 kW and 12 kW are similar with less increase in the inlet temperature. Another study was conducted by Roger Schmidt [34] gave the same conclusion. Herrlin [5] found that once the heat densities increased the temperature conditions improved noticeably and this was attributed to the higher velocity of the cold air. Ratnesh, et al. [2] found similar conclusion where with the increasing of the heat load, the SHI dropped noticeably. In fact, this can be attributed to the buoyancy force, where with higher outlet temperature the hot air will be subjected to more lifting force drifting it away from being recirculated into the cold aisle to the ceiling return vet tiles. Though, the buoyancy force can be beneficial for the ceiling

return infrastructure, it can cause problems for other infrastructures especially for flooded room return infrastructure. In this case, more mixing will be present in the upper part of the data centre.

2.10. CRACs Units Placement

Schmidt, et al. [44] performed a study to report a combined modelling and experimental study towards a detailed predictions of airflow distribution through the perforated tiles in a data centre. Two CRAC units were used in conjunction with five different arrangements of perforated tiles layouts as shown in Figure 11. For case 1 when both CRAC units A and B are on there is some back flow near unit B. The flow from both CRAC units are split into two streams, one is forward to the opposite CRAC unit and the other one is backflow. But, the velocity of the air jet from CRAC unit B is high thereby there is a backflow and large pressure variations near this CRAC unit. Whereas, once unit A is off the simulation shows that there is backflow and large pressure variations near unit B because of the large longitudinal velocities near this unit. Also it was noticed by Fakhim, et al. [45] the perforated tiles flowrates are normally significantly lower or higher than average. The tiles near the CRAC units form reversed airflow consistent with Patankar [38] result. This is due to the low static pressure in the high velocity regions.

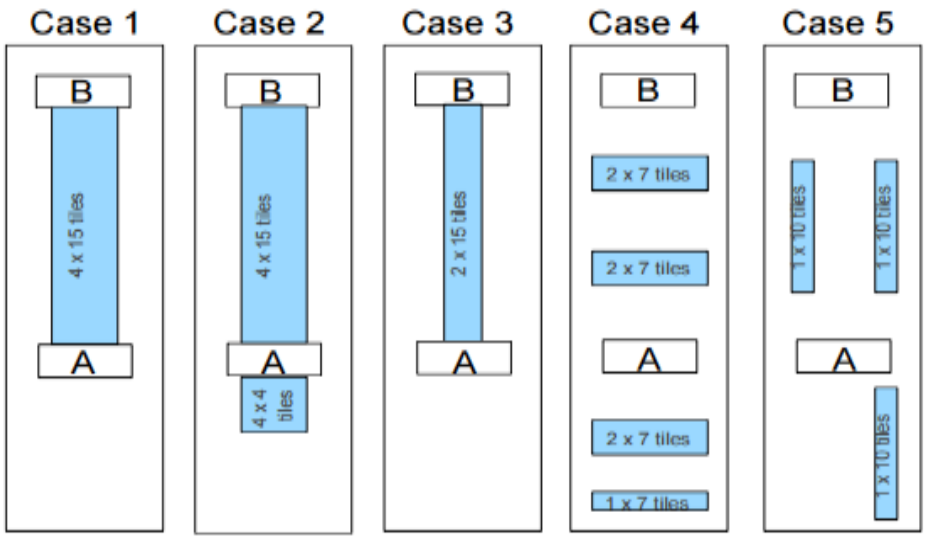

Figure 11: CRAC units and perforated tiles arrangements [33].

In addition, Patankar [46] performed a study in the IBM plant in Poughkeepsie. The key conclusions of the study are that the number of CRAC units in operation affect the airflow distribution across the perforated tiles strongly. Where if the CRAC units discharge chilled air in the same direction, the airflow distribution will be improved. However, if the CRAC units discharge the chilled air in opposite direction the non-uniformity of the airflow would be increased as their airstreams will collide. Also, once there is one a CRAC unit in operation, there will be a reverse flow near this unit consistent with [33, 45].

Rambo and Joshi [31] reported that the high flow rates of CRAC units in the raised floor plenum cause complex flow pattern and hence the pressure variations within the plenum will cause mass airflow variations across the perforated tiles. However, this non-uniformity may be used in advantageous manner by localizing the high-power racks near the tiles with high flowrates. Additionally, the orientation of the CRAC units, because of the symmetry, has no effect on the perforated tiles flowrates. It was also noticed that once the CRAC units located in the same side they give the highest flow rates and once they are in opposite to each other they give uniformly flow rates through the perforated tiles; however, their result is inconsistent with the conclusion found by Patankar [46].

2.11. Room Infrastructure

2.11.1. Cold and Hot Aisles

According to AHRAE (2004) recommendations the cold and hot aisle widths should be 0.9 m and 1.2 m, respectively [5]. Ratnesh, et al. [2] investigated the, geometry parameter, cold aisle width. It was found that the SHI decreased with the increasing of the cold aisle width. This was because of the perforated tiles airflow area decreased and hence the velocity of the chilled air jets, entering the data centre, decreased. This in turn increased the static pressure within the cold aisle and; consequently, more of hot air infiltration into the cold aisle was prevented. Additionally, unlike the velocity in the cold aisle, the velocity in the hot aisle is low as it depends on the CRAC units induced draft and hence any increasing in the hot aisle width will decrease the static pressure within the hot aisle. In addition, in the hot aisle, the static pressure increased with the decreasing of the hot aisle width and this enhanced the hot air mixing and reduced the CRAC units' inlet temperatures. With respect to the average RHI it was noticed that the cold aisle width has limited impact.

2.11.2. Ceiling Height

In case of ceiling return infrastructure Ratnesh, et al. [2] found that the presence of the ceiling plenum changed the airflow pattern drastically. For example, when the hot aisle spacing decreased, combined with ceiling vent tiles located upper the hot aisle, the static pressure within the hot aisle increased, and because of the low pressure above the hot aisles near the return vent, more hot air forced directly up into the return vents caused in a lower SHI and more RHI. In contrast, larger hot aisle, reduced this beneficial, caused more air mixing within the data environment which allowed more hot air infiltration into the cold aisle. The ceiling height was following the same trend of the hot aisle, where once the ceiling height decreased, the pressure gradient between the ceiling and the hot aisle increased. This forced the hot air directly up into the return vents caused a lower SHI and more RHI. However, increasing the ceiling space reduced the mixing of the cold air with

the hot air above the top of the central servers and hence the RHI for those rows decreased [2]. Furthermore, Rambo and Joshi [31] found that the overhead return infrastructure increased the size of the recirculation zone and the width of the CRAC exhaust jets producing marginally more uniform pressure field in the data centre and hence more uniform airflow rates through the perforated tiles. In addition, the ceiling height does not have significant effect on the cold aisle airflow distribution but it has major effect on the exhaust air recirculation [37]. Shrivastava, et al. [47] stated that increasing the ceiling height from 9 to 12 ft improved the thermal conditions in the data centre room as increasing the ceiling height provides more space for the exhaust air to rise up and does not recirculate directly into the cold aisle. However, increasing the ceiling above this limit does not have any significant effect on the thermal performance.

2.12. Free Cooling Solutions

The free cooling concept depends on using either outside cold air or outside natural source of cold water. Free cooling considered the best way for saving energy required for the cooling system in data centres [48]. It was found that the free cooling has high efficiency due to the fact that the heat pipe system used in free cooling has excellent heat transfer performance under small temperature difference operating conditions [49]. According to Tom Harvey [50] around 75% of Northern American data centres can utilise free cooling in their cooling systems. Liquid cooling solutions for data centre cooling have many advantages such as energy savings, reduction the need of mechanical equipment and also they are capable of supporting high density power data centres [51]. Additionally, Google will build a data centre in Europe by investing 200 million Euros because of the cold weather conditions [52]. Likewise, Facebook will construct green data centre in Sweden due to the same reason [53]. Pawsey Supercomputing Centre in Australia innovated geothermal solution for cooling the centre's supercomputing systems which has been estimated to save approximately 14.5 million litres of water every year [54].

2.13. Aisle Containment Solutions

Cho and Kim [13] used a CFD modelling to analyse different air distribution systems by describing two performance metrics, Rack Cooling Index (RCI) and Return Temperature Index (RTI) in high density data centre. It was detected that the hot air re-circulation takes place in the upper part of the cold aisle. Therefore, they suggested a physical partition to separate the hot aisle and the cold aisle to minimize the hot air re-circulation. To prevent the hot air recirculation in underfloor distribution system they used additional barrier installation on the server racks. They found that by using under floor recirculation system without barriers the server intake temperature below 1.8 m high is near the tile temperature but above this limit there is hot air recirculation, due to insufficient supply flow rates, which increases the server intake temperature. By installing a solid partition, the air recirculation is greatly reduced in the upper part of the cold aisle. It was also noticed the average server outlet temperature is reduced from 15 °C without installing the vertical partition to about 10 °C after the vertical partitions were installed. Nada, et al. [55] found that the roof top containment of the cold aisle is better than the side containment as it eliminates the cold air bypass and hot air recirculation for the upper part of the cold aisle. Srinarayana, et al. [29] and Nada, et al. [55] also found that the top containment is better that the side panel containment because of the majority of the hot air recirculation from the top part of the cold aisle.

2.14. Thermal Indices

Cooling performance efficiency is one of the most important parts to be explored in data centres; therefore, many performance metrics have been developed to evaluate cooling performance efficiency in data centres. Bhagwat, et al. [4] argued that because it is significantly difficult to use CFD models to characterize and design efficient cooling systems for data centres, there is necessity to explore alternative way not using very much computational processes and simultaneously provide a trustworthy vision enabling decision makers to make sound decisions. In recent years, to control the thermal management and the air distribution performance both in design and operational stage, several thermal metrics were introduced [56] [57]. By using these indices, the thermal and

airflow performance can be improved which can lead to improve the energy consumption of the data centres and hence the operational costs can be reduced [56]. The most important and most widely used thermal indices in order to evaluate data centres thermal performance is shown in Table 2.

Table 2: Summary of thermal indices used in evaluation of data centres thermal performance [56].

Index	Information provided	Input Measures	Formula	Benchmark	
SHI	Recirculation extent within cold aisles	Airflow supply, inlet and outlet temperatures	(1)	target	0
				good	< 0.2
RHI	Effectiveness utilization of cold airflow	Airflow return, supply and outlet temperatures	(2)	target	1
				good	> 0.8
RCI_{Lo}	Rack cooling condition in respect of cold threshold values	Rack intake air temperatures distribution	(3a)	ideal	100%
				good	≥ 96%
				acceptable	91 ÷ 95%
				poor	≤ 90%
RCI_{Hi}	Rack cooling condition in respect of hot threshold values	Rack intake air temperatures distribution	(3b)	ideal	100%
				good	≥ 96%
				acceptable	91 ÷ 95%
				poor	≤ 90%
β Index	Presence of recirculation and over heating	Local airflow inlet supply and outlet temperatures	(4)	target	0
NP	Airflow infiltration into underfloor plenum	Airflow plenum, supply and return temperatures	(5)	negligible	
BP	Bypass extent within data center	Plenum airflow, return and outlet temperatures	(6)	ideal	0
				good	0 ÷ 0.05
				acceptable	0.05 ÷ 0.2
R	Recirculation extent within cold aisles	Airflow supply, inlet and outlet temperatures	(7)	target	0
				good	< 0.2
RTI	Presence of recirculation or bypass phenomena	Airflow return, supply and outlet temperatures	(9)	target	100%
				good	95 ÷ 105%
				poor	<70% Λ>130%

2.15. Data Centre Numerical Simulations

Numerical modelling, Computational Fluid Dynamics (CFD), has been extensively used to study the data centre thermal performance as it is challenging to study data centres

experimentally especially prior to building a real data centre. It is widely used in data centres especially in predicting air velocity, pressure distribution and heat transfer for room and chip levels. Real data centre construction costs a lot of money; therefore, a reliable data centre simulation can be done to help the designers to generate a set of guidelines to building designers when design data centres for optimal thermal performance. It is also a capable tool for predicting the hot spots and identify the problematic areas to avoid potential failure of critical equipment. The most effective and economical way to build an efficient cooling system for a data centre for a new facility is by using CFD modelling. The first time that CFD used to publish results for data centre was in 2000, since then it has been widely used due to it is ability to give reliable data about fluid flow and heat transfer characteristics [58].

Some argue that CFD can give accurate results for provisioning of air conditioning units, CRAC units, though in large scale data centres where in case of high heat dissipation the provisioning of the air conditioning units is a key problem [59]. According to Shrivastava, et al. [47], it is difficult to generate large data sets for a real data centre due to the difficulty of the thermal experimental measurements for different locations within the data centre room making CFD modelling the best alternative. Numerous researchers, as shown in Table 3, have utilised numerical modelling using the k-ε model. Schmidt, et al. [60] pointed out that the k-ε model is widely accepted as the most appropriate method to be used in the data centre numerical simulations.

Table 3: Turbulence models used in the previous studies.

Author	Year	Turbulence Model
Yuan, et al. [61]	2018	k-ε
Song [62]	2017	k-ε
Norouzi-Khangah, et al. [8]	2016	k-ε
Nada, et al. [55]	2016	k-ε
Priyadumkol and Kittichaikarn [63]	2014	k-ε
Fakhim, et al. [42]	2013	k-ε
Srinarayana, et al. [29]	2013	k-ε
Bhagwat, et al. [4]	2013	k-ε
Almoli, et al. [16]	2012	k-ε
Bhagwat, et al. [64]	2012	k-ε
Fernando, et al. [65]	2012	k-ε
Cho and Kim [13]	2011	k-ε
Fakhim, et al. [45]	2011	k-ε
Ibrahim, et al. [66]	2010	k-ε
Shrivastava, et al. [47]	2009	k-ε
Cho, et al. [28]	2009	k-ε
Herrlin and Belady [67]	2006	Not stated
Tang, et al. [68]	2006	Not stated
Bhopte, et al. [37]	2006	k-ε
Rambo and Joshi [41]	2006	k-ε
Beitelmal and Patel [69]	2007	k-ε
Radmehr, et al. [70]	2005	k-ε
Roger Schmidt [34]	2005	k-ε
Karki, et al. [71]	2004	k-ε
Schmidt and Cruz [43]	2003	k-ε
Patel, et al. [40]	2002	Not stated
Ratnesh, et al. [2]	2002	Not stated
Kang, et al. [32]	2002	k-ε
Chandrakant D. Patel [72]	2001	k-ε

The CFD numerical simulations are normally carried out by specialised commercial CFD software packages such as FLOTHERM and TILEFLOW. However, the license pricing for these tools is beyond the capacity of individuals. Thus, there should be some alternatives to overcome this problem by using the open source CFD tools. Though, the demonstration of using open source CFD tools has not been well proved. The only study which has been found that demonstrated the use of the open source software tool OpenFOAM (Open source Field Operation and Manipulation) has been conducted by Summers, et al. [73]. In this study, they demonstrated OpenFOAM accuracy despite the fact the it needs more time to achieve proficiency in its use. Moreover, use of open source software OpenFOAM has many advantages such as the financial cost and advanced physical modelling. Although, mesh generation of a real data centre and representation of data centre components such as blowers, IT servers may not be feasible by using OpenFOAM with simple boundary conditions typically be used to represent these complicated components.

Most of the CFD simulations in data centres have been utilized based on steady state analysis, and few of them utilized transient simulations [74]. Where the airflow rates and the IT server power are applied, then the airflow and thermal conditions in data centres have been obtained [66]. Besides, most of the transient simulations have focused on evaluation of equipment responses to system failures [69] and to investigate the effect of the CRAC units malfunctioning on the data centre temperature distribution. Beitelmal and Patel [69] utilised transient CFD numerical simulation and found that when the IT load is available with good organisation the rack inlet temperature can maintain acceptable inlet temperature. Also Schmidt, et al. [75] used transient CFD numerical simulation to explore different failure scenarios of cluster of water cooled chillers in the IBM cooling infrastructure.

The transient CFD modelling can give accurate results; though, it is not easy to be implemented in the data centre cooling simulations as it is time consuming and may take days to finish. VanGilder [76] and Seymour, et al. [77] reported that, it is not easy to get sufficient details with high accuracy to capture the IT cooling conditions by using transient simulations. Therefore, many researchers developed alternative ways to evaluate the data

centres transient thermal performance. For instance, Khankari [78] developed zero-dimensional heat transfer model, by applying simple energy balance, to investigate the time available for the IT servers to reach the critical temperature during power shutdown. Kummert, et al. [79] studied the effect of chiller unit's failure on the room temperature variations by developing detailed transient model of a data centre chilled water cooling plant. Although, these different methods achieved more computational efficiency by eliminating the special non-uniformity in the CFD simulations, they are not appropriate for real time data centre thermal management [74].

2.16. Numerical Experimental Discrepancy

Shrivastava, et al. [80] used experimental works to be compared with their CFD modelling using the k-ε model. Figure 12 shows numerical and experimental comparison in their study. It is clearly shown by the figure that there is a significant difference between the numerical and experimental results. In general, they found that the variations in more than 83% of the calculated rack inlet temperatures between the measured temperature values and the numerical values is about ± 7 ºC. Although, the authors attributed the disagreement between the measured and the numerical results to the uncertainty in the measurements and the simplifications in the numerical models, using the k-ε model might be the main source of the error. Patankar [46] and Schmidt and Cruz [43] compared some experimental results with CFD predictions and found that the average root mean square of the error is at least 10% and in some cases exceeds 100%. Chandrakant D. Patel [72] reported that the numerical experimental discrepancy is about 12% at the top of the racks with overhead air supply. Fernando, et al. [65] studied the flow patterns similarity between a data centre model and a CFD simulations using k-ε RANS. Table 4 shows the error which indicates that the k-ε RANS model cannot anticipate the right value and direction at the same point. In their study Fulpagare and Bhargav [81] further criticised the k-ε RANS model due to the fact that even if the boundary conditions are matched the tile flow rates, the solution over the domain is not necessarily correct or even unique.

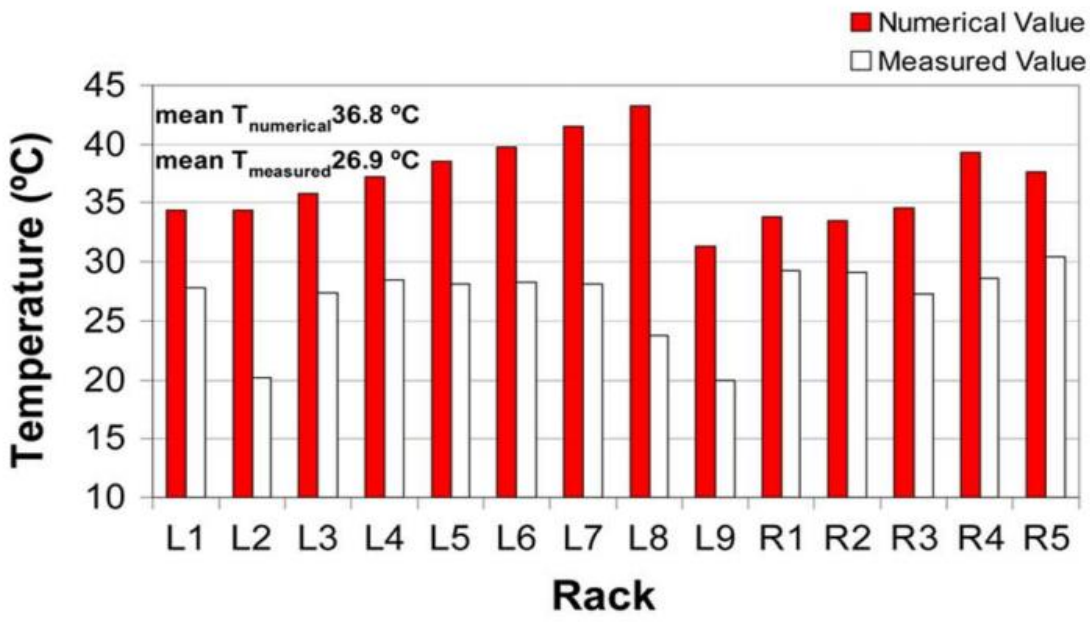

Figure 12: Numerical and experimental comparison [80].

Table 4: Average error of flow velocity between data centre model and CFD simulations using k-ε RANS model, adapted from [65].

Item	**Average Error**
Total Velocity	16.46%
Velocity U	135.79%
Velocity V	138.00%
Velocity W	244.00%

Karki, et al. [71] performed a study to compare experimental measurements with numerical results computed by using k-ε RANS model. They argued that their numerical values have small discrepancy with the experimental values; therefore, k-ε RANS model was recommended to be used in the data centre numerical simulations. However, only the perforated tile flow rates captured by the numerical model were compared with the experimental results. Other comparisons have been performed by Nada, et al. [55], Norouzi-Khangah, et al. [8] by comparing experimental temperature values with numerical temperature values captured by using k-ε RANS model. The agreement between the experimental and numerical values is acceptable. The problem of their comparison is that they picked up points away from the aisles where no interesting airflow interaction may take place. Therefore, to be able to make sure all the results of the k-ε RANS model is precise a holistic comparison should be considered as the discrepancy may appear due to the complex interactions of the airflow inside the data centre room especially in the cold and hot aisles.

2.17. Research Gap

Many techniques have been used in the literature such as CFD modelling, experiments, and thermal indices approach. Based on the literature tendency, more improvements could be achieved in the future to many features of data centres; however, no indication that the turbulence modelling would attract attention to be improved. k-ε RANS model is widely used in the data centre numerical simulations. Even though some papers argued that the k-ε RANS turbulence model is the best choice in the data centre numerical simulation, the discrepancy between the numerical and the experimental results are significantly large especially in the cold and hot aisles. Moreover, no clear attempt was made to compare the k-ε RANS model results with more robust turbulence model. Therefore, in this study, results using the k-ε RANS model will be carried out and compared with the more robust turbulence model k-ω SST SAS to identify the limitations of the k-ε RANS model for three different layouts.

The cooling power optimisation has been attracted attention to be improved in many ways as illustrated in the literature. However, the thermal analysis of different data

centre components such as the rack level thermal analysis, and the effect of the server arrangement with different heat generation on the data centre thermal performance and energy consumption have not been well proven to be studied. Therefore, these two gaps will be addressed in two separate chapters in the thesis.

2.18. Summary

Data centre is known as the facilities that house IT servers and data storage systems. The raised floor data centre is the dominant configuration with 80% among the rest of the other configurations. It consists of racks arranged in cold/hot aisle arrangement to eliminate the possibility of hot air infiltration into the cold aisle. There is increasing demand in internet and clouding services which makes data centres need expanding in steep curve. This has resulted in increasing in power consumption of data centres. Hence, exceptional cooling approaches should be developed to save the cooling energy of data centres as the cooling system may consume around 50% of the data centre total energy. However, great effort has been made to investigate data centres cooling leading to enormous improvement in the thermal performance and hence increasing the cooling effectiveness and energy saving.

Chapter 3: CFD Modelling of Air-Cooled Data Centre

3.1. Introduction

In this chapter, the mathematical background and Computational Fluid Dynamic (CFD) modelling will be described for the subsequent chapters. The turbulence models used to simulate the data centres will be clarified with their relevant equations. The boundary conditions that will be implemented in OpenFOAM will be explained. Also, the behaviour of the fluid flow inside the data centre will be classified whether it is laminar or turbulent. In this study, two turbulence models will be used the k-ω SST SAS and k-ε RANS models. The results of these turbulence models will be compared with some experimental works to identify which of them is correctly anticipate the thermal and fluid flow distribution within the data centre.

3.2. Computational Fluid Dynamics (CFD)

Computational Fluid Dynamics (CFD) can be defined as the assessment of any system that contains fluid flow and heat transfer by using computer based simulations [82]. CFD has the ability to capture the fluid flow complex interactions. Also, it is very powerful tool and used in wide range of engineering applications such as aircraft and vehicles aerodynamics, chemical reactions and biomedical engineering and in many other fields. In CFD, the fluid flow and heat transfer interactions are described by mathematical differential equations which in turn can be converted into a set of algebraic equations that are solvable by using the CFD packages such as OpenFOAM and ANSYS.

The CFD simulation consists of three main parts as follows:

1. Pre-processing.
2. Solving.
3. Post-processing.

In pre-processing stage, which is considered the first stage of the CFD simulation, the mesh of the fluid domain is generated and then the physical properties and boundary conditions are set.

In the solving stage, the fluid flow and heat transfer governing equations are solved by using the Finite Volume Method (FVM) or Finite Element Method (FEM). The FVM is used in most of the commercial software including OpenFOAM. By the FVM, the partial differential equations will be converted from continuum along the whole fluid domain into a set of discrete algebraic equations at each node throughout the fluid domain.

The last step of the simulation process is the Post-processing step. The results, generated by the solver, can be visualised and analysed qualitatively or quantitatively. For example, Paraview can be used to generate streamlines, vector plot and contour plots. Also, there are many utilities such as probing and sampling can be used to generate the required data and this data can be manipulated by using MATLAB or Python or any another relevant software.

3.3. Turbulence Modelling

Turbulence modelling is needed when the flow regime is turbulent by presence of chaotic changes in fluid flow characteristics. In contrast to turbulent flow, in the laminar flow the fluid layers flow in parallel layers with no interference between them. The turbulent flow has many special features; for instance, it is random, diffusive, rotational, and dissipative. It is normally highly unsteady and three dimensional and changes by un-expectable manner. Diffusivity causes rapid mixing which in turn increases momentum, heat and mass transfer. Also, the rotational nature of the turbulent flow causes great deal of fluctuating vorticity as shown in Figure 13. There are many factors that may increase turbulence generation such as low fluid viscosity, high flow rates and surface roughness.

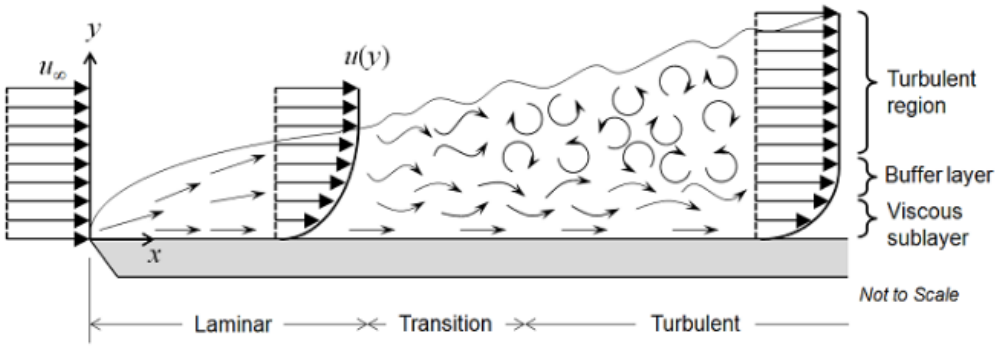

Figure 13: Fluid flow phases, laminar, transition and turbulent, image credit: COMSOL [83].

Once the dimensionless Reynolds number (Re) exceeds the critical value a series of complex actions take place within the flow causing the flow to transform from laminar to turbulent flow. The Re is the ratio of inertia forces to viscous forces as equation 3.3.1 clarifies.

$$\mathrm{Re} = \frac{\rho u D_h}{\mu} \qquad 3.3.1.$$

Where, ρ is density of the fluid, u is mean velocity of airflow, D_h is hydraulic diameter and μ is viscosity of the fluid. Re values for a rectangular duct are highly problem dependent where it can be considered laminar once Re<2300 and turbulent if Re>4000.

Even for steady and uniform boundary conditions there will be a chaotic motion imposed in the fluid in case of turbulent flow. All airflow properties such as velocity, pressure and temperature will have chaotic behaviour and will fluctuate around their mean as shown in Figure 14 for velocity. Where, U is the average velocity, u′ is fluctuations of the velocity.

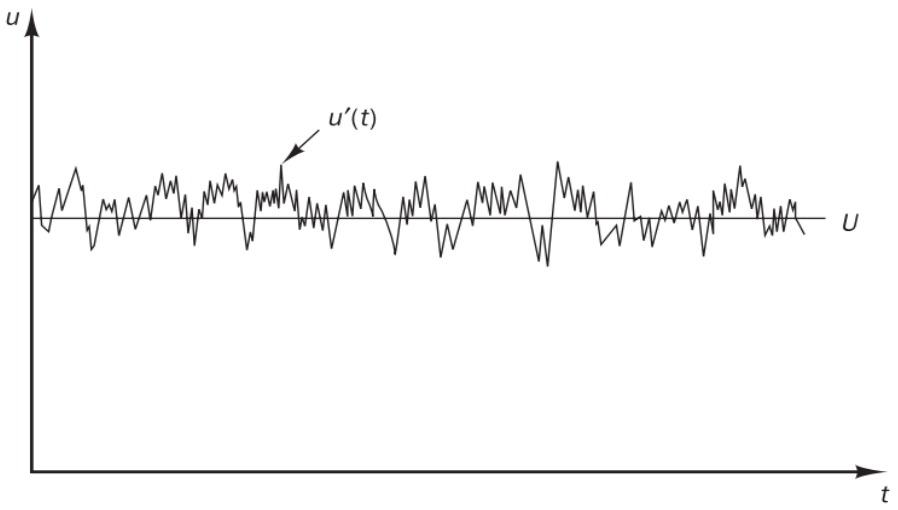

Figure 14: Velocity fluctuations around mean value in turbulent flow [82].

The viscous shear stress deformation work increases internal energy at the expense of kinetic energy, so the flow needs continuous supply of energy, which normally is extracted from the mean flow, to make up for the viscous losses. Typically, the largest eddy extracts energy from the mean flow and the energy transfers from the largest eddy to the smallest eddy which dissipates energy at last because of the viscous effect, this process is known as vortex stretching.

Turbulent flows are modelled by a number of modelling approaches for CFD. These are typically Direct Numerical Simulation (DNS), Large Eddy Simulation (LES), Detached Eddy Simulation (DES) and Reynolds-Averaged Navier Stokes (RANS). DNS requires extremely fine mesh resolve and small time steps to resolve all the scales of motion. Though, it is the most accurate, it requires astronomical computational requirements which limits its use to fundamental flow studies. Large Eddy Simulation (LES) depends on the spatial filtering to limit the scales that are resolved; it is time dependent and three dimensional. In LES the filter size should be chosen first, with all the scales larger than the filter size resolved and all scales less than the filter size will be modelled. The large eddies are much more energetic and also the main transporters of the conserved quantities e. g. mass, momentum and energy. Whereas, the smaller eddies are typically far weaker than the large eddies and therefore have very limited part in mass,

momentum and energy exchange. Moreover, the unresolved eddies effect on the resolved eddies should be described by the sub-grid-scale stresses SGS.

DES is a hybrid of RANS and LES where the turbulence in the boundary layer will be modelled by the RANS, and the large detached eddies outer the turbulent boundary layer will be resolved by the LES. Detached-Eddy Simulation is "a three-dimensional unsteady numerical solution using a single turbulence model, which functions as a sub-grid-scale model in regions where the grid density is fine enough for a large-eddy simulation, and as a Reynolds-averaged model in regions where it is not" [84].

In RANS simulations, the details of the turbulent fluctuations are not resolved as many engineering applications do not require resolving all of turbulent fluctuations, and RANS models have substantially reduced computation requirements. Usually, the turbulence effect on the mean flow would be required [82]. RANS simulations have many turbulence models such as mixing length model, two equation models, k-ε and k-ω, and Reynolds stress equation model. Generally, RANS turbulence models are simpler, economical to run and accurate enough to be used in many industrial applications. Due to these properties of RANS, it is the most common technique used in industrial simulations [82].

3.4. Reynolds-Averaged Navier Stokes Equations

The Reynolds-Averaged Navier Stokes equations (RANS) basically depends on the time averaging for the Navier Stokes equation. The Navier Stokes equations for turbulent and incompressible flow could be stated as [82]:

Continuity

$$\nabla . U = 0 \qquad 3.4.1.$$

Reynolds average momentum equations in x, y, and z directions

$$\rho\frac{\partial(\boldsymbol{U})}{\partial t}+\rho\nabla(\boldsymbol{U})U=-\frac{\partial\bar{P}}{\partial x}+\nabla(\mu\,\nabla\,U\,)+\left[-\rho\frac{\partial(\overline{u'^2})}{\partial x}-\rho\,\frac{\partial(\overline{u'v'})}{\partial y}-\rho\frac{\partial(\overline{u'w'})}{\partial z}\right]+S_{Mx} \quad 3.4.2.$$

$$\rho\frac{\partial(\boldsymbol{V})}{\partial t}+\rho\nabla(\boldsymbol{U})V=-\frac{\partial\bar{P}}{\partial y}+\nabla(\mu\,\nabla\,V\,)+\left[-\rho\frac{\partial(\overline{u'v'})}{\partial x}-\rho\,\frac{\partial(\overline{v'^2})}{\partial y}-\rho\frac{\partial(\overline{v'w'})}{\partial z}\right]+S_{My} \quad 3.4.3.$$

$$\rho\frac{\partial(T)}{\partial t}+\rho\nabla(\boldsymbol{U})W=-\frac{\partial\bar{P}}{\partial z}+\nabla(\mu\,\nabla\,W\,)+\left[-\rho\frac{\partial(\overline{u'w'})}{\partial x}-\rho\frac{\partial(\overline{v'w'})}{\partial y}-\,\rho\frac{\partial(\overline{w'^2})}{\partial z}\right]+S_{Mz} \quad 3.4.4.$$

Where, overbar indicates the time averaged variables. The S_M accounts for the force term which might be buoyancy or gravity.

For non-isothermal problems such as data centres, there is one more scalar transport equation which accounts for energy and can be stated as (in temperature form):

$$\rho\frac{\partial(T)}{\partial t}+\rho\nabla(\boldsymbol{U})T=\nabla(\Gamma_t\,\nabla\,T\,)+\left[-\rho\frac{\partial(\overline{u'T'})}{\partial x}-\rho\frac{\partial(\overline{v'T'})}{\partial y}-\,\rho\frac{\partial(\overline{w'T'})}{\partial z}\right]+S_T \quad 3.4.5.$$

Where, Γ_t is turbulent diffusivity.

The right-hand side of the momentum equations include the turbulence stresses which are known as the Reynolds stresses. The Boussinesq eddy viscosity assumption, which introduced by Boussinesq in 1844, is the bases of all two equations models. The Reynolds stress tensor, τ_{ij}, that appears in the right-hand side of the momentum equations is proportional to the mean rate strain tensor, S_{ij}, and can be related by the following means:

$$\tau_{ij}=-\rho\overline{u'u'} \quad 3.4.6.$$

$$\tau_{ij}=2\mu_t S_{ij}-\frac{2}{3}\rho k\delta_{ij} \quad 3.4.7.$$

$$\tau_{ij}=2\mu_t(\frac{\partial U_i}{\partial x_j}+\,\frac{\partial U_j}{x_i})-\frac{2}{3}\rho k\delta_{ij} \quad 3.4.8.$$

Where μ_t, the turbulent eddy viscosity, is typically calculated by the two transport variables of the turbulence model. The k is the turbulent kinetic energy per unit mass.

3.5. k-ε Turbulence Model

The most common turbulence model used in numerical simulations is the k – ε turbulence model which established for the first time by Launder [85]. This turbulence model was developed as improvement of the mixing length model. Although; this model has a superior performance outside the boundary layer for fully developed flow, it has unsatisfactory performance inside the boundary layer, in case of high stream line curvatures and with high buoyancy forces. There are two transport equations in this model, the turbulent kinetic energy (k) and the turbulent dissipation rate (ε).

The turbulent kinetic energy, (k):

$$\frac{\partial(\rho k)}{\partial t} + \frac{\partial(\rho k u_i)}{\partial x_i} = \frac{\partial}{\partial x_j}\left[\frac{\mu_t}{\sigma_k}\frac{\partial k}{\partial x_j}\right] + 2\mu_t E_{ij}E_{ij} - \rho\varepsilon \qquad 3.5.1.$$

The turbulence dissipation rate, (ε):

$$\frac{\partial(\rho \varepsilon)}{\partial t} + \frac{\partial(\rho \varepsilon u_i)}{\partial x_i} = \frac{\partial}{\partial x_i}\left[\frac{\mu_t}{\sigma_\varepsilon}\frac{\partial \varepsilon}{\partial x_j}\right] + C_{1\varepsilon}\frac{\varepsilon}{k}2\mu_t E_{ij}E_{ij} - C_{2\varepsilon}\rho\frac{\varepsilon^2}{k} \qquad 3.5.2.$$

The transport equations terms are:

k or ε	+	k or ε	=	k or ε	+	k or ε	-	k or ε
rate of change		convection transport		diffusion transport		production rate		destruction rate

Where, u_i is the velocity vector in corresponding direction, E_{ij} is the rate of deformation, when fluid flow moves with presence of velocity gradient it tends to deform and E_{ij} describes this deformation. μ_t is the turbulent viscosity.

The turbulent viscosity could be computed as:

$$\mu_t = \rho C_\mu \frac{k^2}{\varepsilon} \qquad 3.5.3.$$

The values of the empirical constants are:

$C_\mu = 0.09$ $\sigma_k = 1$ $\sigma_\varepsilon = 1.30$ $C_{1\varepsilon} = 1.44$ $C_{2\mu} = 1.92$

3.6. k-ω SST Turbulence Model

The original form of $k-\omega$ model was published by Kolmogorov in 1942. This model is a two-equation model to represent the turbulent properties of the flow, turbulent kinetic energy k, and specific dissipation ω. The first variable is the turbulent energy in the flow and the second variable could be thought as the turbulence scales i. e. time and length scales. Although, this model has superior performance in the boundary layer, it has unsatisfactory performance away from the boundary.

k-ω SST is a more sophisticated model, Shear Stress Transport (SST), was proposed by Mentor [86], to combine $k-\omega$ with $k-\varepsilon$ models to get the best of each model. This model has satisfactory performance in case of flow separation and adverse pressure gradient. The proposed model, SST, is working with the help of blending function F_1, where near the wall $F_1 = 1$ activating Wilcox model which is the most recent and accurate version of the $k-\omega$ model, and $F_1 = 0$ away from the wall activating the $k-\varepsilon$ model [87]. In addition; this model has been widely validated against many applications such as turbomachinery blades, wind turbines, free shear layers, zero pressure gradient and adverse pressure gradient boundary layers with good results [88].

The k-ω SST turbulent kinetic energy:

$$\frac{\partial(\rho k)}{\partial t} + U_j \frac{\partial(\rho u_j k)}{\partial x_j} = \rho P - \beta^* \rho \omega k + \frac{\partial}{\partial x_j}\left[(\mu + \sigma_k \mu_t)\frac{\partial k}{\partial x_j}\right] \qquad 3.6.1.$$

Specific dissipation rate:

$$\frac{\partial(\rho\omega)}{\partial t}+\frac{\partial(\rho u_i\omega)}{\partial x_j}=\frac{\gamma}{\upsilon_t}P-\beta\rho\omega^2+\frac{\partial}{\partial x_j}\left[(\mu+\sigma_{\omega 1}\mu_t)\frac{\partial\omega}{\partial x_j}\right]+2(1-F_1)\frac{\rho\sigma_{\omega 2}}{\omega}\frac{\partial k}{\partial x_j}\frac{\partial\omega}{\partial x_j} \quad 3.6.2.$$

Closure coefficients of the turbulence model:

$$\mu_t=\frac{\rho a_1 k}{\max(a_1\omega,\Omega F_2)}$$

$$F_1=tansh[[\min[\max\left(\frac{\sqrt{k}}{\beta^*\omega y},\frac{500\upsilon}{y^2\omega}\right),\frac{4\sigma_{\omega 2}k}{CD_{k\omega}y^2}]]^4]$$

$$P=\tau_{ij}\frac{\partial u_i}{\partial x_j}$$

$$CD_{k\omega}=\max(2\rho\sigma_{\omega 2}\frac{1}{\omega}\frac{\partial k}{\partial x_j}\frac{\partial\omega}{\partial x_j},10^{-20})$$

$$F_1=tansh[\max(2\frac{\sqrt{k}}{\beta^*\omega d},\frac{500\upsilon}{d^2\omega})]$$

The turbulence model constants:

$\sigma_k=0.85$ $\sigma_{\omega 1}=0.65$

$\beta=0.85$ $\sigma_{\omega 2}=0.856$

$\beta^*=0.09$ $a_1=0.31$

3.7. Scale Adaptive Simulation (SAS)

Scale Adaptive Simulation (SAS), is a DES version of the k-ω SST model, was developed by Menter, et al. [89]. The basic principle of k-ω SST SAS is by adding an additional production term, the SAS term, to the ω equation to be sensitive to resolve the unsteady flow fluctuations [90]. While, the flow in the boundary layer is solved based on the k-ω SST turbulence model. The velocity gradients length scale is much smaller than the averaged-velocity gradients length scale when the flow equations resolve turbulence. Therefore, the von Karman length scale, $L_{vk,3D}$, which is calculated based on the ratio of the first to the second velocity gradients, is appropriate quantity to be used to detect flow unsteadiness based on the second velocity gradients which has length scale much smaller than that based on the time averaged-averaged gradients.

The SAS term allows resolving turbulence spectrum in the regions where the flow in the limit to go unsteady. The result of that is to reduce the damping effect of the turbulent viscosity on the resolved fluctuations by reducing turbulent kinetic energy k, and turbulent dynamic viscosity μ_t, this process will prompt the momentum equations to switch from steady to unsteady mode [87]. Moreover, the advantage of the SAS is that it allows to resolve the turbulent spectrum down to the mesh limit without explicit time step or mesh dependency. Also, it solves the flow inside the boundary layer as SST RANS model and the unsteady flow away from the boundary layer as LES like solution. This behaviour what makes SAS like LES solution [91].

The additional term, $Q_{SST-SAS}$, that added to ω equation is based on transformation of $k-\sqrt{k}L$ [86, 92].

$$Q_{SST-SAS} = \rho F_{SAS}.\max[\tilde{\zeta}_2 k S^2 \frac{L}{L_v k} - \frac{2k}{\sigma\Phi}.\max\left(\frac{|\nabla\omega|^2}{\omega^2}, \frac{|\nabla k|^2}{k^2}\right), 0] \qquad 3.7.1.$$

The derivation and constants of the $k-\sqrt{k}L$ model can be found in [92].

3.8. OpenFOAM

In 2007 the OpenCFD Ltd released OpenFOAM as open source under the GNU General Public License [93]. OpenFOAM is a C++ library which consists of executables applications and utilities [94]. The solvers fall into applications category; whereas, the utilities are designed to perform data manipulation such as probing and sampling. OpenFOAM includes pre-processing and post-processing environments as utilities to ensure common environment to all data manipulation.

3.9. Boundary Conditions

The boundary conditions implementation is a vital part to successfully represent the fluid flow behaviour as they are approximation to physical reality. They are also affect the solver behaviour as any incorrect posing of the boundary conditions can lead to simulation failure. In OpenFOAM, there are three main categories of the boundary conditions, basic, constraint and derived boundary conditions. In all boundaries, the velocity vectors, pressure, temperature and the turbulence parameters, k, ε and ω will be imposed. In the next sections, the imposed boundary of the data centre simulations will be described.

3.9.1. Inlets and Outlets Boundary Conditions

The fluid flow in data centres is extremely complicated as there are many inlets and outlets, and also there are complex interactions between different airflow streams. The fluid flow in this thesis is air which enters the data centre through perforated tiles. The flow regime at the entrance should be identified whether it is laminar or turbulent. The Re number at the entrance of the perforated tiles is around 5×10^5 which considered turbulent.

For the inlet boundary conditions, except for the IT server's inlet, the velocity vector and temperature considered to be constant and the turbulence parameters calculated based on the turbulence intensity at each inlet. Whereas, at the outlet of the return vents, the velocity boundary condition is `pressurInletOutletVelocity` which prevents

any reverse flow into the domain by switching itself into `fixedValue` boundary condition in the case of reverse flow. Table 5 shows the boundary conditions imposed in OpenFOAM.

Table 5: Inlets and outlets boundary conditions for velocity U, pressure P and temperature T.

Field	**U**	**P**	**T**
	Mathematical formulation	**Mathematical formulation**	**Mathematical formulation**
	OpenFOAM description	**OpenFOAM description**	**OpenFOAM description**
Perforated Tiles (Inlet)	$U = U_{inlet}$	$\nabla P.\, n = 0$	$T = T_{crac-out}$
	`type fixedValue;` `value uniform (0 0 1.48);`	`type zeroGradient;`	`type fixedValue;` `value uniform 285.15;`
Servers Inlet	$U = U_{inlet}$	$P_p = P_{total} - 0.5\|U\|^2$	$\nabla T.\, n = 0$

	`Type surfaceNormalFixedValue;`
	`refValue uniform 0.72;`
		`type totalPressure;`
		`p0 uniform 0;`
		`U U;`
		`phi phi;`
		`rho none;`
		`psi none;`
		`gamma 1;`
		`value uniform 0;`
			`type zeroGradient;`

Servers Outlet	$U = U_{out}$	$P_p = P_{total} - 0.5\|U\|^2$	$T = T_{server-out}$

	`Type surfaceNormalFixedValue;`
	`refValue uniform -0.72;`
		`type totalPressure;`
		`p0 uniform 0;`
		`U U;`
		`phi phi;`
		`rho none;`
		`psi none;`
		`gamma 1;`
		`value uniform 0;`
			`Type fixedValue;`
			`Value uniform 300.15;`

CRAC Units Inlet	$\nabla U.n = 0$	$\nabla P.n = 0$	$\nabla T.n = 0$
	`Type pressureInletOutletVelocity;` `value uniform (0 0 0);`	`type zeroGradient;`	`type zeroGradient;`

3.9.2. Perforated Tiles Boundary Condition

In this study, the cold airflow through the vent tiles is assigned as a fixed momentum at the perforated tiles inlet matching the server racks flowrates without resolving the perforated tiles geometry. However, in reality, different air jets enter data centre affect the downstream airflow due to the higher momentum imposed by the pores' air jets as well as air jets interactions. As a general practice Porous Jump Model (PJ), Body Force Model (BF) and Modified Body Force Model (MBF) are used to avoid resolving the pores geometry in case of performing rapid simulations for the perforated tiles [95]. Instead, the effect of pores of the vent tiles on the airflow and velocity distribution across the domain compared to assigning fixed momentum is investigated to study the validity of using constant momentum across the tile.

The computational model is a small room with 800 mm height and 100 mm length and width. The first and second models are aimed to resolve the tile geometry with a perforated tile that has 25% porosity with two geometries 16 and 64 square pores with pore sizes 12.5 mm and 6.25 mm, respectively. The square and circular pores have similar profile for velocity and pressure distribution [96]. Therefore, to get better mesh quality the square pores were chosen. One large pore with 25% of the tile area at the middle of the tile is considered for the third model. The inlet of the fourth model domain is square open area with no pores, but the inlet airflow is specified by assigning constant momentum over the tile. The models' tiles geometry is illustrated in Figure 15 (a-d). The air quantity entering the domain is the same for all models with 3×10^{-3} m^3/sec. The outlet pressure was set as atmospheric pressure whereas at the inlet the airflow was set as volumetric flow rate boundary condition. The mesh was resolved to achieve mesh independent study at grid size ~45,000 cells. As the turbulence model used is an SAS, the resolvedness index

over the domain was calculated with a result over 80% which the threshold value for such simulations. The details of this approach are explained in section 3.12. In addition, it should be noted that the validation of the numerical simulations is explained in section 4.3.

Figure 16 shows the effect of the pore size on the velocity distribution. The figure shows that for the first two models where the pores are resolved there are air jets near the pores. Although, for both models the jets decay after a certain height, the jets for smaller pores decay faster. For the model with a uniform air flow through one large pore 25% of the tile area, the airflow behaves like a large jet imposing much higher z-momentum. Arghode and Joshi [95] studied the effect of the pore size on the airflow rate. They concluded similar conclusion where with higher pore size (less pore number) the airflow rate at the top is much higher and they attributed that with higher pore size larger portion of jets are at the perimeter of the tile which behave as a free jet entraining higher amount of air. Figure 16 (d) shows the air velocity profile for the model with assigning the air flow through the whole tile, 100% of tile area. The behaviour of this model airflow velocity is similar to the models with resolving the pores except the presence of the jets near the pores. Though, the presence of the jets in the first two models causes weak turbulent eddies as the flow is highly turbulent due to the higher Re number at the pores.

From the previous analysis, assigning fixed momentum at the tile behaves similar to resolving the pores. Additionally, in [95] it is stated that with very small pore sizes, higher number of pores, the flow field obtained is similar to airflow obtained from PJ model and the downstream excess momentum is negligible which implicitly suggests that assigning fixed momentum across the tile acts as using PJ model. Therefore, to save considerable amount of the computational time by resolving the pores which needs another level of mesh resolution near them, the airflow at the inlet of the perforated tile will be considered as a fixed momentum without resolving the details of the pores.

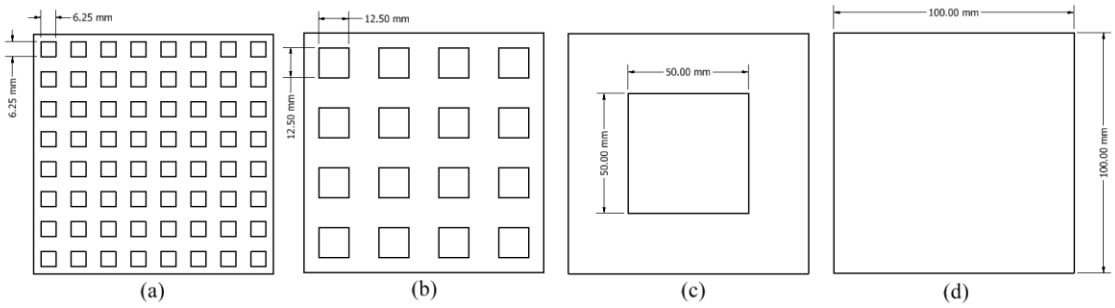

Figure 15: The inlets of the room: (a) perforated tile open area with pore size = 6.25 mm and porosity = 25%. (b) perforated tile open area with pore size = 12.50 mm and porosity = 25%. (c) perforated tile open area with one large pore size = 50 mm and porosity = 25%. (d) uniform inlet tile open area, 100%.

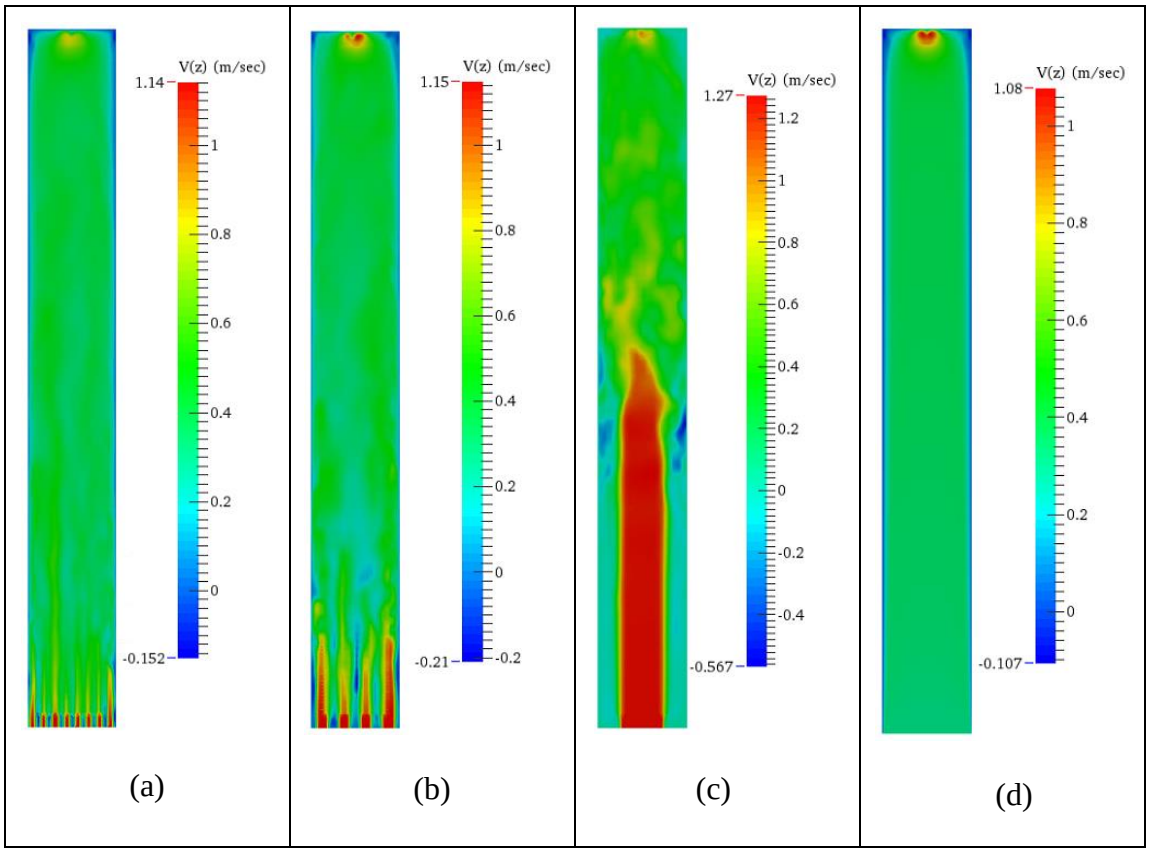

Figure 16: Comparison of velocity contours over across section plane at (x=0.015m) for: (a) perforated tile open area with pore size = 6.25 mm and porosity = 25%. (b) perforated tile open area with pore size = 12.50 mm and porosity = 25%. (c) perforated tile open area with one large pore size = 50 mm and porosity = 25%. (d) uniform inlet tile open area, 100%.

3.9.3. Turbulence Fields Initialisation

The turbulence fields initialisation is based on the formulas shown in Table 6. The estimation of inlet and initial conditions are based on the following:

- Flow speed U.
- Turbulence intensity: $I = 0.16Re^{-\frac{1}{8}}$, where Re is the Reynolds number of the flow at the inlets.
- Characteristic length scale: $L = 0.07d_h$, where d_h is the hydraulic diameter of the inlets.
- $C_\mu = 0.09$, is empirical constant.

Table 6: Turbulence fields initialisation formulas.

Fields	Mathematical formula
Turbulent kinetic energy, k	$k = 0.75((\|U\|I)^2$
Turbulent dissipation rate, ε	$\varepsilon = \frac{C_\mu^{0.75} k^{1.5}}{L}$
Specific turbulent dissipation rate, ω	$\omega = \frac{C_\mu^{-0.25} k^{0.5}}{L}$

Table 7: Inlets and outlets boundary conditions for the kinetic energy k, turbulent dissipation rate ε and specific turbulent dissipation rate ω.

Field	k	ε	ω
	Mathematical formulation	**Mathematical formulation**	**Mathematical formulation**
	OpenFOAM description	**OpenFOAM description**	**OpenFOAM description**
Perforated Tiles (Inlet)	$k = k_{inlet}$	$\varepsilon = \varepsilon_{inlet}$	$\omega = \omega_{inlet}$
	`type fixedValue; value uniform 5.8e-3;`	`type fixedValue; value uniform 7.22e-4;`	`type fixedValue; value uniform 1.98;`
Servers Inlet	$k = k_{inlet}$	$\varepsilon = \varepsilon_{inlet}$	$\omega = \omega_{inlet}$
	`type fixedValue; value uniform 2.22e-3;`	`type fixedValue; value uniform 1.4e-4;`	`type fixedValue; value uniform 1.57;`
Servers Outlet	$k = k_{inlet}$	$\varepsilon = \varepsilon_{inlet}$	$\omega = \omega_{inlet}$
	`type fixedValue; value uniform 2.22e-3;`	`type fixed Value; value uniform 1.4e-4;`	`type fixedValue; value uniform 1.57;`
CRAC Units Inlet	$\nabla k.n = 0$	$\nabla \varepsilon.n = 0$	$\nabla \omega.n = 0$
	`type zeroGradient;`	`type zeroGradient;`	`type zeroGradient;`

3.9.4. Wall Treatment

Wall is the most common boundary conditions used in the numerical simulations [82]. The no slip boundary condition is normally imposed at the stationary walls for the velocity vectors. Because of the chaotic flow nature and high gradients near the wall, it is not straight forward to treat the turbulence at this region. The regions of the boundary layer can be divided into four main regions; at the wall where the velocity is zero, the viscous sublayer where the viscous effect dominates, $y^+ < 5$, buffer region where both turbulent shear and viscous effects dominate $5 < y^+ < 11$ and the log-law region where the turbulence dominates $11.06 < y^+ < 300$ [83]. Therefore, there are two special

approaches can be applied near the wall. The first one is to solve the turbulence up to the wall; however, this approach needs the mesh to be very fine near the wall. The second one does not require solving the flow near the wall, instead it uses the wall function approach to start solving the turbulent flow at some distance from the wall where the y^+ should be > 11.06 [97].

The wall boundary condition implantation starts with the assessment of [82]:

$$y^+ = \frac{\Delta y_p u_*}{\nu} \quad 3.9.1.$$

$$u_* = \sqrt{\frac{\tau_w}{\rho}} \quad 3.9.2.$$

$$\tau_w = \mu(\frac{\partial u}{\partial y})_{y=0} \quad 3.9.3.$$

Where Δy_p is the distance between the wall and first node P, ν is the kinematic viscosity, u_* is the frictionless velocity, τ_w is the wall shear stress, ρ is the fluid density, μ the dynamic viscosity. Table 8 shows the boundary conditions imposed at the walls.

Table 8: Wall boundary conditions.

Field	Mathematical formulation	OpenFOAM description
U	$U = 0$	`type fixedValue;` `value uniform (0 0 0);`
T	$\nabla T.\, n = 0$	`type zeroGradient;`
P	$\nabla P.\, n = 0$	`type zeroGradient;`
k		`type kqRWallFunction;` `value uniform 2e-3;`
ε		`type epsilonWallFunction;` `value uniform 1e-4;`
ω	$\nabla \omega.\, n = 0$	`type zeroGradient;`

3.10. Numerical Solvers

The physics of data centre contains high temperature differences and hence the solver that used must solve the temperature transport equation and at the same time account for the buoyancy forces. Therefore, in this thesis, `buoyantBoussinesqPimpleFoam` will be used to generate the results. However, the standard form of this solver is developed for the RANS turbulence models whereas in this thesis the SAS turbulence model will be used which is a part of the LES turbulence models. Hence, this solver will be compiled to be able to call the SAS turbulence model. The compilation process should be applied carefully to modify a specific part of the solver code with considering the solver file structure. This process can be conducted because the OpenFOAM is an open source tool and hence the access to the source codes and modify them are possible. The compilation process is explained in Appendix A.

3.11. The Basic Configurations of Air Distribution Systems

In this study, the most commonly used air distribution systems in the current data centre buildings will be modelled. The basic configuration of the first layout is the Raised Floor with Flooded Room Return-A (RF/RR-A), where the CRAC (Computer Room Air Conditioning) units and the room return vents are perpendicular to the IT server racks as illustrated in Figure 17. The basic configuration of the second air distribution system is Raised Floor with Flooded Room Return-B (RF/RR-B), where the CRAC units are parallel to the racks with room return vents as shown in Figure 18. The last configuration, illustrated in Figure 19, is Raised Floor supply with Overhead Return (RF/OR); it has a ceiling return infrastructure.

All the modelled data centres have almost identical foot print. The RF/RR-A room has a layout with 3 m (height) x 11.3 m (length) x 7.5 m (width) with four room return vents at the inlet of the CRAC units. The RF/RR-B room has a layout with 3 m (height) x 9.2 m (length) x 9.6 m (width) with four room return vents at the inlet of the CRAC units. Whereas, the room dimensions of the RF/OR are 3 m (height) x 9.2 m (length) x 9.6 m (width) with three room return vents at the ceiling above the hot aisles. Additionally, there

are 12 perforated tiles for each row of the racks distributed across the cold aisles with 0.5 m (length) and 0.432 m (width) for all configurations. Each one of the data centres consists of four rows of racks; each row has 12 racks. Each of these racks have 13 servers uniformly distributed (location-wise) within each rack. The details of heating the load of each model will be described in the corresponding sections. Each data centre has four rows of racks mounted in the room, organized back to back, thus, creating a cold aisle and hot aisle arrangement. Each server dissipates 0.6 kW and the air mass flow rate is 0.0398 kg/sec (0.0336 m^3/sec) Vent tiles are located on the floor in the cold aisles to supply uniform cold air into the data centre room. There are four CRAC units; each supply 4.12 kg/s (3.36 m^3/sec) of cold air.

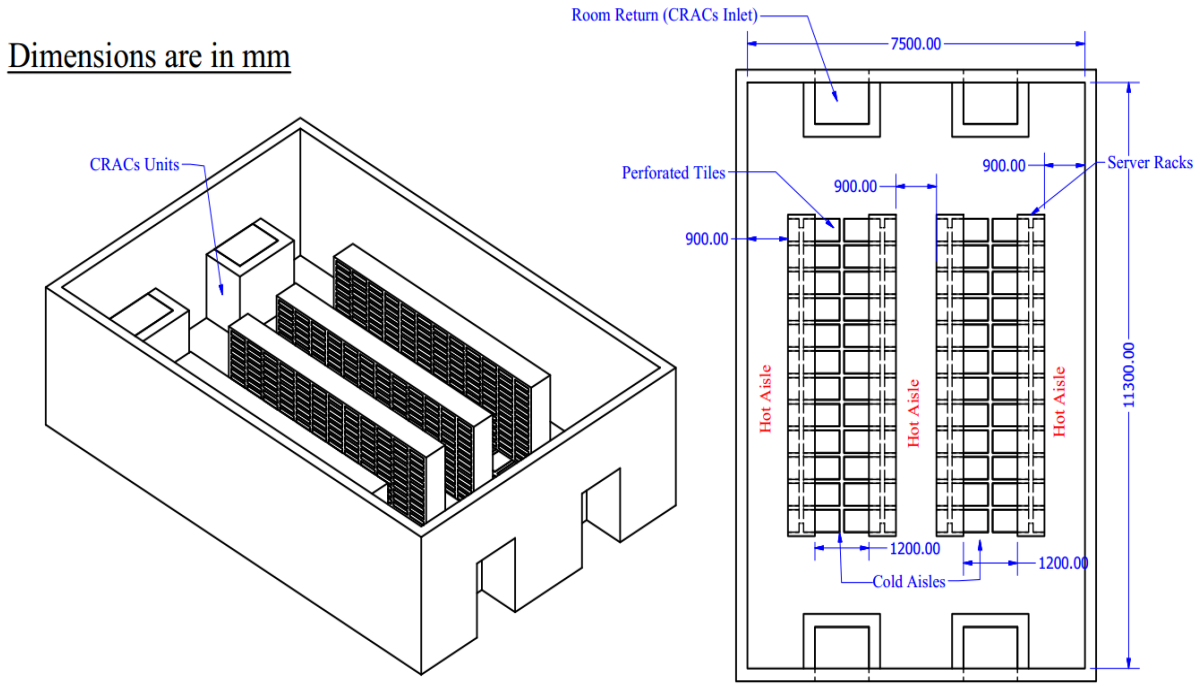

Figure 17: Schematic diagram of the Raised Floor with Flooded Room A (RF/RR-A) data centre.

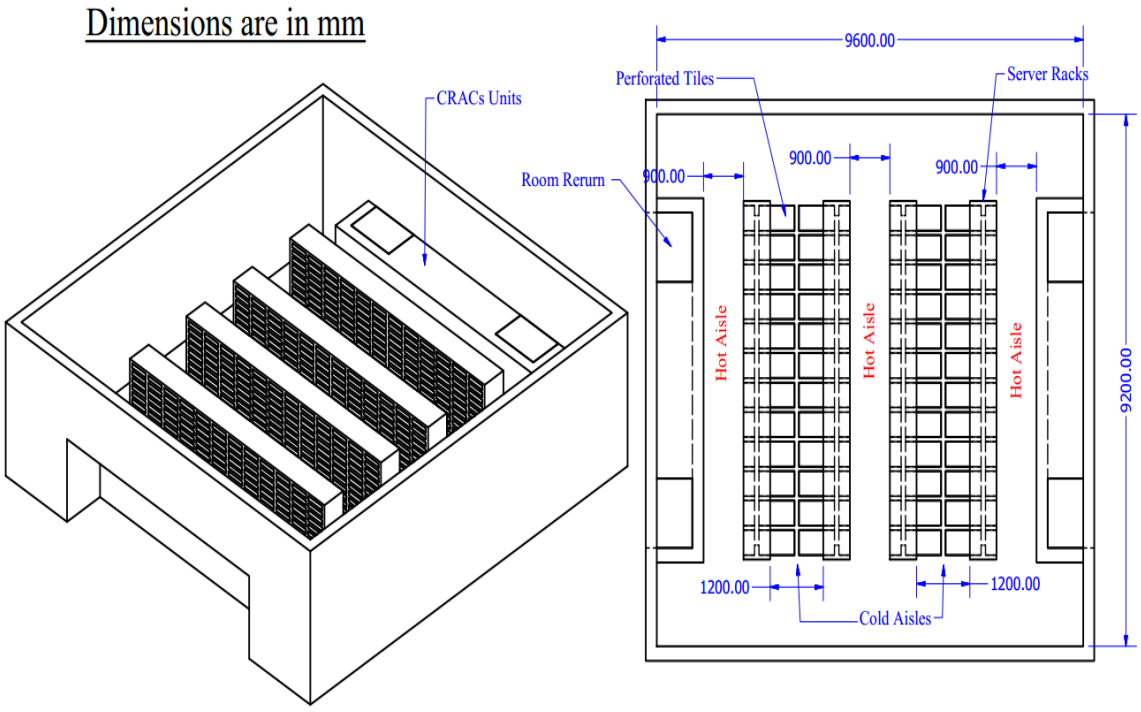

Figure 18: Schematic diagram of the Raised Floor with Flooded Room B (RF/RR-B) data centre.

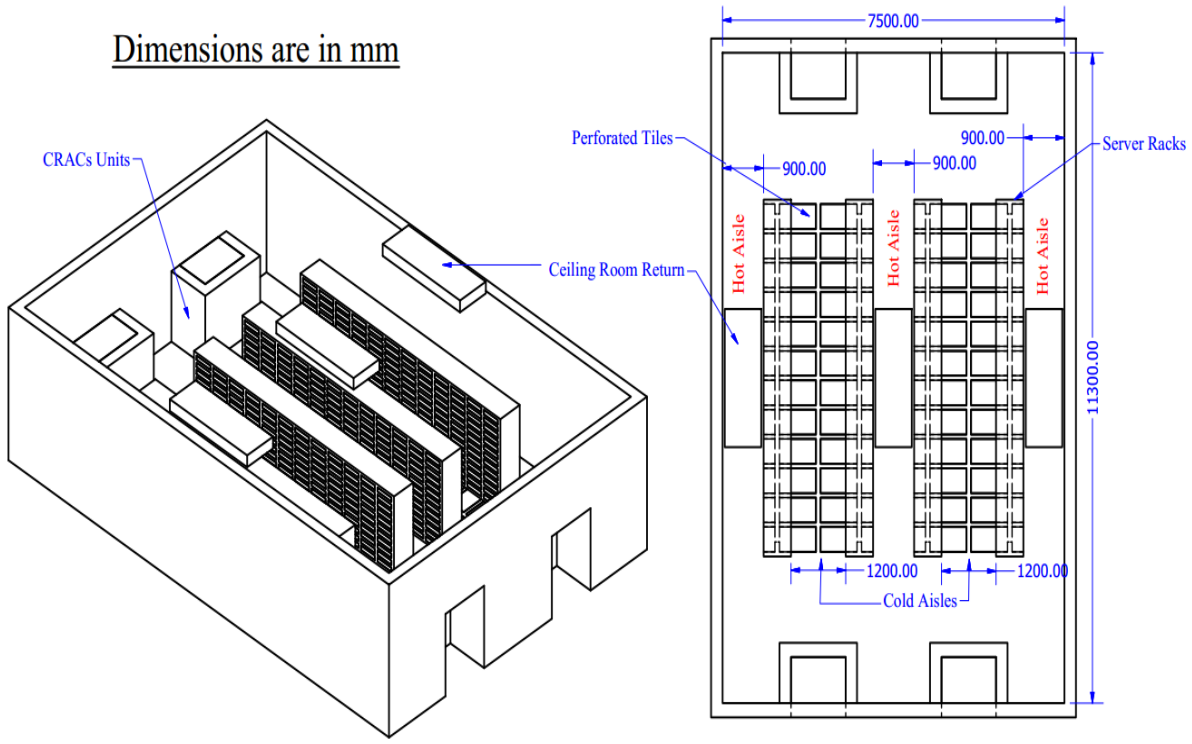

Figure 19: Schematic diagram of the Raised Floor with Overhead Return (RF/OH) data centre.

3.12. Mesh Quality

Meshes for the simulations generated using `SnappyHexMesh` (see details in Appendix B). It is important to save computational time and thus it is good practice to make the mesh as coarse as possible while at the same time assuring the solution is not affected by the mesh resolution. A mesh refinement is used procedure is to make sure the mesh is fine enough to be invariant with finer grid size and to be course enough to save in computational time. In this research both RANS and SAS simulations were conducted. Each approach has different mesh constraints. Therefore, for the RANS meshes a mesh independence study will be used, while for the SAS simulations (considered similar to LES) the mesh quality assessment proposed by Celik, et al. [98] was used. The mesh independence study is conducted on RF/RR-A configuration which is shown in Figure 17.

3.12.1. Mesh Independence Study for RANS Simulations

The accepted method to perform a mesh independence study is to probe a variable at the same location for each mesh resolution. Once the variable becomes invariant with the mesh resolution it indicates that there is no need for further refinement. The temperature values (in Kelvin) for 11 points along a random line at 2.5 m above the raised floor is shown in Table 9. These points were probed to figure out the optimum mesh resolution. It can be seen from the Table 9 that the temperature values remain stable with all mesh grid cells refinements. The small variation between the grid cells is because the solver is transient and the RANS simulation is considered as mildly transient which may result in slight change in the value of the probed variable. Therefore, the medium mesh resolution was selected for the domain since it is enough to have good results for the RANS simulations.

.

Table 9: Temperature (in Kelvin) for 11 points along a random line at 2.5 m above the raised floor for the mesh independence study of RANS simulations.

Points along line at 2.5 m above the raised floor	Coarse mesh (0.87 million cells)	Medium mesh (1 million cells)	Fine mesh (1.25 million cells)
1	299.87	299.49	299.53
2	299.95	299.29	299.46
3	300.00	299.99	299.64
4	300.15	300.12	300.11
5	300.13	300.13	300.13
6	300.11	300.14	300.15
7	300.10	300.14	300.14
8	300.00	300.10	300.11
9	299.96	299.90	299.84
10	299.99	299.87	299.56
11	300.01	299.39	299.61

3.12.2. Resolvedness of the SAS simulations

Like LES, the SAS model strongly depends on the mesh resolution; therefore, the SAS mesh resolution was treated as LES for assessment. Celik, et al. [98] proposed the

resolvedness index to assess meshes for LES simulations. This index depends on the ratio of the resolved turbulent energy (k_{res}) to the total kinetic energy in the flow (k_{tot}) which is the sum of the resolved kinetic energy and the modelled part of the kinetic energy, the sub-grid scale kinetic energy (k_{SGS}). Pope [99] suggested that the resolved kinetic energy over the domain for LES should be at least 80% of the total kinetic energy. The resolvedness index and the resolved kinetic energy can be defined as:

$$LES\_IQ_k = \frac{k_{res}}{k_{tot}} = \frac{k_{res}}{k_{res} + k_{SGS}} \quad 3.12.1.$$

$$k_{res} = \frac{1}{2}(\overline{u'^2} + \overline{v'^2} + \overline{w'^2}) \quad 3.12.2.$$

The computational demand increases with the increasing of the mesh resolution. Therefore, the first run of SAS was with same mesh as RANS mesh resolution, 1 million cells. However, as Figure 20 shows that the resolvedness index over the domain is very poor. The resolvedness over most of the domain is below 50 % which well below the threshold of the index. In the regions where high jets velocities enter the domain it is almost zero. As a result, this mesh resolution will not be enough to capture all the flow features.

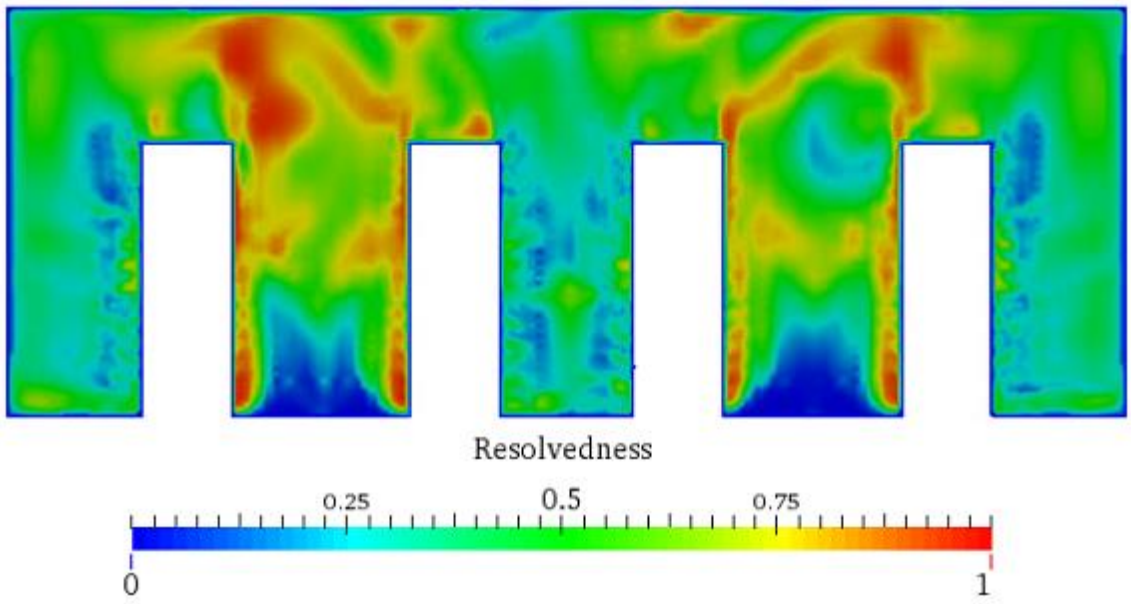

Figure 20: Resolvedness contour over the domain for 1 million cells.

Further refinement has been performed to enhance the resolvedness as shown in Figure 21. This figure shows that for 3.5 million cells that resolvedness has been enhanced dramatically. It can be noticed that the resolvedness over most of the domain is around 100%. Though, in the regions at the entrance of the cold air through the perforated tiles, the resolvdness drops noticeably to around 50%. These regions are small and are located away from the interesting regions such as the IT server intake. Therefore, this mesh resolution was fine enough to get accurate results with the k-ω SST SAS model.

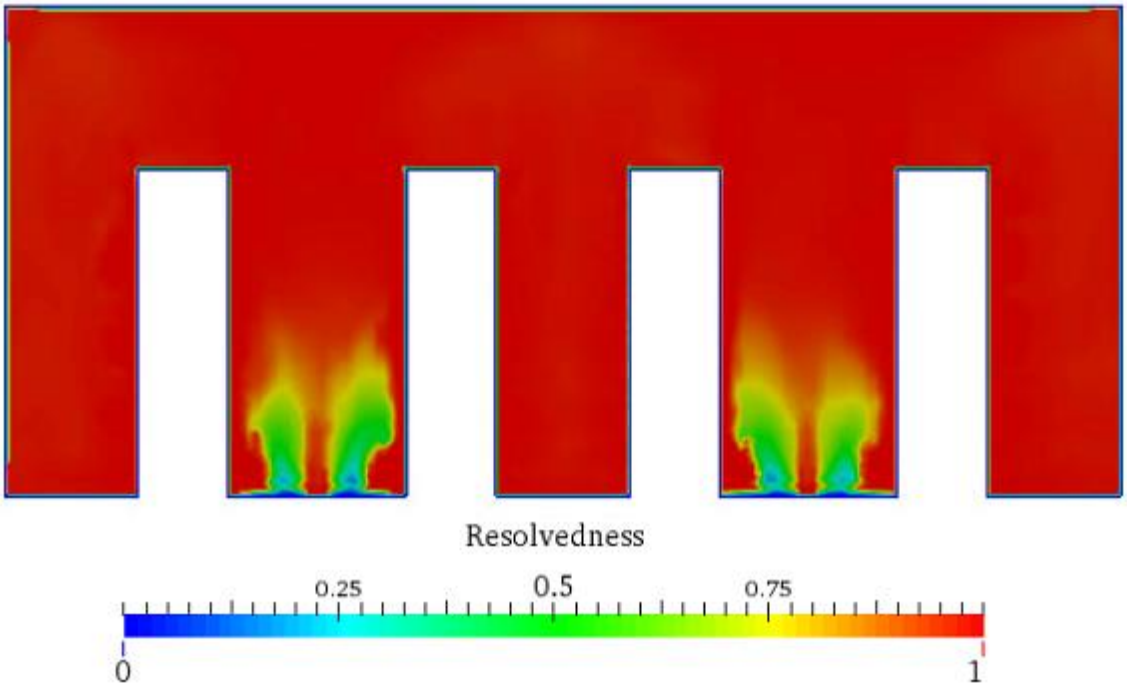

Figure 21: Resolvedness contour over the domain for 3.5 million cells.

3.13. Summary

In this chapter, an introduction to CFD and the mathematical background behind it were introduced along with the turbulence models used in this thesis and their relevant equations. The open source CFD toolbox, OpenFOAM, was introduced with the boundary conditions that imposed to data centre numerical simulations. Based on large body of the literature, there are some studies argued that the RANS simulations may impose significant errors in data centre modelling. Therefore, the implementation of the SAS simulation in the data centre was demonstrated by compiling an existing solver to be used in the subsequent chapters to validate the use of RANS. The basic configurations that will be modelled in this thesis were clarified. The mesh quality is vital in any numerical simulation; therefore, both the RANS and SAS mesh quality was examined to specify the right mesh for each technique.

Chapter 4: Evaluation of the SAS Simulation Modelling for Data Centre Simulations

4.1. Introduction

The main objective of this chapter is to find the limitations of using k-ε RANS model in data centre numerical simulations, as it is widely used in this field as the literature review showed that. The secondary objective of this chapter is to investigate the performance of three different air distribution system especially for the room return infrastructure as no evidence in the literature this issue has been conducted. Each air distribution system will be modelled by two different turbulence models k-ω SST SAS and k-ε RANS models. Various comparisons, including statistical comparisons of the IT servers' intake temperature, will be established between these turbulence models to understand the limitations of using the k-ε RANS in the data centre numerical simulations by comparing the RANS results with the SAS turbulence model. Also, a comparison with some available experiments will be conducted to validate using the proposed turbulence models.

In this study, there are three basic configurations each involves different type of return vents will be considered. The candidate configurations are:

1- Raised Floor with Flooded Room A (RF/RR-A).
2- Raised Floor with Flooded Room B (RF/RR-B).
3- Raised Floor with Overhead Room Return (RF/OH).

4.2. Numerical Simulations Parameters

The details of the data centres geometry being modelled are described in section 3.11. Each data centre has four rows of racks mounted in the room organized back to back creating cold aisle hot aisle arrangement. Each row has 12 racks, each rack has 13 servers Each server dissipating 0.6 kW and mass flow rate 0.0398 kg/sec (0.0336 m^3/sec). Vent tiles are located on the floor in the cold aisles to supply uniformly cold air into the data centre room. There are four CRAC units each supply 4.12 kg/sec (3.36 m^3/sec) of cold air.

The simulations have been conducted by using the open source software tool OpenFOAM. The solver of the k-ε RANS model was the `buoyantBoussinesqPimpleFoam`; whereas, for the k-ω SST SAS model a modified version of this solver was used to perform a SAS solution. The solver compilation process details are explained in Appendix A. The variables used in the numerical simulations are summarised in Table 10.

Table 10: The parameters used in the numerical simulations.

Parameters	**Value**
Return vent locations	Perpendicular, parallel, overhead
No. of racks	48
Heat load per rack	7.8 kW
No. of servers per rack	13
Heat load per server	0.6 kW
Rack load distribution	Uniformly Distributed
Temperature rise across rack	15 °C
Supply vent total volume flow rate	16.88 m^3⁄sec
Supply vent airflow temperature	285.15 K (12 °C)
Turbulence models	k-ε RANS, k-ω SST SAS

4.3. Validation of Numerical Models

4.3.1. Validation of the Turbulence Models Against Vented Enclosure Experiment

In this section, different comparisons will be established to examine the capability of using the proposed turbulence models and the relevant boundary conditions to model the fluid flow and heat transfer inside the data centre room. Tiong [100] carried out experiments on a vented enclosure to study the effect of vents on the temperature inside

the enclosure. The enclosure has a square cross-section with 1.2 m (height) x 0.6 m (length) x 0.6 m (width) and has two upper vents and four bottom vents as shown in Figure 22. The walls of the enclosure have been made of Perspex which has low thermal conductivity to measure the effect of ventilation on the temperature across the enclosure. There is an electrical heater and a fan to force the hot air to enter the enclosure through a grille at the bottom of the enclosure. The enclosure can be considered a good model for simple data centre room where the electrical heater is similar to the servers and the vented room looks like data centre room. The difference is that in a real data centre there are racks that create more complicated air flow interactions throughout the room.

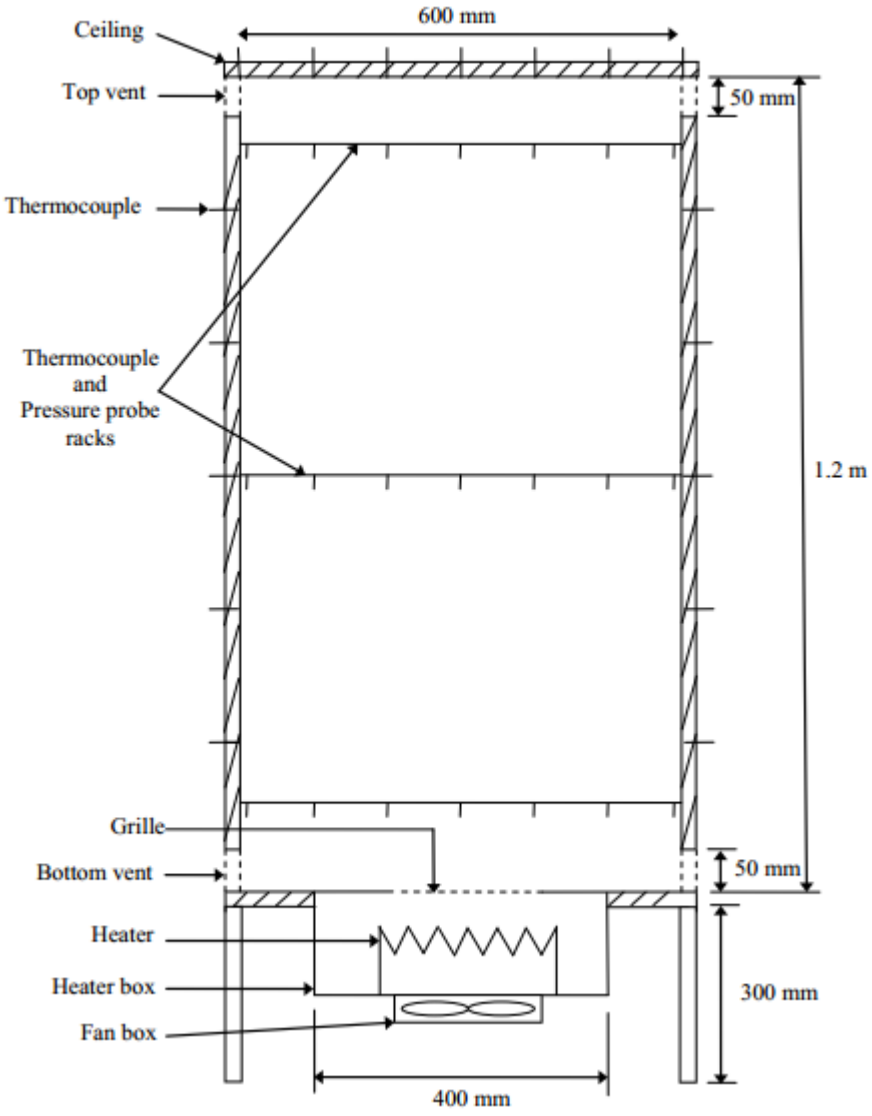

Figure 22: Diagram showing the enclosure for the experimental investigation by Tiong [100].

To investigate the mesh resolution effect on the solution, resolvedness index over the domain for the SAS turbulence model applied to this experimental geometry was performed for 0.61 million cells as illustrated in Figure 23. It was found that for this mesh, the resolvedness index over most of the domain was 100%. The same mesh was used for the k-ε RANS because it needs less mesh density than the SAS turbulence model. In addition, Figure 24 (a-c) shows a comparison for the temperature variations between the turbulence models and the experiment across the top-vented vertical walls facing each

other. The temperature variations were measured at three different planes (heights). The bottom plane is at height of 0.1 m from the base of the enclosure whereas the middle and the top planes are located at heights of 0.6 m and 1.1 m, respectively. Data from 7 locations were measured across each plane. It can be seen the highest temperature for the turbulence models and the experiment is at the middle of the bottom plane because this point is directly above heat source. Whereas, the middle and the top plane temperatures are closer to the average temperature of the air within the enclosure. Figure 24 (d) displays the temperature contour at the middle of the enclosure for the k-ω SST SAS and k-ε RANS models. Both models have similar temperature contours except that the k-ω SST SAS model shows slightly more mixing.

Additionally, the pressure at the middle of the top plane in the experiment was found to be 5.9 Pa, and for the SAS and k-ε models, the pressures were found to be 5.3 Pa and 5.4 Pa, respectively, as illustrated by Table 11. Also, the hot air was found to flow out of the enclosure at a speed of 3.09 m/sec in the experiment, and for the SAS and k-ε RANS, were found to be 3.01 m/sec and 2.98 m/sec, respectively, as shown in Table 12. The small discrepancy between the turbulence models and the experiment might be attributed to the accuracy of the experimental measurements. However, the overall agreement between the turbulence models and the experimental results for the temperature, pressure and velocity variations for the vented enclosure are good indicating that these turbulence models and the relevant boundary conditions can be used to simulate the airflow and temperature variations in real data centre models.

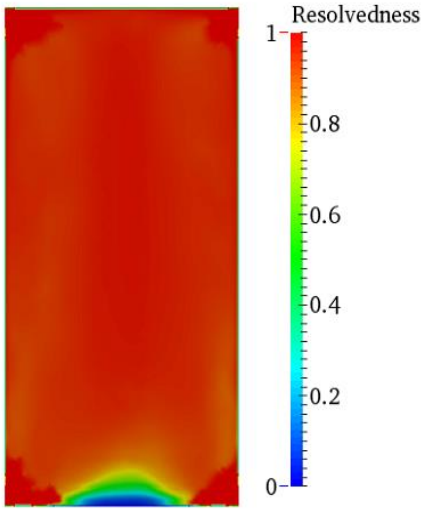

Figure 23: Resolvedness contour over the domain for the vented enclosure for 0.61 million cells.

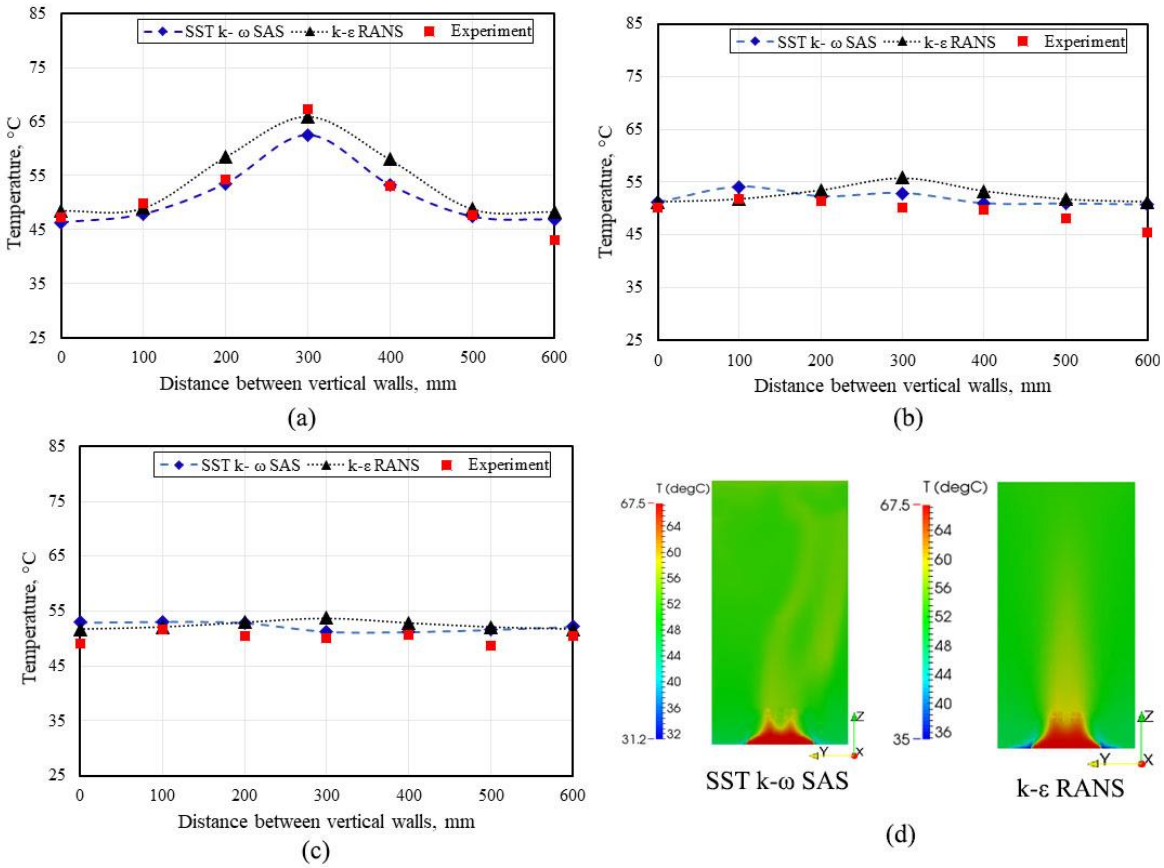

Figure 24: Variation of the of air temperature within the enclosure across the vertical walls that having the top vents. (a) Bottom plane. (b) Middle plane. (c) Top plane. (d) Temperature contours obtained from the present study of the turbulence models for the vented enclosure considered by Tiong [100].

Table 11: Comparison of pressure values for the vented enclosure at the middle of the top plane between the present study and Tiong [100].

	k-ε RANS	k-ω SST SAS	Tiong [100]
P (Pa)	5.4	5.3	5.9

Table 12: Comparison of average velocity of air flowing out of the enclosure through the top vents between the present study and Tiong [100].

	k-ε RANS	k-ω SST SAS	Tiong [100]
V (m/s)	2.98	3.01	3.09

4.3.2. Validation of the Numerical Model Against Square Cavity Results

The buoyancy forces might be important for data centre airflow movement as there are high temperature differences. Therefore, the viability of using the proposed solver to account for buoyancy will be studied by comparing this solver results with the bench mark numerical solution for natural convection of air in a square cavity carried out by De Vahl Davis [101]. The geometry of the square cavity is a 2-dimensional with hot left and cold right vertical walls alongside insulated upper and lower walls with T_h=1 and T_c=0 and $\Delta x = \Delta y$ as shown in Figure 25. Three different cases were studied using different Raleigh (Ra) number for each case, 10^3, 10^4,10^5. These Ra numbers considered as laminar regimes. For the simulations, the same mesh size was generated for all cases with 120×120.

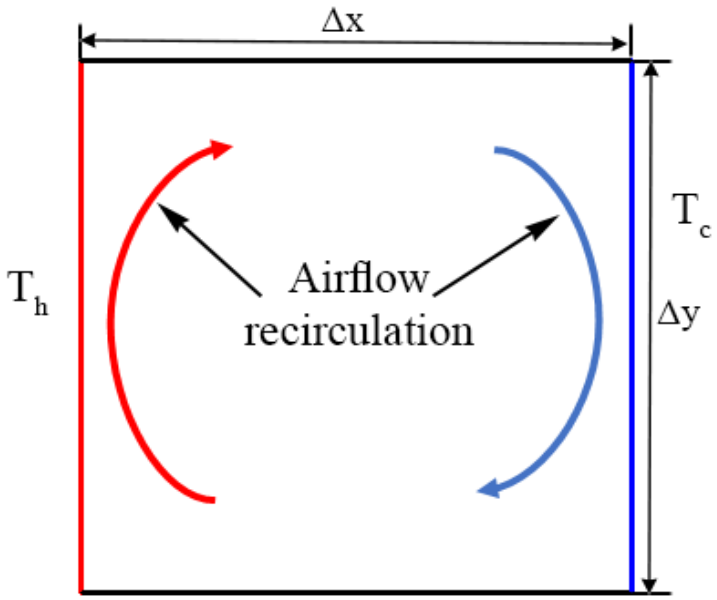

Figure 25: Square cavity geometry adapted from [102].

Table 13 shows the temperature contours and isotherms lines inside the cavity. The results show that with low Ra number there is slight isotherm curvature within the cavity. However, with the increase of the Ra number there is almost zero-line curvature at the top right and bottom left of the cavity because the thin thermal layers. This resulted from the high temperature gradients at these regions because air recirculation. Table 14 shows the streamlines inside the cavity. For the lowest Ra number, the airflow recirculation is almost symmetrical about the centre point of the cavity. For higher Ra numbers, the airflow started to elongate into the corners where at the highest Ra number two separate recirculation zones with zero velocity appear. The results of the present study is almost identical to the results of De Vahl Davis [101] for both the temperature isotherm lines and streamlines which means that this solver is suitable tool to be used with data centre numerical simulations.

Table 13: Comparison of temperature isotherm lines inside the cavity between present study and De Vahl Davis [101].

Ra	Present Study	De Vahl Davis [101]
10^3	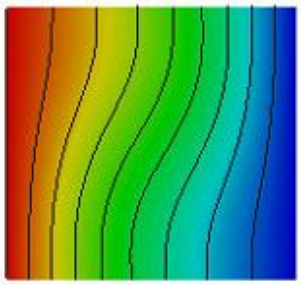	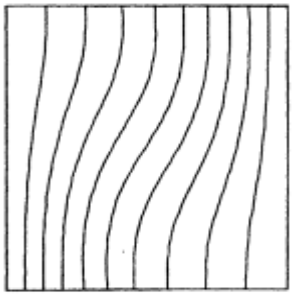
10^4	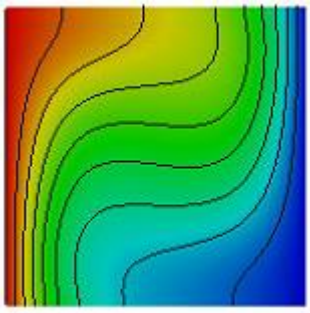	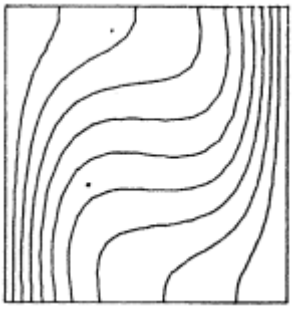
10^5	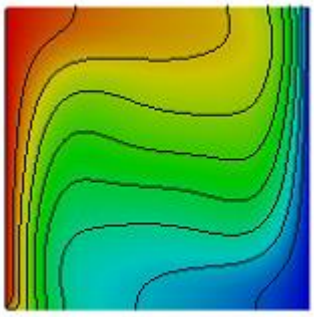	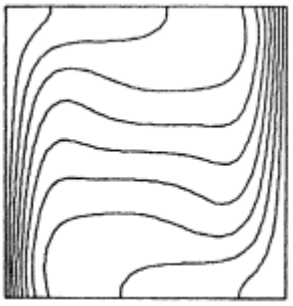

Table 14: Comparison of streamlines inside the cavity between the present study and De Vahl Davis [101].

Ra	Present Study	De Vahl Davis [101]
10^3	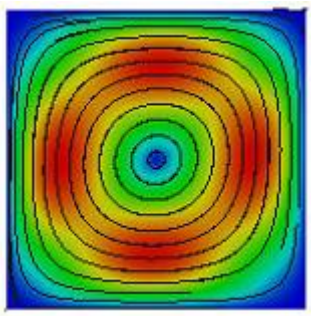	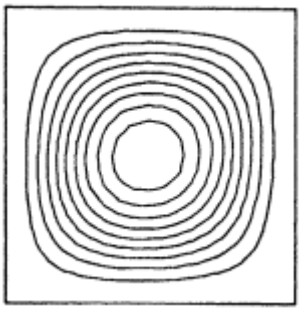
10^4	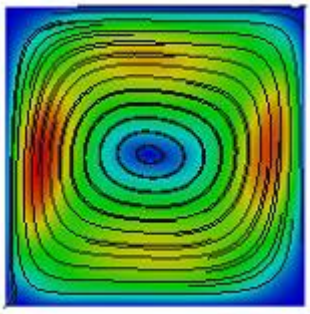	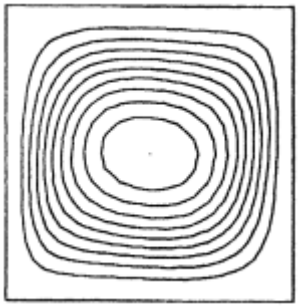
10^5	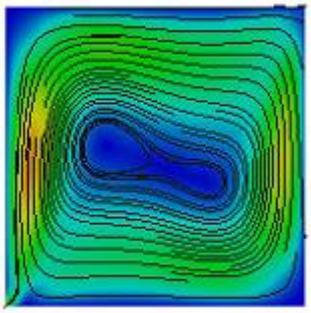	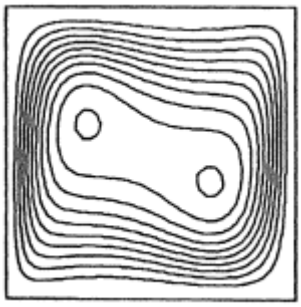

4.4. Comparison of results for Typical data centres

In this thesis, the pressure and temperature quantitative analysis for the SAS simulations are based on the time-averaged results; whereas, the pressure and temperature contours are based on the instantaneous values. In this section, the pressure variations through the cold and hot aisles were explored to know how each turbulence model predicts

the pressure variations within the aisles and to understand the differences between the modelled data centre configurations. The OpenFOAM postprocessing sample utility was used to know how the pressure changes within the cold and hot aisles. Five vertical lines located at the centre point of each aisle from the floor up to the ceiling where 100 points have been sampled over each line in each aisle. The previous experiments [103, 104] were carried out for a RF/OR configuration, thus, the comparison was established for the same configuration.

The pressure variations within the cold and hot aisles for both turbulence models for a RF/OR are shown in Figure 26 (a-b). For the SAS model, the pressure in the middle of the cold aisle, z = 1 m, is comparable to the pressure of the data centre room space, the pressure above the racks, z > 2 m. Whereas, the pressure of the RANS in the middle of the cold aisle is noticeably higher than the pressure above the racks.

Moreover, for the RF/RR-A, as Figure 26 (a) shows, the k-ω SST SAS detected the static pressure drop in front of each server in the hot aisles in the expense of dynamic pressure because of the servers' air jets; whereas, the k-ε RANS partly detected these variations. This can be an indication that the SAS better detects the airflow interactions within the hot aisles. It can be also noted that for the RF/OR, even the SAS model did not show significant pressure fluctuations at the middle of the hot aisle. This can be attributed to the fact that the hot air is directly drawn by the return vent located at the ceiling, which means that the hot air jets do not pass at the centre of the hot aisles. It is also noted that for the RF/OR and RF/RR-A the pressure predicted by the k-ω SST SAS model is higher than the pressure anticipated by the k-ε RANS by amount of 3.5X, this can be attributed to that the SAS may detect the complex airflow interactions inside the aisles where the airflow could have high flow swirling around the racks which may not be detected by the k-ε RANS which in turn affect the pressure distribution inside the data centre room.

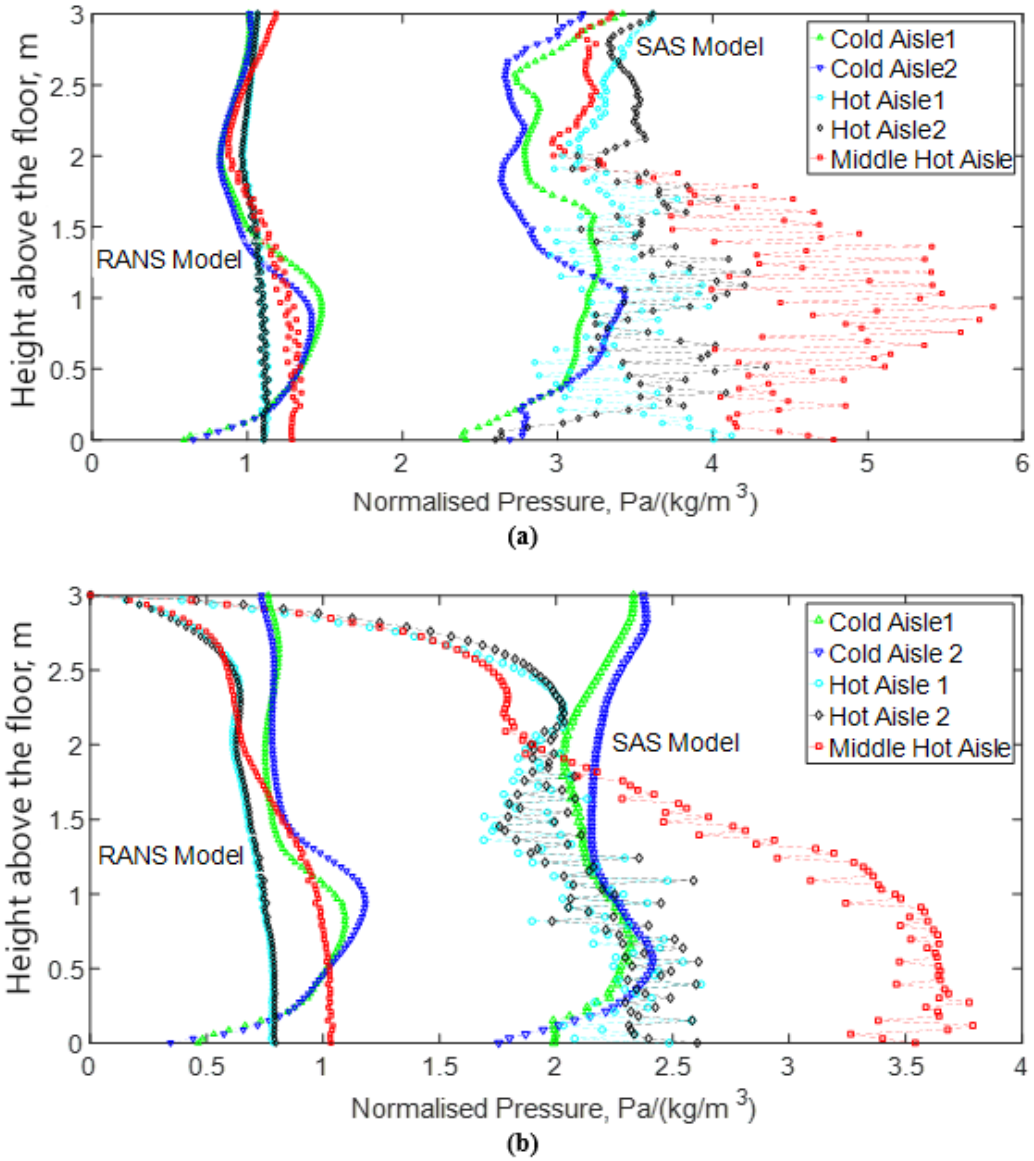

Figure 26: Time-averaged pressure variations within the cold and hot aisles: (a) RF/RR-A. (b) RF/OR.

Two experimental studies were compared with this study. The first one was conducted by Sundaralingam, et al. [103] in the Data Centre Laboratory (DCL) at the Georgia Institute of Technology. The cold aisle pressure measurements were taken at the centre plane of the cold aisle and compared to the pressure above the middle racks. The pressure was measured with simple PVC tube, where the end of the tube was left open in

the cold aisle and the other end of the tube above the racks was connected to the measurement port of the differential pressure sensor. The tube port of the reference pressure was left open. The second experiment which compared the cold aisle pressure to the data centre room space pressure was conducted by Arghode, et al. [104]. In this experiment, the aisle pressure was measured using the differential pressure sensor, Sensitron SPD 100-L025. The sensor measures mass flow rate. The mass flow rate was associated with differential pressure across the flow path.

Both experiments compared the cold aisle pressure to the pressure above the middle racks. Comparison between the experimental results and the turbulence models of cold aisle pressure referenced to the data centre room space pressure for RF/OR is illustrated in Table 15. The measured cold aisles pressure for the experiments differed at small magnitudes from the reference pressure by amount of -0.08 Pa [103, 104]. These results match the results of the k-ω SST SAS model, where the pressure distribution in the middle of the cold aisles is comparable to the data centre room space pressure for this study. However, in the case of the k-ε RANS model, the pressure distribution in the middle of the cold aisle is significantly higher than the data centre room space pressure. The pressure above the racks is higher than the pressure of the middle of the cold aisle for the k-ω SST SAS and the k-ε RANS by amount of 0.004 Pa (0.2%) and 0.4 Pa (33.15%), respectively as illustrated by the Table 15. Additionally, for both turbulence models the pressure in the hot aisle located in the middle of the data centre room is higher than the pressure in the lateral hot aisles where these two aisles almost have identical pressure.

Table 15: Numerical experimental comparison of cold aisle pressure referenced to the data centre room space pressure for RF/OR.

	k-ε RANS	k-ω SST SAS	Experimental Results [103, 104]
ΔP (Pa)	0.4 (33.15% higher)	0.004 (0.2% higher)	-0.08

In addition, Figure 27 (a) shows the RF/OR with one cold aisle, the temperature contour plots of the experiment conducted by Sundaralingam, et al. [103]. The temperature contours for the SAS simulations are based on the instantaneous values. The total cooling load in the experiment is less than the servers heat dissipation; whereas, in the present study the total cooling load is matching the heat dissipation of the server racks. Qualitatively the figure shows that the hot air infiltration is not uniform in the cold aisle from the upper part of the cold aisle, instead, a significant portion of the hot air is infiltrated from both sides of the cold aisles. On the other hand, Figure 27 (b) shows the temperature contours of the k-ω SST SAS where this turbulence model can detect the hot air infiltration at the rack ends. However, the k-ε RANS partly detects both the upper and the hot air infiltration from the end racks as shown in Figure 27 (c).

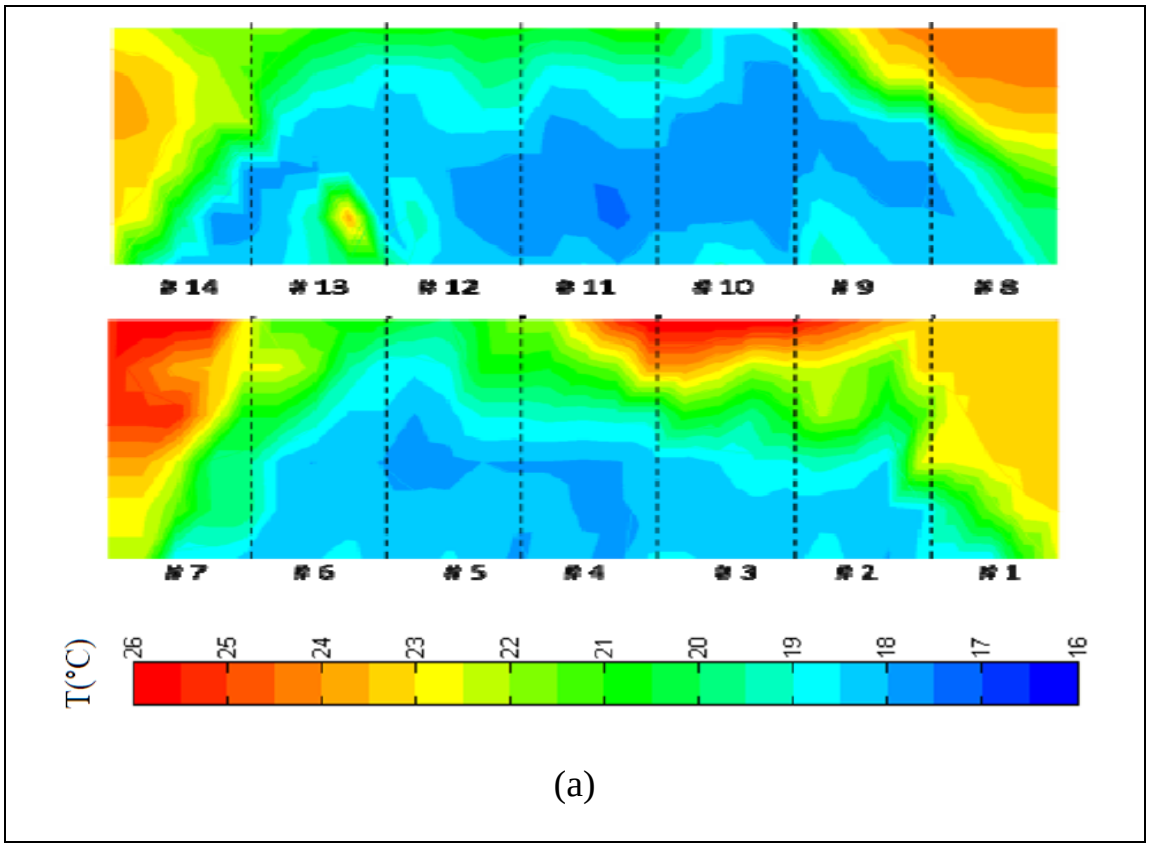

(a)

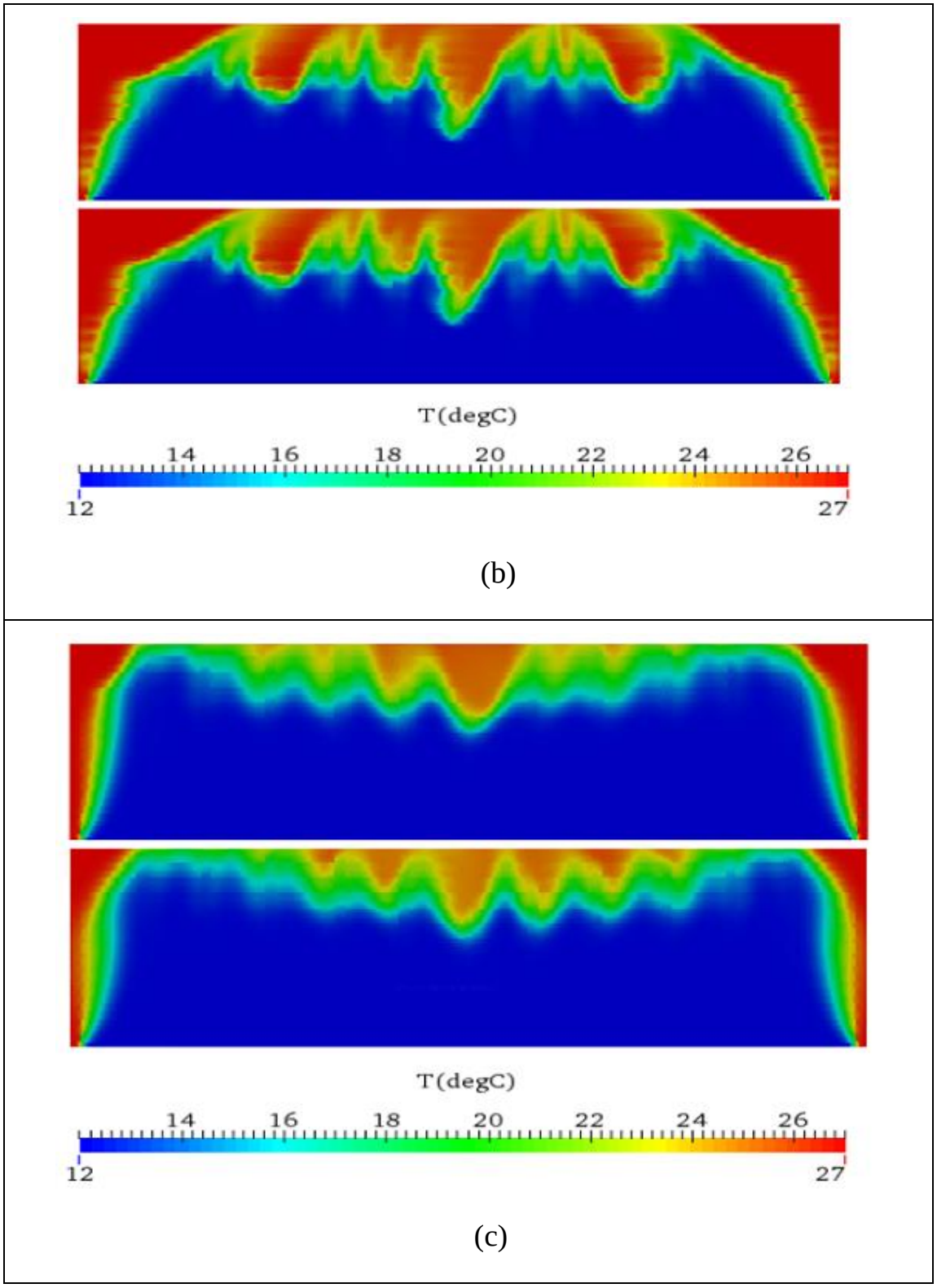

Figure 27: Instantaneous temperature values contours at the intake of the IT server racks for RF/OR, (a) Experimental results of [103]. (b) k-ω SST SAS, (c) k-ε RANS.

Although, the comparison between the turbulence models and the vented enclosure experiment suggested that both turbulence models give almost identical results to the bench mark experiment. They give different results for the data centre simulations. In fact, this can be attributed to that in data centre room there are racks, which can cause flow swirling around their edges, and extremely complicated airflow streams because of equipment airflow. These issues can strongly deteriorate the performance of the turbulence models especially the RANS simulations. Moreover, in the light of the fact that the SAS simulations are much more robust than the RANS simulations in the complicated airflow regimes and also the pressure distribution comparison showed that the SAS simulations detected the right pressure distribution within the data centre room, it can be suggested that the SAS simulations projected the right results for the data centre numerical simulations.

4.5. Rack Inlet Temperature

To evaluate how the k-ε RANS turbulence model predicts the servers' inlet temperature, the temperature contour at the inlet of the same IT server racks was captured and compared with the more robust model k-ω SST SAS. Also, a statistical comparison will be stablished for the average rack inlet temperature between the turbulence models. The root mean square error (RMSE) will be used as a measure of the differences between the average rack inlet temperature of the RANS and SAS models. The RMSE can be defined as:

$$\mathrm{RMSE} = \sqrt{\frac{1}{N}\sum_{i=1}^{N} T_i^2} \qquad 4.5.1.$$

Where N denotes to the number of sampled temperatures per each rack, T_i is the difference (error) between the SAS and RNAS temperature values.

Figure 28 shows the temperature distribution at the inlet of the servers' rack for the k-ω SST SAS turbulence model for the first air distribution system, RF/RR-A. It is clearly shown by the figure that the hot air is not only infiltrated from the top portion of the cold aisle but also from both sides of the racks. This means that the servers at the top and the sides of the cold aisle will be subjected to excessive heat, which may lead to serious damage in these servers. It is also clearly shown in the figure that the hot air infiltration affected the servers located at both sides of the rack from the top to the bottom of the rack. The anticipation of the overheated racks was not straight forward where some servers at the top portion of the rack surprisingly received cold air. In fact, this temperature distribution reflects the effect of the pressure and airflow distribution. Thus, the pressure variations within the cold aisle allows for the hot airflow to infiltrate to the middle or even to the lower part of the cold aisle.

In addition, Figure 29 shows the temperature distribution at the inlet of the same server rack for the k-ε RANS model. The figure displays how the k-ε RANS model predicts the temperature at the inlet of the IT server racks. It shows that the hot air infiltration affects the upper part of the IT server racks, while the middle and lower part of the IT server racks is well maintained in good cooling conditions. Moreover, the RANS model does not show excessive heat at the servers in the sides of the racks. There is a significant difference between the k-ε RANS model and the k-ω SST SAS turbulence model in predicting the hot spots in front of the IT server racks. The number of number problematic servers detected by the SAS simulations is higher than that detected by the RANS simulation. This indicated that the RANS results may give misleading results as it was widely used in the current data centre numerical simulations. Figure 31 shows the difference between the SAS and the RANS rack's average temperature for the racks shown in Figure 30 for RF/RR-A. The agreement in general is good for the middle racks, where the RMSE for these racks is 3.19 ℃ with a standard deviation of 1.59 ℃. However, for the racks located in the sides of the cold aisle, the agreement is very poor with RMSE 6.85 ℃ , which has a 0.62 ℃ standard deviation. The overall agreement is shown in Figure 32 with the help of a frequency histogram. The RMSE between the SAS and RANS for the avergae inlet rack temperature for 75 % of the racks is higher than 2 ℃. However, the mean absolute error is 3.8 ℃ with a 2.01 ℃ standard deviation.

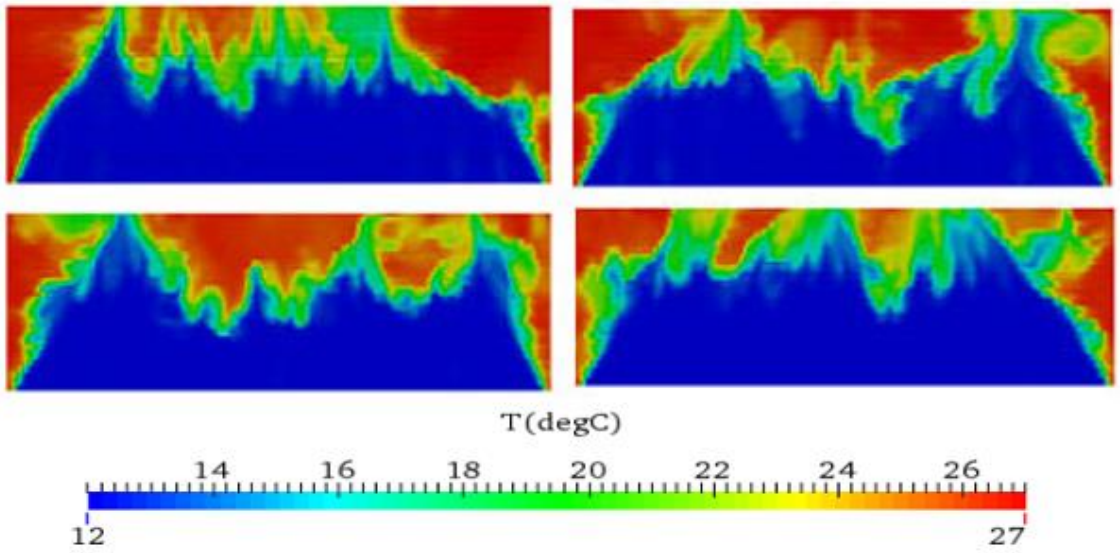

Figure 28: Instantaneous temperature values contours for the k-ω SST SAS turbulence model in front of the IT server racks for RF/RR-A.

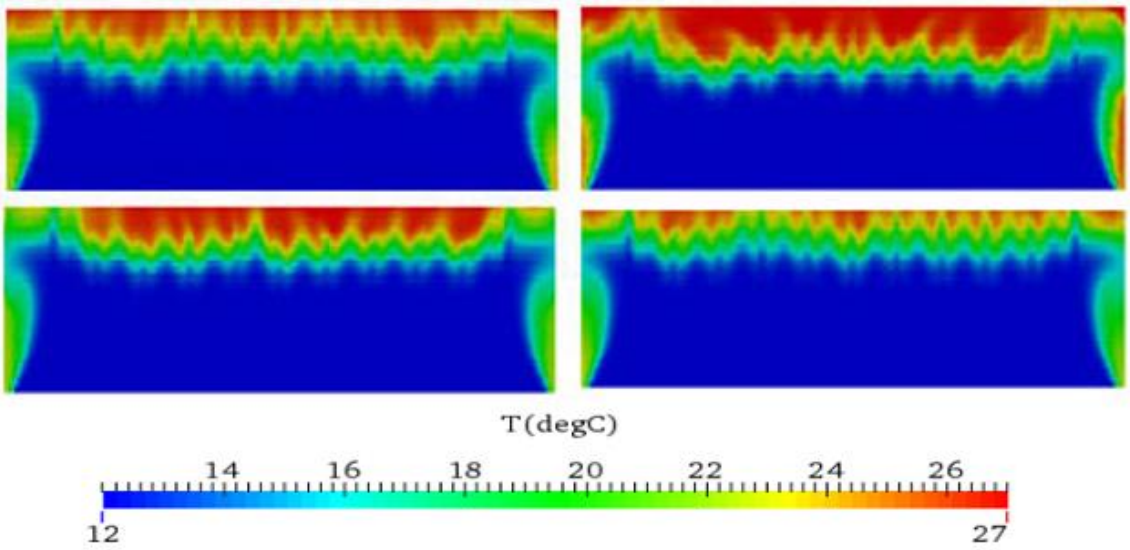

Figure 29: Temperature contours for the k-ε RANS model in front of the IT server racks for RF/RR-A.

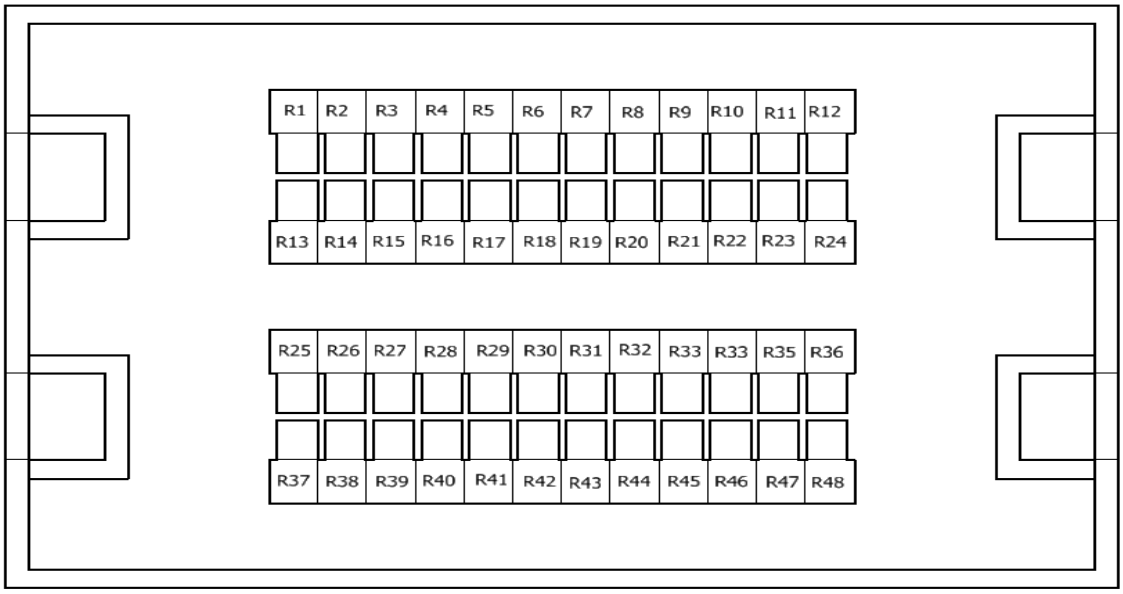

Figure 30: Rack locations along the aisles.

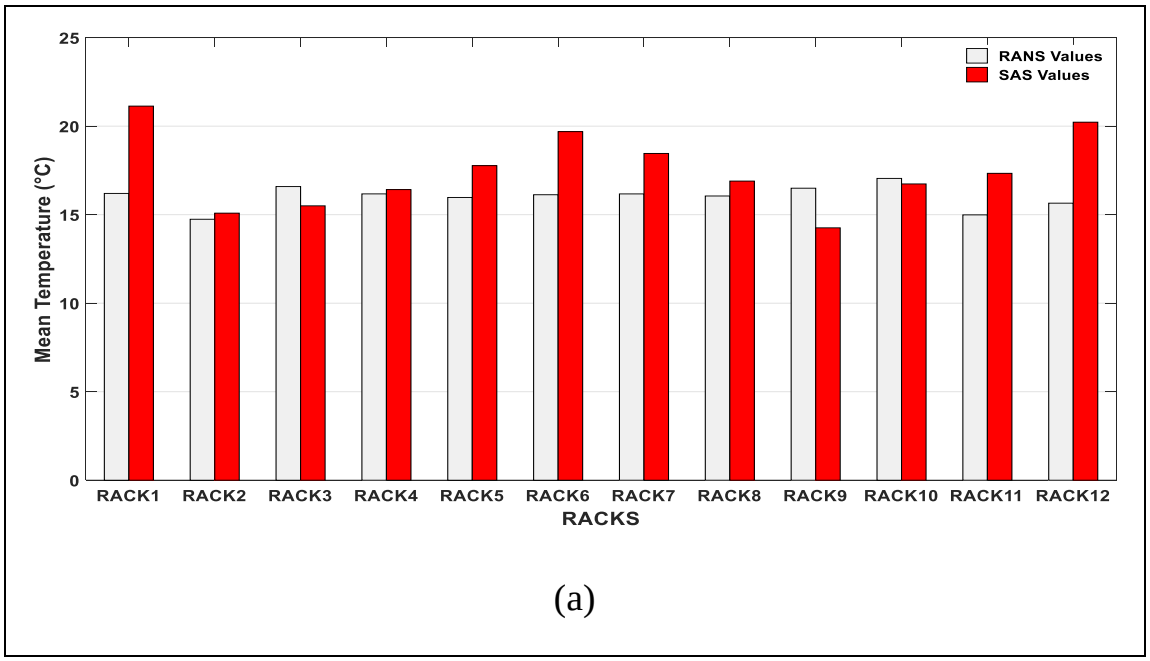

(a)

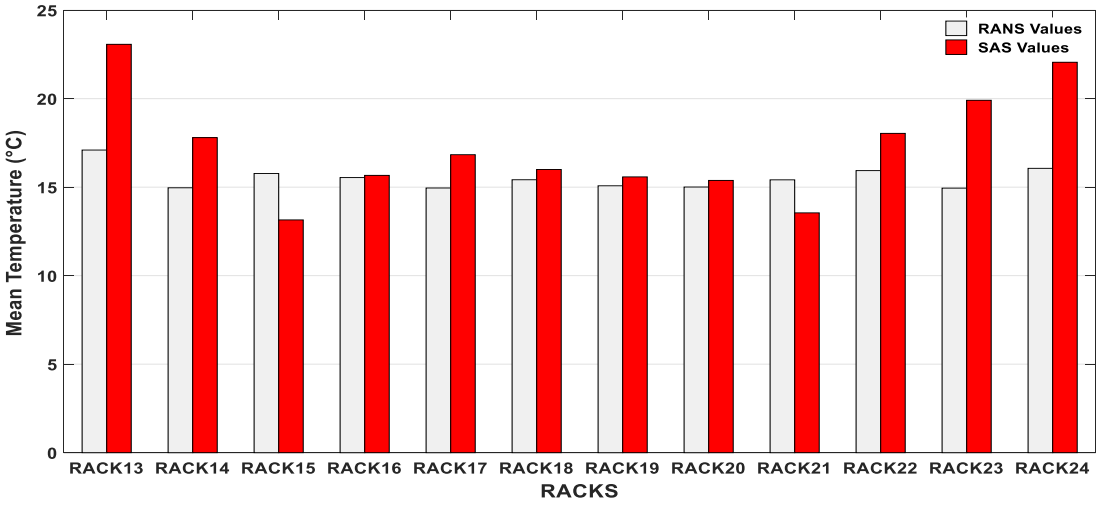
RANS Values
SAS Values
Mean Temperature (°C)
0
5
10
15
20
25
RACK13 RACK14 RACK15 RACK16 RACK17 RACK18 RACK19 RACK20 RACK21 RACK22 RACK23 RACK24
RACKS

(b)

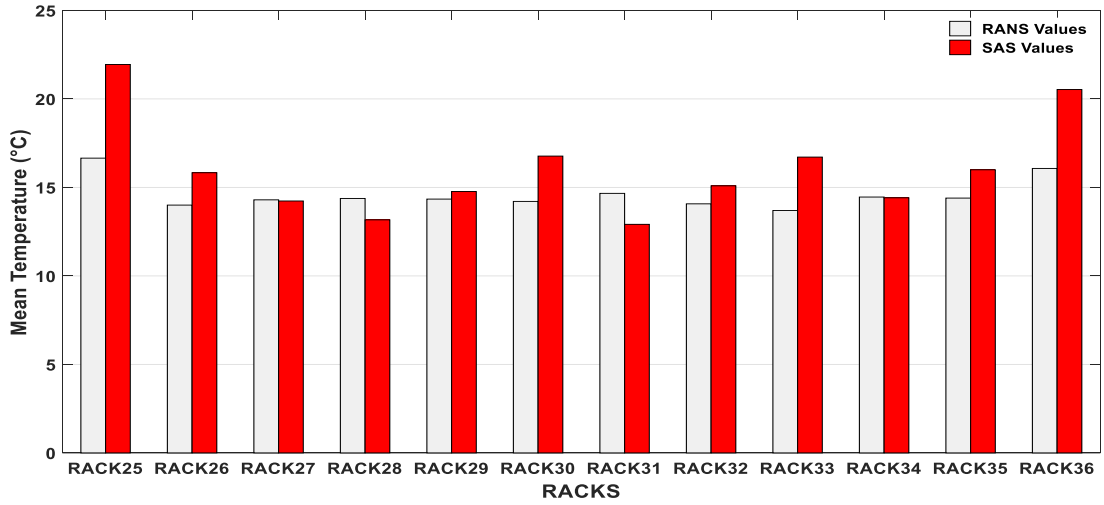
RANS Values
SAS Values
Mean Temperature (°C)
0
5
10
15
20
25
RACK25 RACK26 RACK27 RACK28 RACK29 RACK30 RACK31 RACK32 RACK33 RACK34 RACK35 RACK36
RACKS

(c)

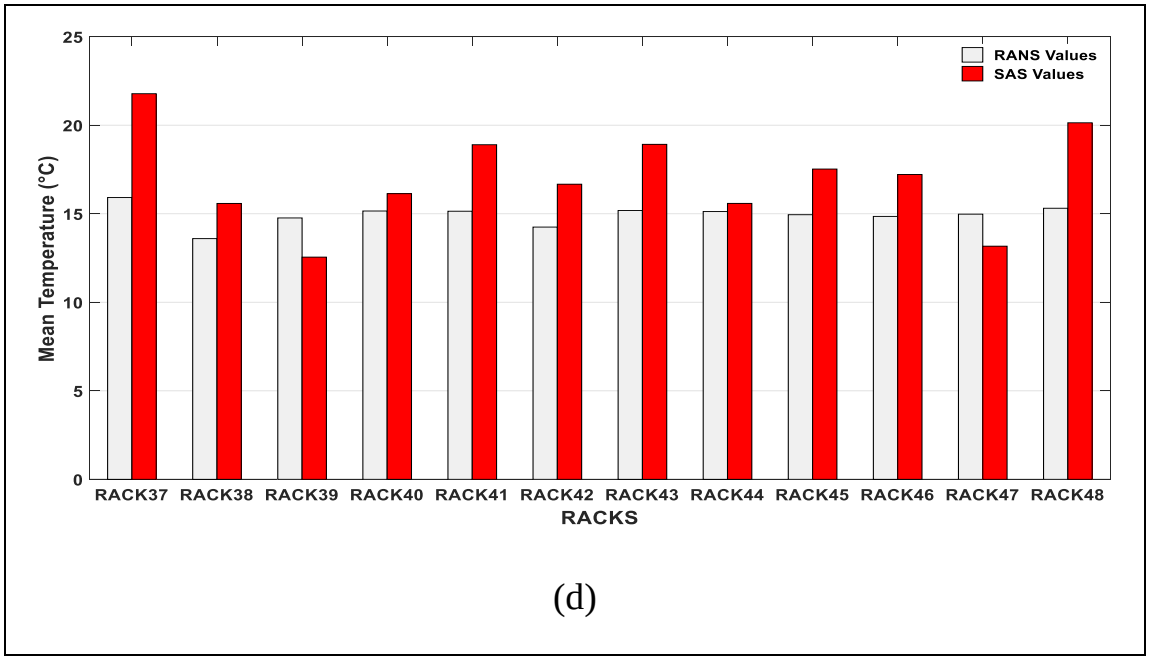

Figure 31: (a)-(d) Comparison of time-averaged inlet rack temperature between SAS and RANS simulations of the RF/RR-A.

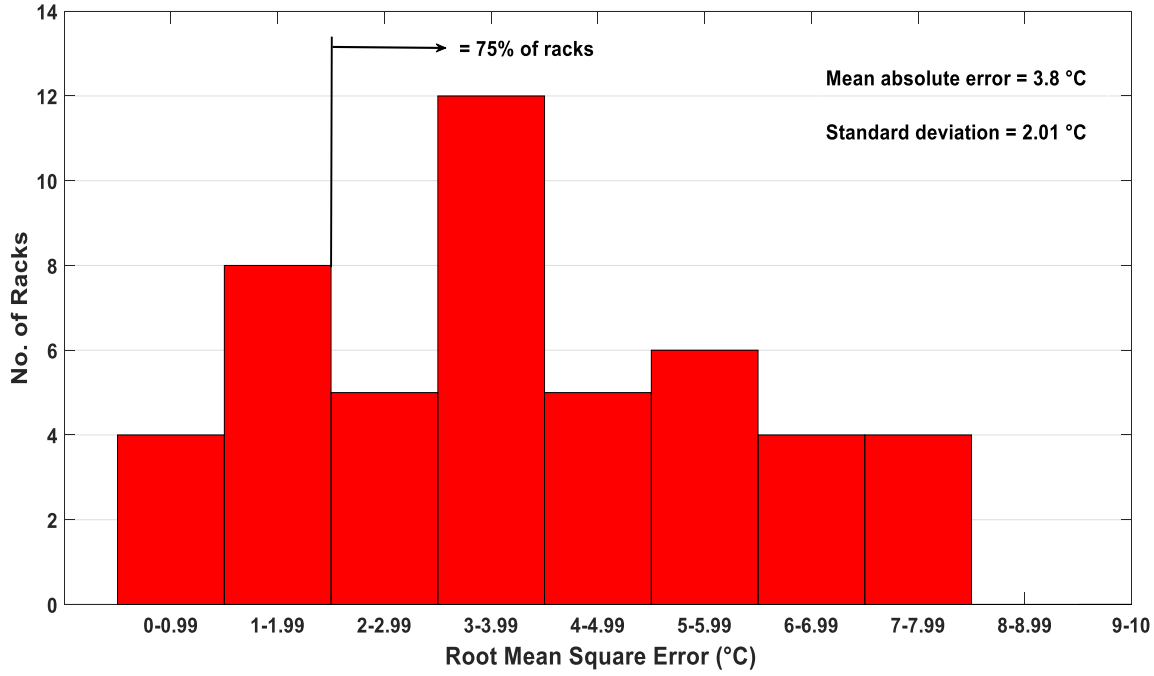

Figure 32: Frequency histogram of RMSE between SAS and RANS simulations of mean inlet rack temperature of RF/RR-A.

The temperature contours of RR/RR-B for SAS and RANS simulations are shown in Figure 33 and Figure 34. The difference between the results of this configuration is noticeably less than the difference between the results of the RF/RR-A configuration. For the RF/RR-B, the k-ε RANS model can detect some of the hot air infiltration from the sides of the racks unlike the RF/RR-A. It is also noted that the hot air infiltration from the top portion of the racks for the SAS simulation is slightly less than that for the RF/RR-A. The hot air infiltration from the upper part of the racks of the k-ε RANS model is less than that for the RF/RR-A. In fact, this might be attributed to the room return location. Figure 34 shows the average inlet temperature comparison between the SAS and the RANS for RF/RR-B. The discrepancy between the turbulence models is apparently due to the racks at the end of the cold aisles. The agreement in general is good for the middle racks, where the RMSE for these racks is 2.58 ℃ with a standard deviation of 1.78 ℃. However, for the end racks, the agreement is very poor where the RMSE is 5.37 ℃ with a standard deviation of 1.41 ℃. This result is slightly better than the result of the RF/RR-A. The overall agreement is shown by the frequency histogram shown in Figure 36. The RMSE between the SAS and the RANS for the avergae inlet rack temperature for 58.33 % of the racks is higher than 2 ℃. However, the mean absolute error is 3.04℃ with 2 ℃ standard deviation.

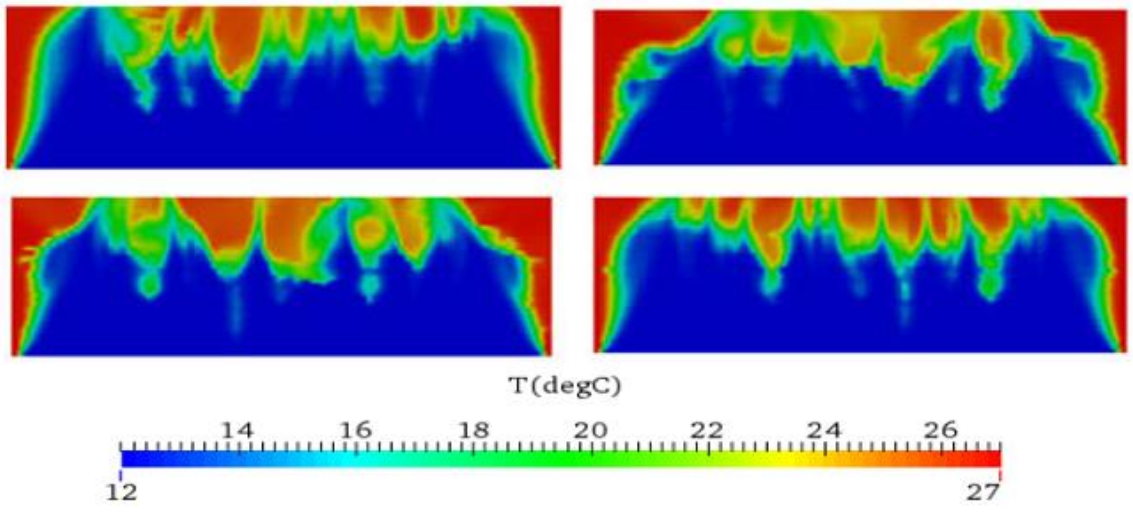

Figure 33: Instantaneous temperature values contours for the k-ω SST SAS turbulence model in front of the IT server racks for RF/RR-B.

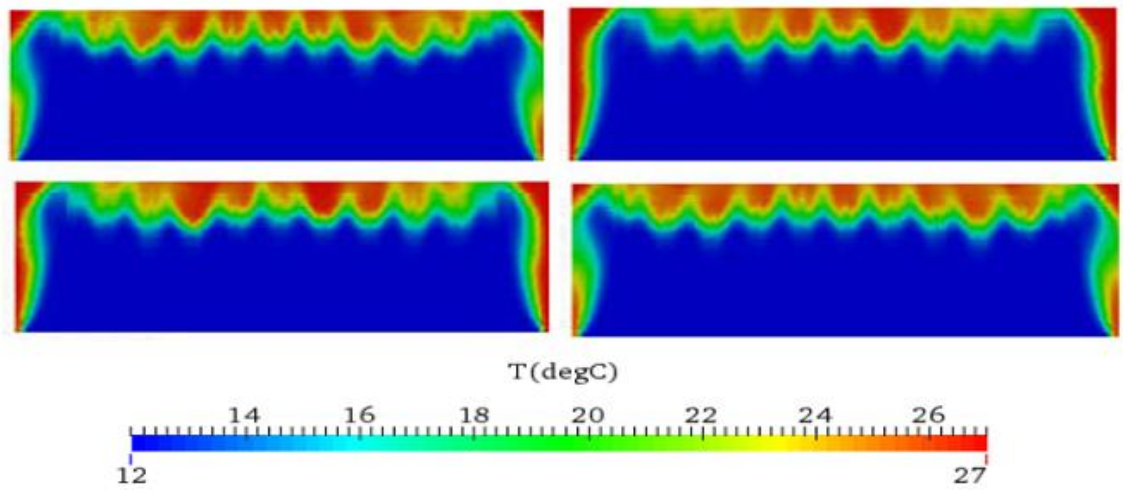

Figure 34: Temperature contour for the k-ε RANS model in front of the IT server racks for RF/RR-B.

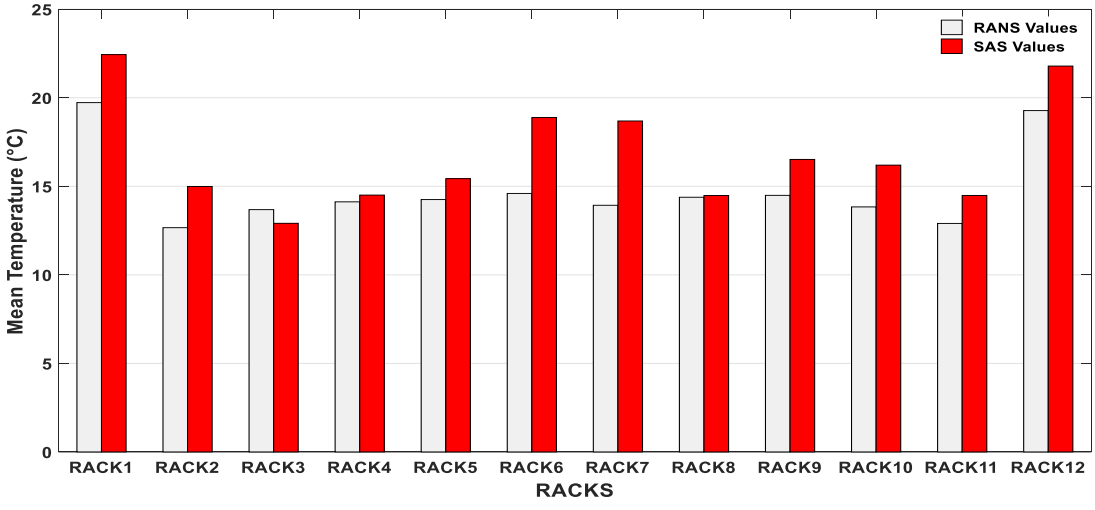

(a)

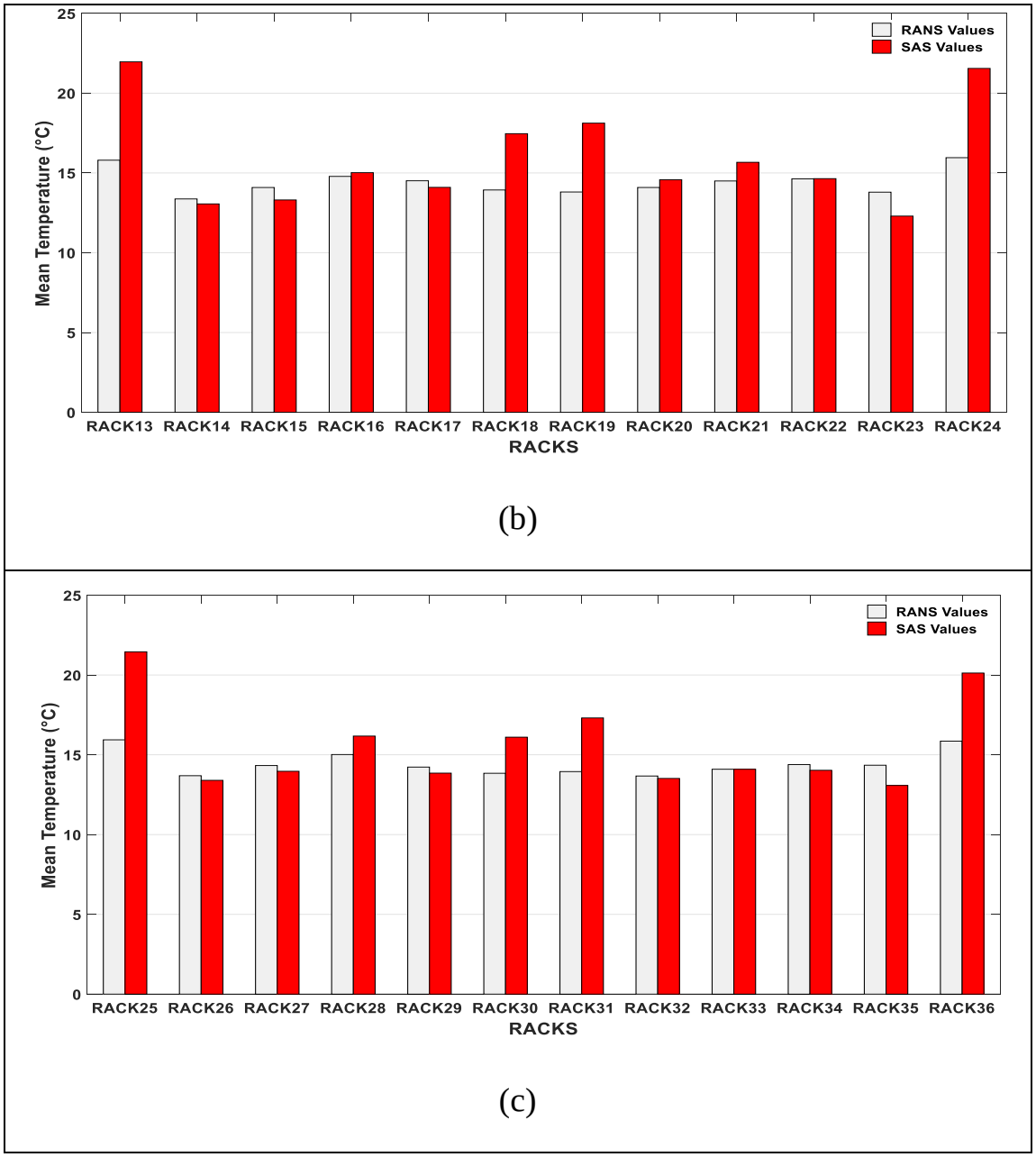
RANS Values
SAS Values
Mean Temperature (°C)
0
5
10
15
20
25
RACK13 RACK14 RACK15 RACK16 RACK17 RACK18 RACK19 RACK20 RACK21 RACK22 RACK23 RACK24
RACKS

(b)

RANS Values
SAS Values
Mean Temperature (°C)
0
5
10
15
20
25
RACK25 RACK26 RACK27 RACK28 RACK29 RACK30 RACK31 RACK32 RACK33 RACK34 RACK35 RACK36
RACKS

(c)

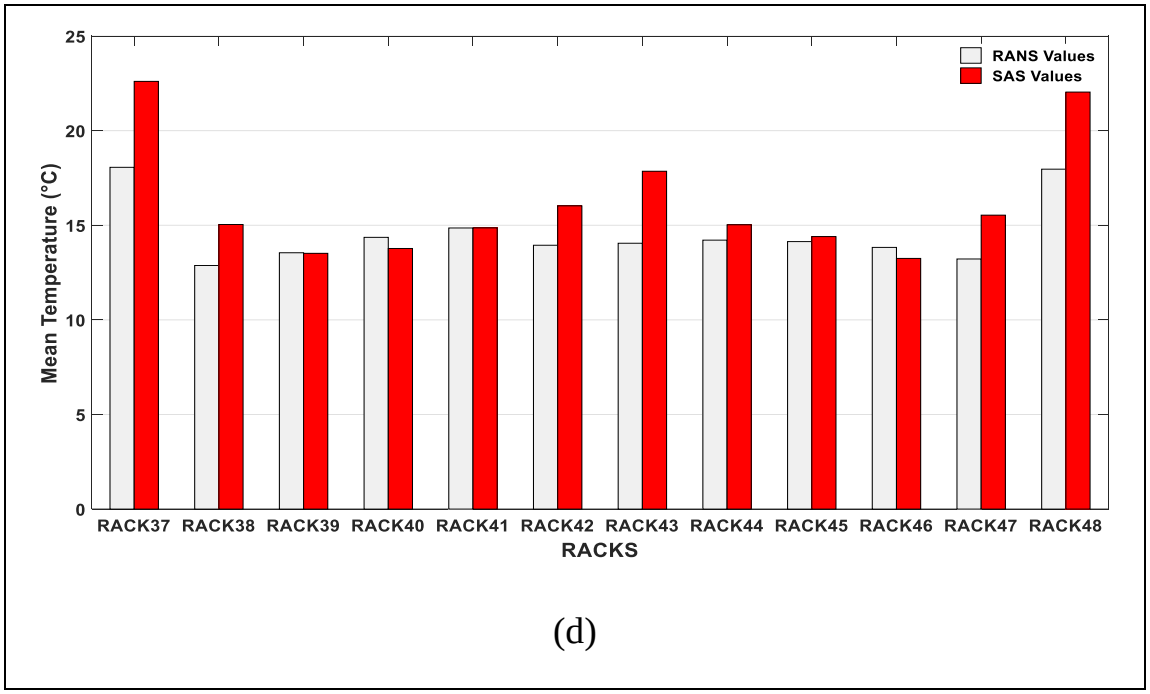

Figure 35: (a)-(d) Comparison of time-averaged inlet rack temperature between SAS and RANS simulations of the RF/RR-B.

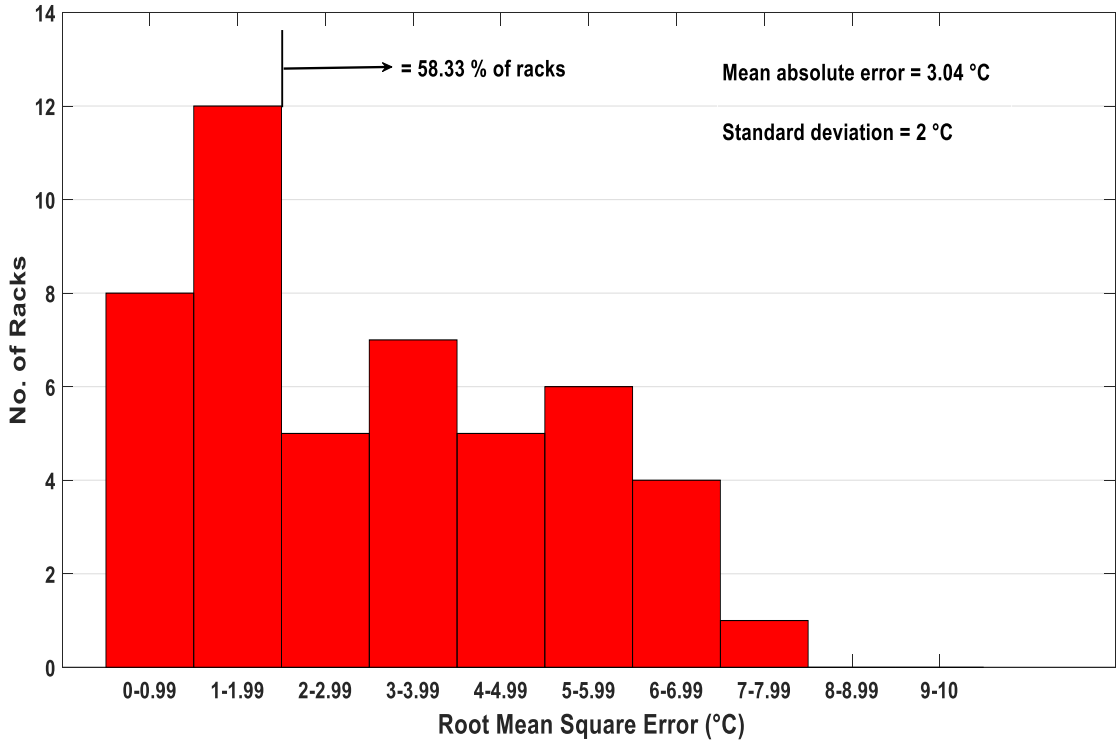

Figure 36: Frequency histogram of RMSE between SAS and RANS simulations of mean inlet rack temperature of RF/RR-B.

Figure 37 and Figure 38 shows the temperature contour for the third configuration, RF/OR for the SAS and the RANS simulations, respectively. The figures show that this configuration has the least discrepancy among others and has the least hot spots for both turbulence models. Figure 39 shows a comparison of the rack inlet average temperature between the SAS and the RANS for the RF/OR configuration. In general, the agreement is good for the middle racks where the RMSE for these racks is 2.69 ℃ with a standard deviation of 1.71 ℃. Moreover, for the end racks the agreement is good as well, where the RMSE is 3.72 ℃ with a standard deviation of 0.76 ℃. The overall agreement is revealed in the frequency histogram shown in Figure 40. The RMSE between the SAS and the RANS for the avergae inlet rack temperature for 66.67 % of the racks is higher than 2 ℃. Whereas, the mean absolute error is 2.86 ℃ with 1.63 ℃ standard deviation. Unlike the RF/RR-A and the RF/RR-B, the discrepancy between the SAS and the RANS results is minimal.

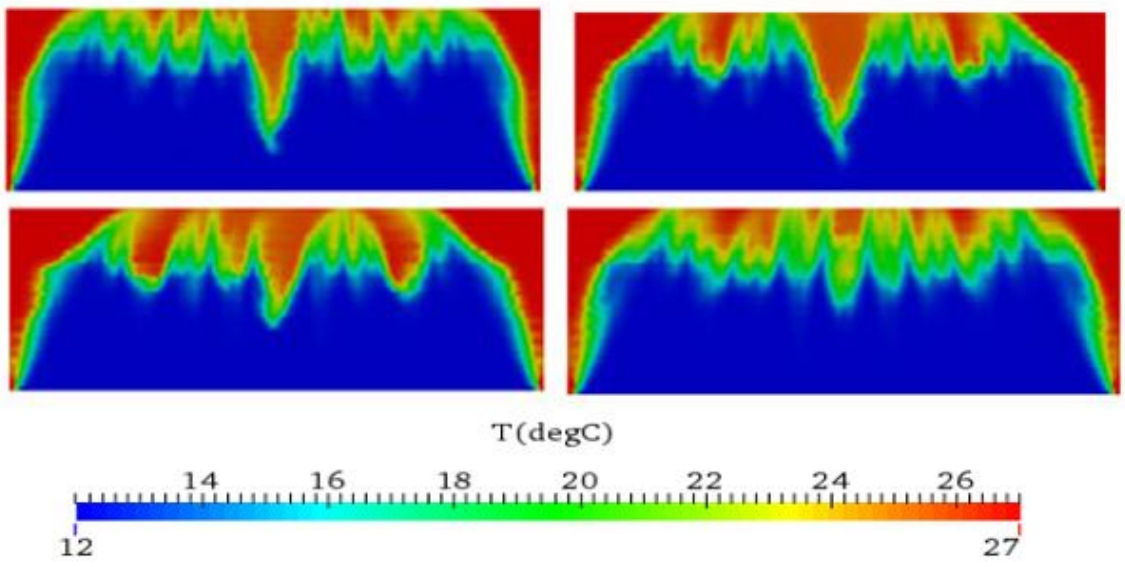

Figure 37: Instantaneous temperature values contours for the k-ω SST SAS turbulence model in front of the IT server racks for RF/OR.

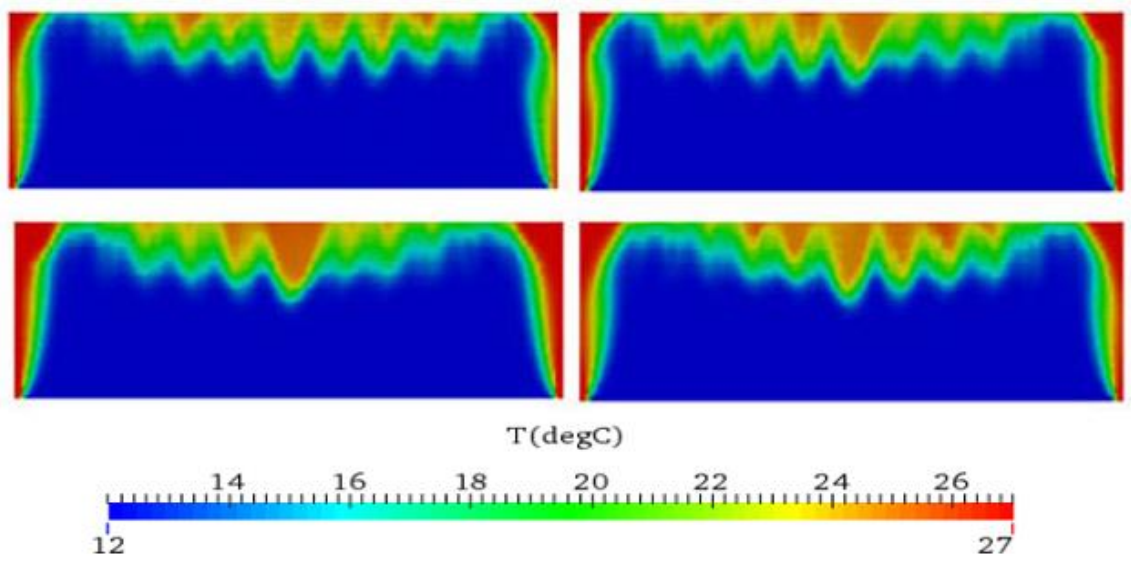

Figure 38: Temperature contour for the k-ε RANS model in front of the IT server racks for RF/OR.

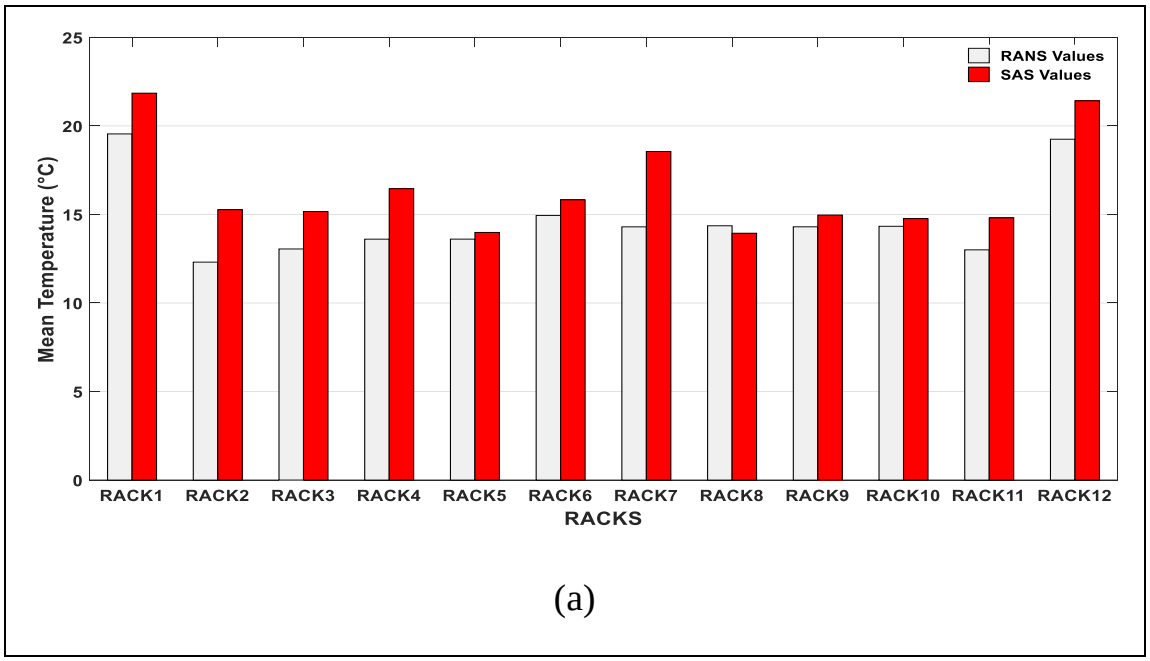

(a)

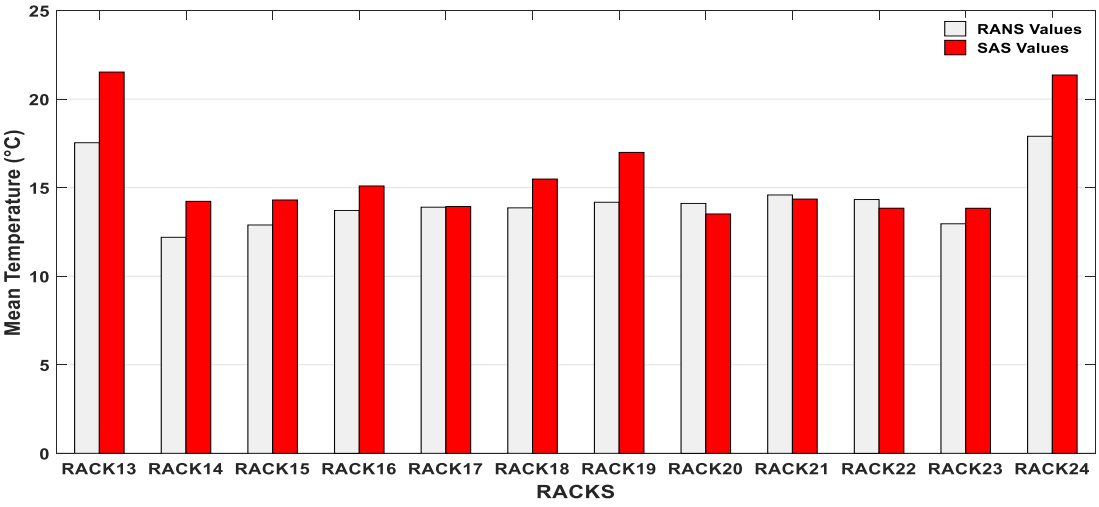
RANS Values
SAS Values
Mean Temperature (°C)
25
20
15
10
5
0
RACK13 RACK14 RACK15 RACK16 RACK17 RACK18 RACK19 RACK20 RACK21 RACK22 RACK23 RACK24
RACKS

(b)

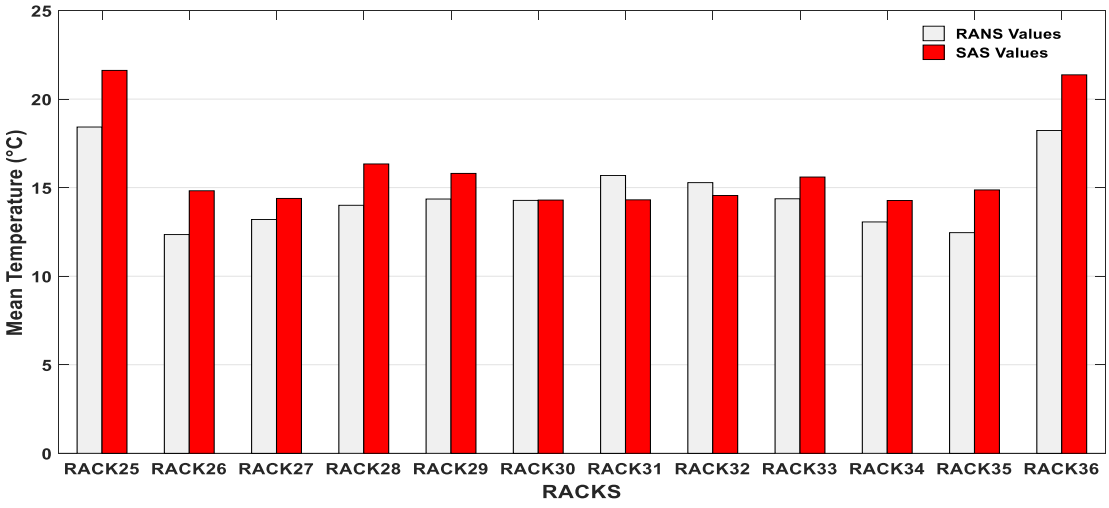
RANS Values
SAS Values
Mean Temperature (°C)
25
20
15
10
5
0
RACK25 RACK26 RACK27 RACK28 RACK29 RACK30 RACK31 RACK32 RACK33 RACK34 RACK35 RACK36
RACKS

(c)

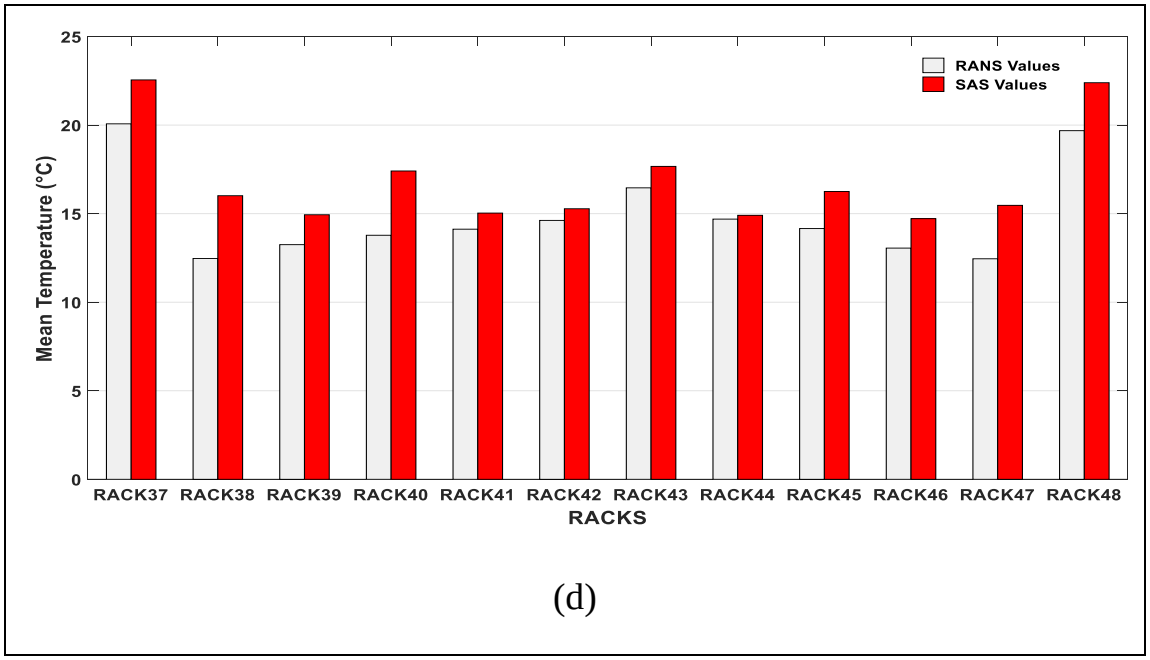

Figure 39: (a)-(d) Comparison of time-averaged inlet rack temperature between SAS and RANS simulations of the RF/OR.

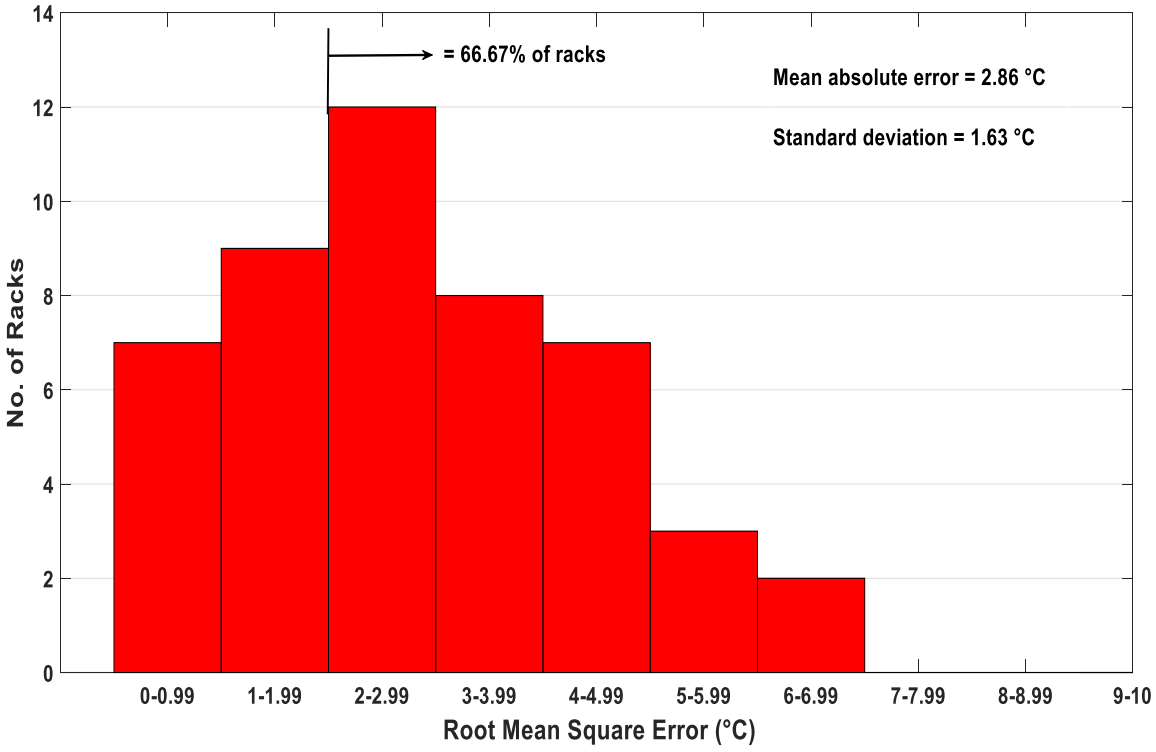

Figure 40: Frequency histogram of RMSE between SAS and RANS simulations of mean inlet rack temperature of RF/OR.

To show the overall agreement, the RMSE values are summarised in Table 16. It is clearly illustrated that the k-ε RANS model does not depict the hot air infiltration for the RF/RR-A and RF/RR-B, especially at the end of the racks. This might be because the mean strain rate has sharp gradients around the rack edges, causing high flow swirling that could not be detected by the isotropic eddy viscosity model, the k-ε RANS model. For the RF/OR, the agreement between the k-ε RANS and the k-ω SST SAS is good for both the overall RMSE and for the end racks RMSE. This might be because of the room return vent locations, where the hot return is directly drawn into the upper part of the data centre room due to the high pressure gradient between the ailes presure and the return vents pressure which may decrease the swirling flow around rack edges.

Table 16: RMSE between SAS and RANS for calculated average inlet temperature.

	Overall RMSE, ℃	**Middle racks RMSE, ℃**	**End racks RMSE, ℃**
RF/RR-A	3.80	3.19	6.85
	SD = 2.01	SD = 2.86	SD = 0.62
RF/RR-B	3.04	2.58	5.37
	SD = 2.00	SD = 1.78	SD = 1.41
RF/OR	2.86 ℃	2.69	3.72
	SD = 1.63	SD = 1.71	SD = 0.76

4.6. Summary

In this chapter and for the first time, the robust turbulence model k-ω SST SAS was applied in the data centre numerical simulations to find the limitations of using the k-ε RANS turbulence model, which is widely used in the current data centre numerical modelling. The turbulence models are validated by comparing their results with an experimental work using a vented enclosure. The comparison showed that both turbulence models anticipated the right temperature, pressure and airflow distribution inside the vented enclosure. Different comparisons with available data centre experimental results showed that the k-ε RANS cannot anticipate the right pressure distribution in the data centre room and the temperature contour at the intake of the IT servers' racks, unlike the k-ω SST SAS turbulence model which anticipated the right pressure distribution in the data centre room and the temperature contour at the inlet of the IT servers' racks. Both turbulence models were used to find the average inlet IT servers temperature. The agreement between the RANS and the SAS for the RF/RR-A is acceptable for the middle racks, where the RMSE for these racks is 3.19 ℃, with a standard deviation of 1.59 ℃. However, for the racks located on the sides of the cold aisle, the agreement is very poor with the RMSE 6.85 ℃ with 0.62 ℃ standard deviation. Likewise, the RF/RR-B has almost the same pattern, where the agreement is good for the middle racks with 2.58 ℃ RMSE and a standard deviation of 1.78 ℃. However, for the end racks, the agreement is very poor where the RMSE is 5.37 ℃ with a standard deviation of 1.41 ℃. This result is slightly better than the result of the RF/RR-A, where the discrepancy between the turbulence models is apparently due to the racks at the end of cold aisles for these two configurations. Unlike the agreement of the RF/OR, which was good, the RMSE for the middle racks is 2.69 ℃ with a standard deviation of 1.71 ℃ and the RMSE for the end racks is 3.72 ℃ with a standard deviation of 0.76 ℃. This means that for the room return configurations, the RANS simulations may give misleading results especially for the end rack temperature distributions unlike the ceiling return configurations where the RANS turbulence model better predicts the end rack temperature distribution.

Chapter 5: The Effect of Server Arrangement on Thermal Performance

5.1. Introduction

Data centre power consumption is steadily increasing relative to the room footprint size and is leading to high volumetric heat generation rates for a given room size [54]. The limited rack cabinets size is another issue where the servers are vertically stacked in 2 m rack long [41]. In today's data centres the IT servers inside a rack may dissipate more than 20 kW of heat, compared to 1 kW in the early 1990s [105]. A standardised single rack can fit 42 1U servers where each server has a height of 0.0445 m and the servers are stacked vertically. Although, a single rack normally accommodates less than 42 1U server to account for cooling or to add routers, switches and many other devices in the future. This trend has the benefit of minimising the data processing equipment to save more rack space to be occupied by more 1U servers. However, in case of populating the rack with its full capacity, the rack may generate more than 16.8 kW of heat. Another issue is that the rack capacity is limited to 42 1U server and with the increasing of computational demand this may not enough to meet the required operations because 1U server has limited computational power. Therefore, there is a need for a more versatile server arrangement within a single rack to get more computational processes and in the same time have acceptable cooling effectiveness. Hence, in this chapter blade server will be integrated with 1U servers in a single rack with different configurations to determine the best possible configuration with respect to the cooling effectiveness. The blade server is a series of servers mounted into a single enclosure to increase the density of computing of a single rack. Each blade server occupies the same space as 7U but has double computational density.

In the case of mounting 1U servers with blade servers in the same rack, there will be high difference in exhaust temperatures. Consequently, the buoyancy force may play a vital role. This may be beneficial if the data processing equipment is arranged in the right way. In contrast, if either 1U servers or blade servers mounted into a single rack the rack

outlet temperatures will be identical and there will be high mixing in the data centre room. Previous rack level analyses have focused on the data processing cabinet, excluding the effect of the servers' arrangement on the room level thermal performance [41, 42]. While, in this chapter the primary objective will consider the effect of different server arrangements on the room level thermal performance.

5.2. Numerical Model

There are various assembly strategies that can be considered to arrange the servers inside the rack cabinet. In this thesis, six different server arrangements are considered to study the effect of these arrangements on room level thermal performance as shown in Figure 41. The basic strategy is to spread the blade servers out across the rack as much as possible. The first candidate strategy may minimize the local heat dissipation at the servers' outlets but it may increase the mixing which may diminish the buoyancy force advantage that may be beneficial to partly prevent the hot air from being returned into the upper part of the servers' inlets. In the second and third configurations, the blade servers are spread between the top and bottom of the rack cabinet to investigate the thermal performance of these candidates.

In the last three strategies, the blade servers are clustered together at the top, middle and bottom of the rack cabinet. Putting the blade servers near the top of the rack cabinet may increase the chance of exhausting the hot air into the upper part of the data centre room without contaminating the cold air; however, minimising the cool air received by these servers does not ensure their reliable operation. Placing blade servers near the lower and middle part of the rack cabinet may ensure that these servers will receive enough cold air but the outlet hot air may thermally contaminate the cold air received by the upper servers. These configurations are considered in this study to cover a wide range of possible servers' configuration schemes and rack heat dissipation profiles.

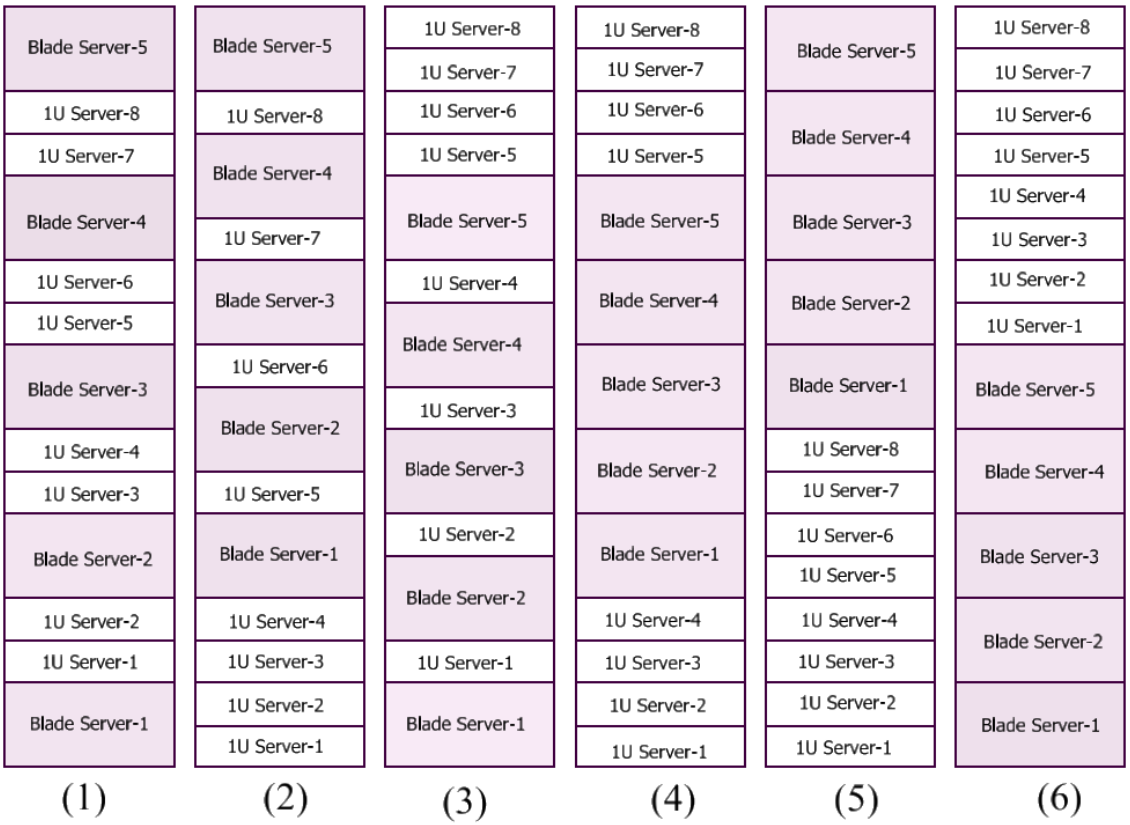

Figure 41: Rack configurations.

The thermal investigation will be carried out on a hypothetical raised floor data centre RF/RR-A as shown in Figure 42. The six server arrangements are shown in Figure 41. The blade servers were considered to have a high heat dissipation rate equal to ~1 kW each at a mass flow rate of ~0.05 kg/sec; whereas, the 1U servers had a heat dissipation rate of ~0.25 kW with an overall mass flow rate of ~0.02 kg/sec. The resulting total rack heat dissipation was ~7 kW. The temperature rise across the servers was maintained constant 10 °C for a 1U server and 20 °C for a blade server to examine the effect of temperature differences on the hot air recirculation without modelling the internal flows inside the data processing cabinet. Table 17 summarises the individual server mass flow rate, temperature rise and heat dissipation rates for all proposed configurations.

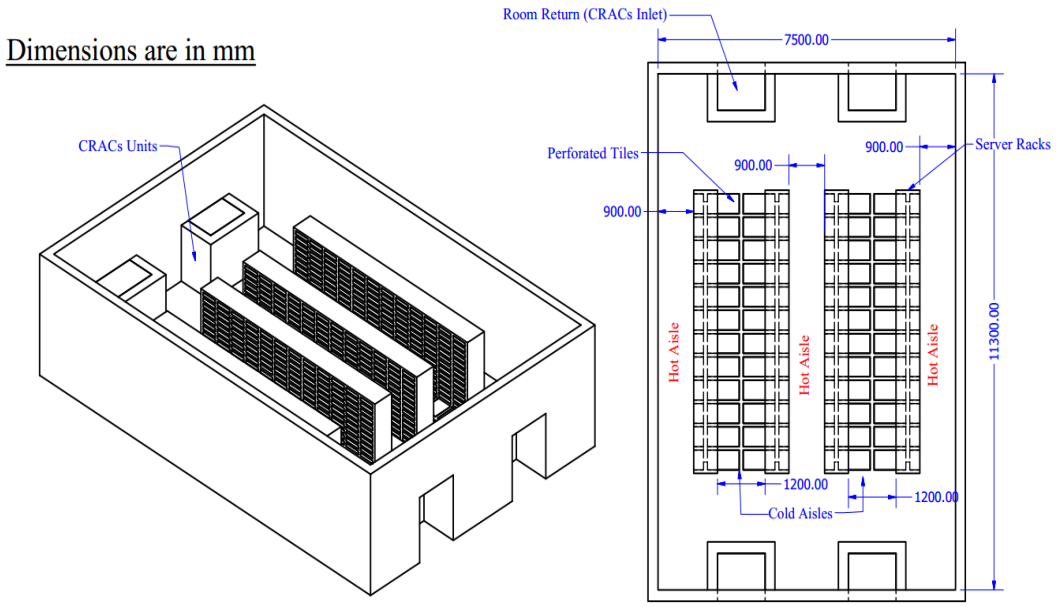

Figure 42: Schematic diagram of the Raised Floor with Flooded Room A (RF/RR-A) data centre.

Table 17: Individual server mass flow rate (kg/s), temperature rise (°C) and heat dissipation (kW).

	$\dot{\mathbf{m}}$ **(kg/s)**	**ΔT (°C)**	**Q (kW)**
1U Server	0.025	10	0.25
Blade Server	0.05	20	1

5.3. Buoyancy Forces

The blade servers have a high temperature rise across the rack, hence the buoyancy forces in the fluid inside the data centre room may be significant. Density variations, especially in natural convection, significantly affects the fluid flow velocity. However, in turbulent regimes the effect of the density variations on the fluid movement may be diminished due to the high fluid velocity. The ratio between the buoyancy forces and inertia forces in the fluid flow can be taken as a measure of the buoyancy force effect on

the fluid flow movement. Reynolds number is the measure of the inertia forces and Rayleigh number (Ra) is used as an indication of the buoyancy forces.

The Reynolds number is the ratio between the inertial and viscous forces which can be evaluated by:

$$\mathrm{Re} = \frac{\rho V L}{\mu} \qquad 5.3.1.$$

Where ρ is fluid density, V is flow velocity, L is a characteristic length and μ is fluid dynamic viscosity. The Ra is the ratio between the buoyancy and viscous forces which can be expressed as the product of the Grashof and Prandtl number (GrPr), where:

$$\mathrm{Gr} = \frac{\beta g \rho^2 \Delta T L^3}{\mu^2} \qquad 5.3.2.$$

$$\mathrm{Pr} = \frac{C_p \mu}{k} \qquad 5.3.3.$$

$$\mathrm{Ra} = \mathrm{GrPr} \qquad 5.3.4.$$

$$\mathrm{Ra} = \frac{\beta g \rho^2 \Delta T L^3 C_p}{k \mu} \qquad 5.3.5.$$

Where β is the thermal expansion coefficient of the fluid, g is the gravitational acceleration, ρ is fluid density, L is a characteristic length, C_p is the specific heat capacity, k is the thermal conductivity and μ is the fluid dynamic viscosity.

Buoyancy forces for the modelled data centre will be investigated at the server exhaust for both the 1U servers and blade servers. The Reynolds number for the 1U server is ~4000 based on the inlet fan hydraulic diameter and the exhaust fan flow rate. For the blade server again using the hydraulic diameter of the inlet fan and the exhaust flow rate the Reynolds number is ~8000. The Re number clearly indicates that the flow near the servers is turbulent. Additionally, the Rayleigh number was calculated based on the height of the servers and temperature rise across the servers. The values were found to be 8.1×10^5

for the 1U server and $4.5x10^6$ for the blade server. The buoyancy ratio to inertial effects at the discharge of the servers (Ra/Re^2) is in order of $O(10^{-1})$ for the blade server and $O(10^{-2})$ for the 1U server demonstrating that the buoyancy forces may play an important role in the fluid motion especially for the blade servers. Therefore, the Scale Adaptive Simulation (SAS) was used to conduct the numerical simulations by using the `buoyantBoussinesqPimpleFoam` solver to account for the buoyancy forces in the fluid flow.

5.4. Results and Discussion

Numerical simulations were carried out for six different server arrangements to explore the best possible configuration scheme with respect to the thermal performance of the data centre. The main source of the temperature rise in front of the servers is the hot air infiltration from the hot aisles and data centre room. Therefore, for each configuration, the hot air infiltration as well as the room level thermal performance for each of the proposed configurations was analysed.

5.4.1. Hot Air Infiltration

Figures 43 to 48 show the z-direction velocity vectors at the middle of the data centre for configurations 1 to 6. These figures illustrate the complex flow field across the data centre room. All the configurations have similar airflow pattern where hot air is exhausted from the outlet of the servers into the upper part of the data centre and the cold aisles which will increase the servers' inlet temperature. However, the hot air infiltration into the cold aisle is clearly affected by the server arrangement.

For configuration 1, as shown in Figure 43, the hot air infiltrates into the middle of the cold aisle which means that the servers in the middle of the cold aisle may be subject to overheating if the return air is at a high temperature. Configurations 1, 2, 3 and 4 have similar airflow distributions as demonstrated in Figures 43 to 46. These configurations

have high mixing for the first three configurations with the blade servers spread out across the rack and for the fourth configuration the blade servers are clustered in the middle of the rack. Whereas, configuration 5 has the lowest hot air infiltration as illustrated by Figure 47. In this configuration, the blade servers were clustered at the top of the rack. Additionally, configuration 6 has the highest airflow jets enter the cold aisle as shown by Figure 48. This implies that the location of the blade server across the rack has significant effect on the hot air infiltration into the cold aisle. The main reason for this may be the difference in the return airflow temperature between these configurations where by spreading the servers across the rack, there is high airflow mixing which will drop the return airflow temperature, unlike when the blade servers are clustered at the top of the cold aisle.

The air recirculation into the cold aisle for all configurations are shown from in Figures 49 to 54. For each configuration two contours presented, one at the intake of the upper servers, at a height of z=1.84 m, and one at a height of z=1.41 m. It is clearly illustrated by the figures that the configurations with high degree of mixing, when the blade servers dispersed across the rack, have strong air recirculation jets especially for the servers located at the height of z=1.41 m. For example, with the blade servers dispersed across the rack or clustered at the middle, the hot air recirculation is comparable. Moreover, configuration 6 is the worst scenario with the blade servers clustered at the bottom of the rack. In this configuration, the 1U server is at the top of the rack which does not allow for the hot air exhausted by the blade servers at the bottom of the rack from escaping into the upper part of the data centre. This decreases the return air temperature which may diminish the density variations between the cold aisle air density and the recirculated air density. In contrast, configuration 5 has the least hot air recirculation as the blade servers were clustered at the top of the rack in contrast to configuration 6.

From the previous analysis, it is clear that the hot air recirculation relies heavily on the power profile across the rack. It can be noted that when the high-power density servers were located at the top of the rack, the hot air recirculation into the cold aisle decreased. This may be attributed to higher return air temperatures and will be investigated in the next section.

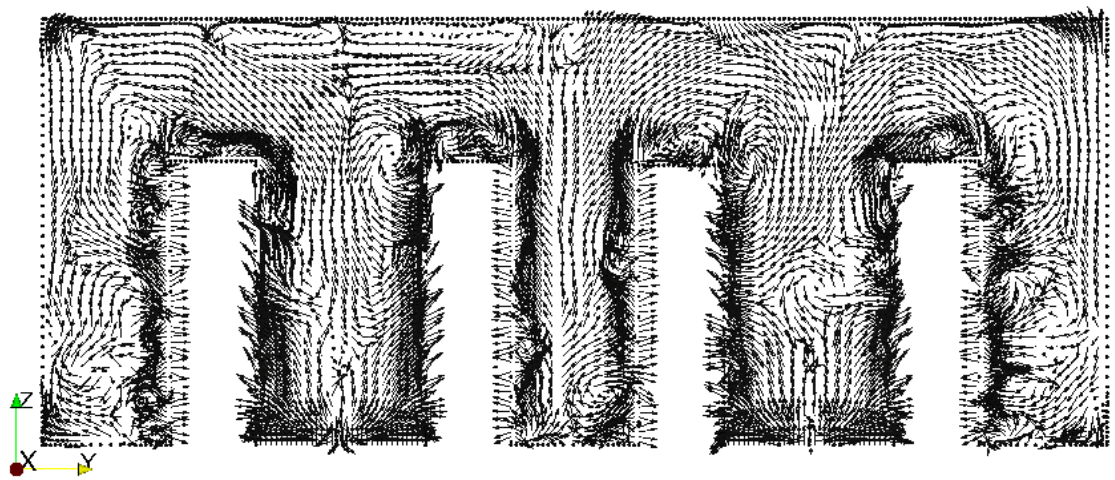

Figure 43: Velocity vectors in the z-direction at the middle of the data centre for configuration 1.

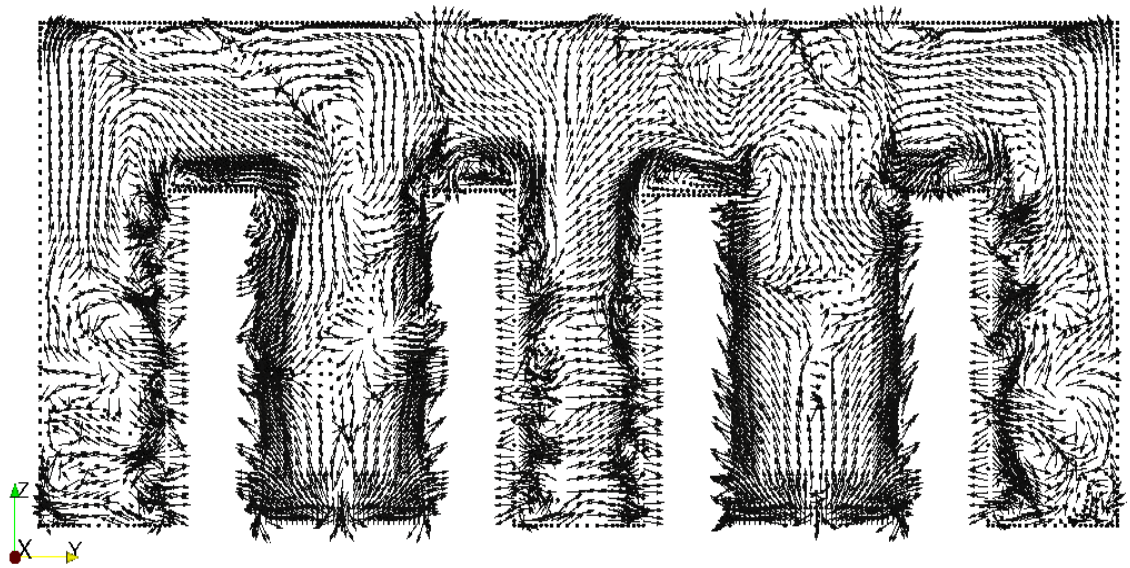

Figure 44: Velocity vectors in the z-direction at the middle of the data centre for configuration 2.

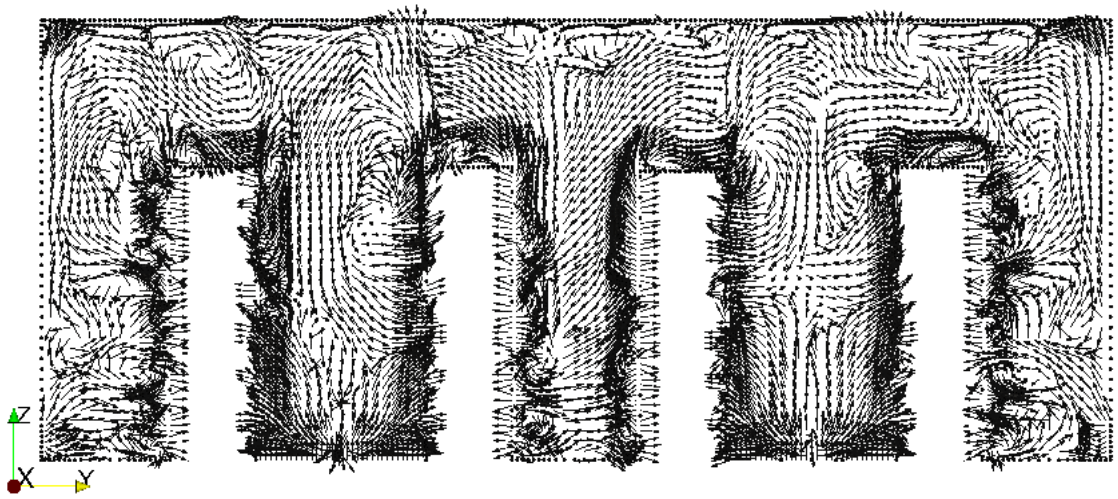

Figure 45: Velocity vectors in the z-direction at the middle of the data centre for configuration 3.

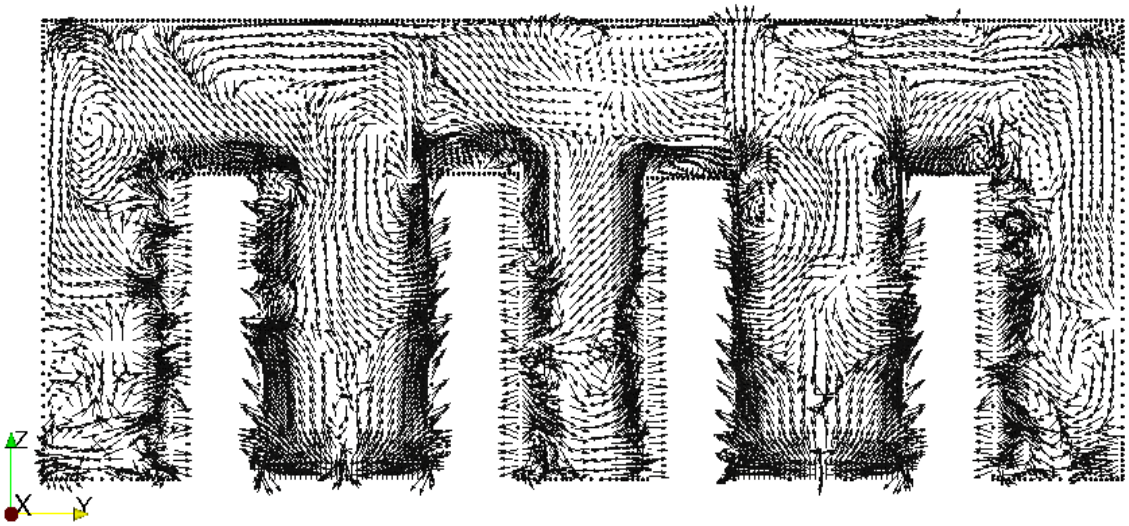

Figure 46: Velocity vectors in the z-direction at the middle of the data centre for configuration 4.

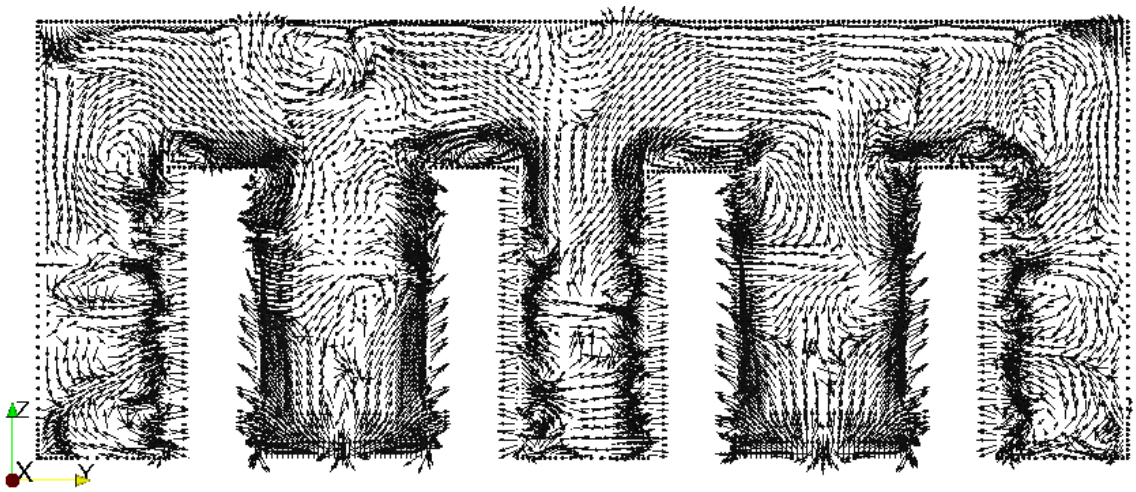

Figure 47: Velocity vectors in the z-direction at the middle of the data centre for configuration 5.

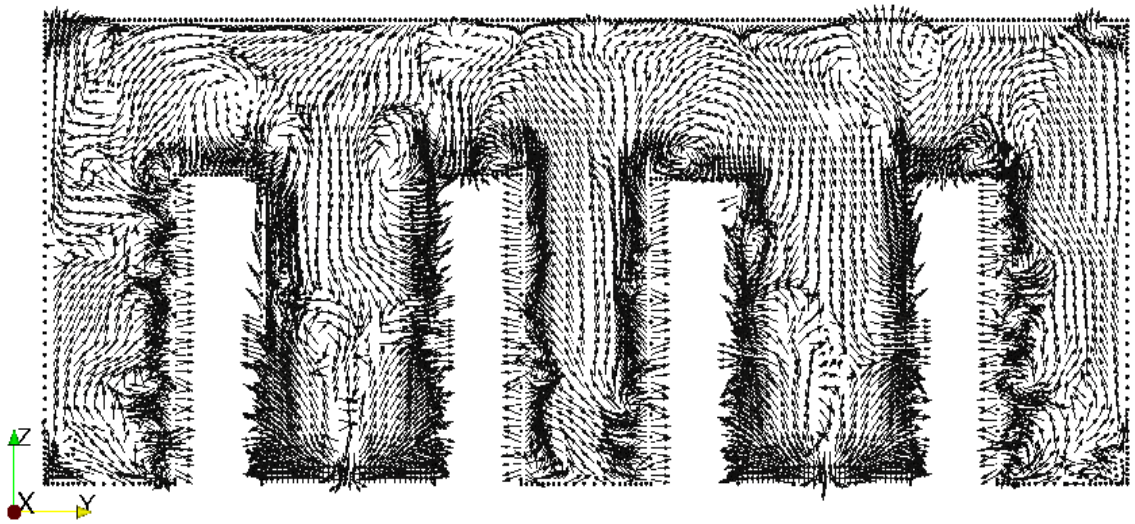

Figure 48: Velocity vectors in the z-direction at the middle of the data centre for configuration 6.

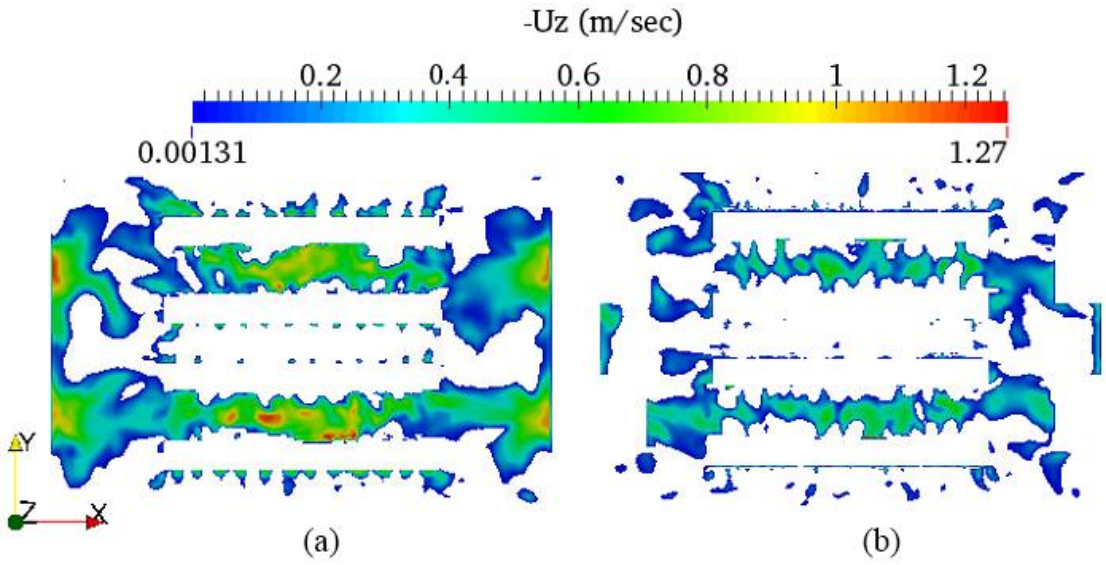

Figure 49: Hot air infiltration contour for configuration 1: (a) at height of $z = 1.84\ m$. (b) at height of $z = 1.41\ m$.

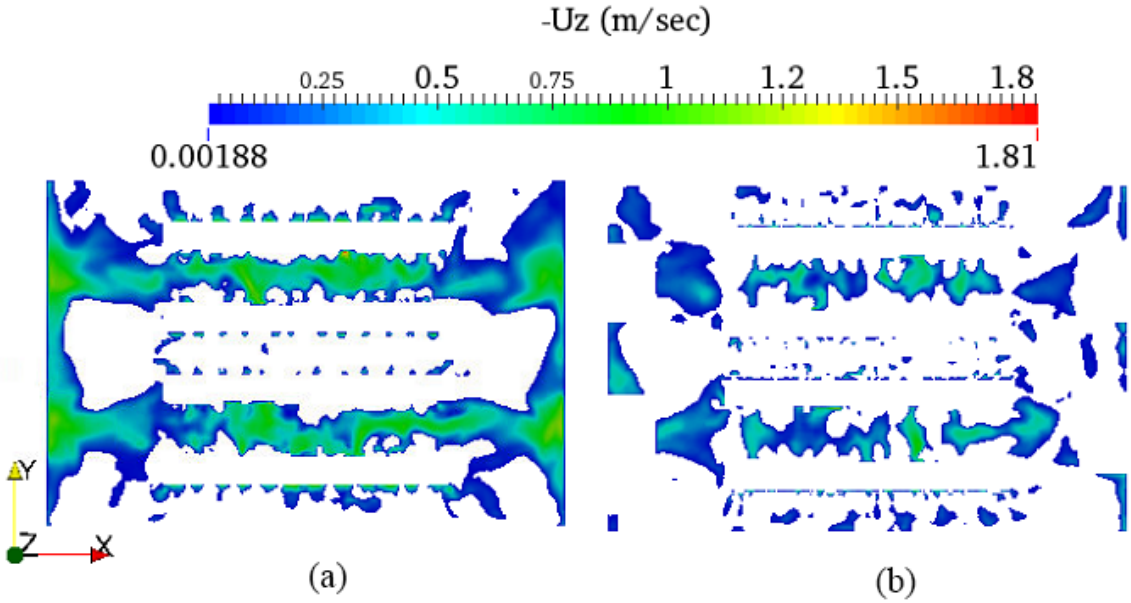

Figure 50: Hot air infiltration contour for configuration 2: (a) at height of $z = 1.84\ m$. (b) at height of $z = 1.41\ m$.

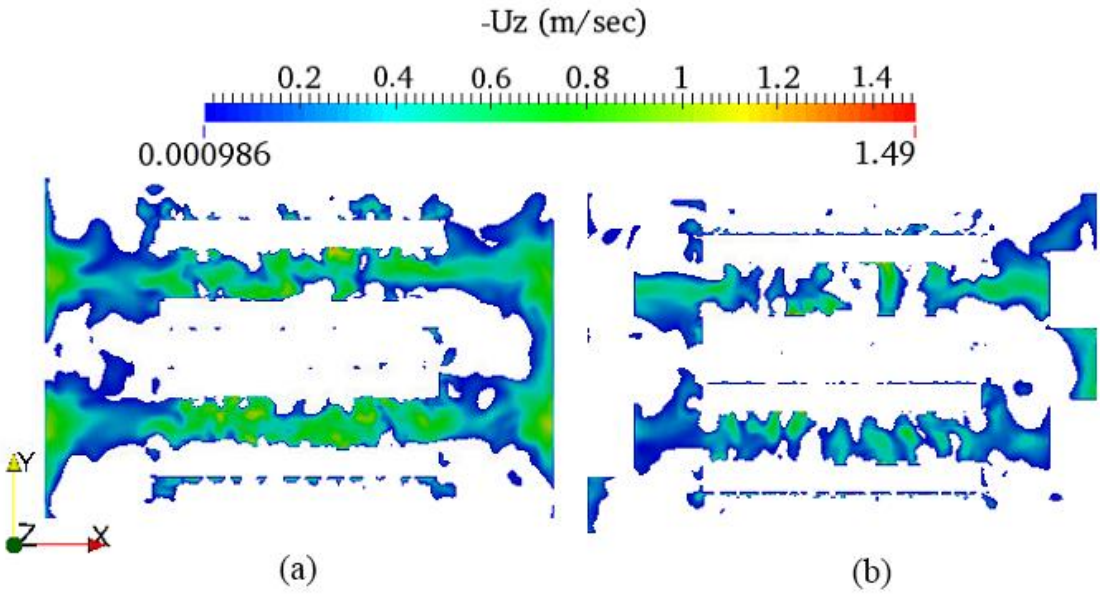

Figure 51: Hot air infiltration contour for configuration 3: (a) at height of $z = 184\ m$. (b) at height of $z = 1.41\ m$.

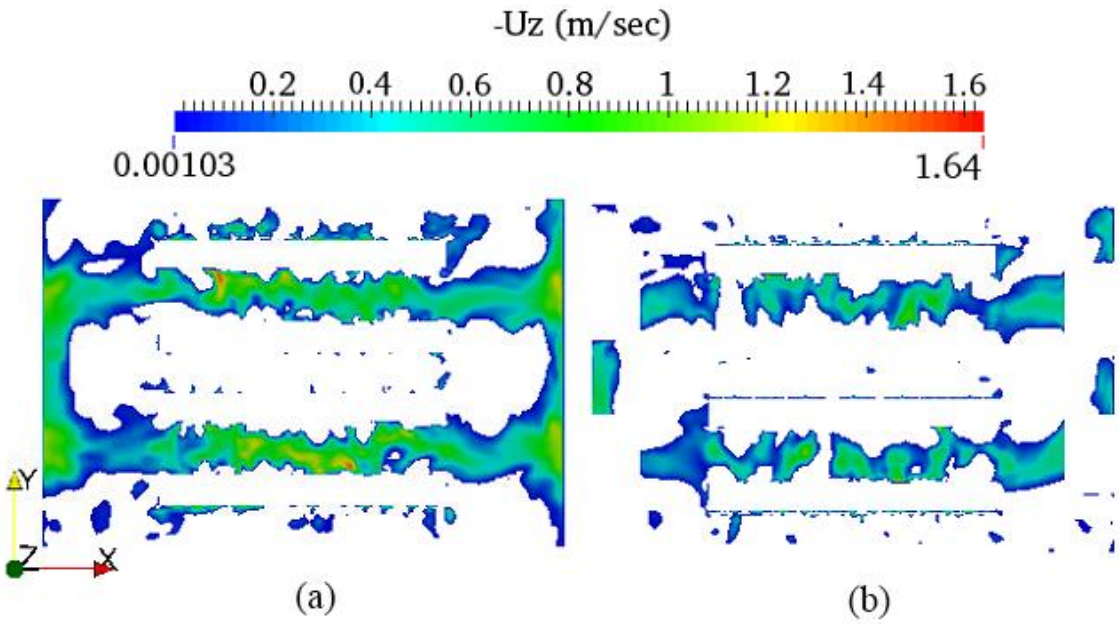

Figure 52: Hot air infiltration contour for configuration 4: (a) at height of $z = 1.84\ m$. (b) at height of $z = 1.41\ m$.

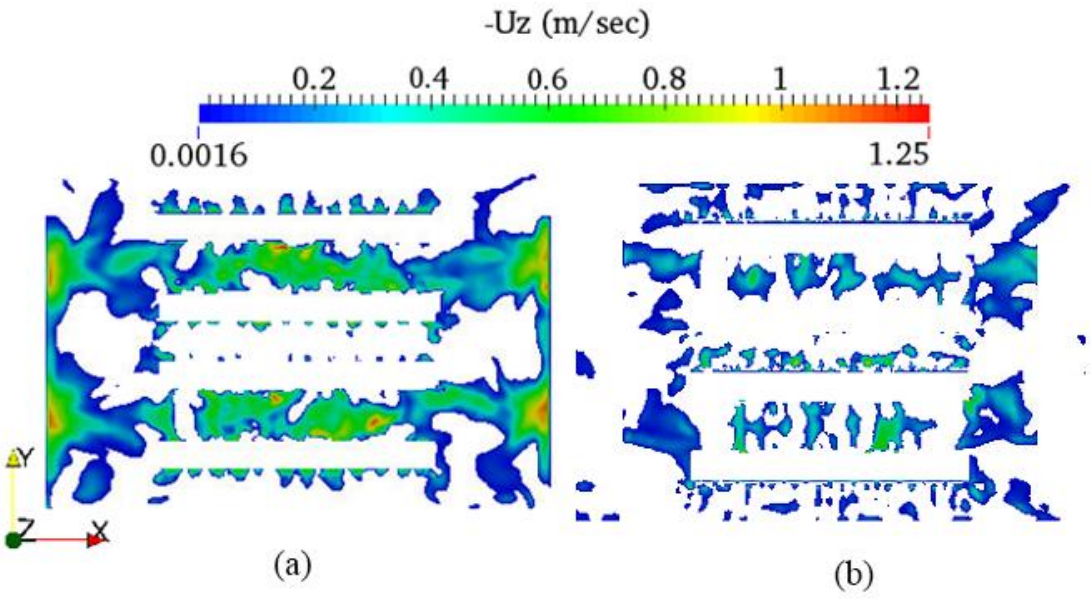

Figure 53: Hot air infiltration contour for configuration 5: (a) at height of $z = 1.84\ m$. (b) at height of $z = 1.41\ m$.

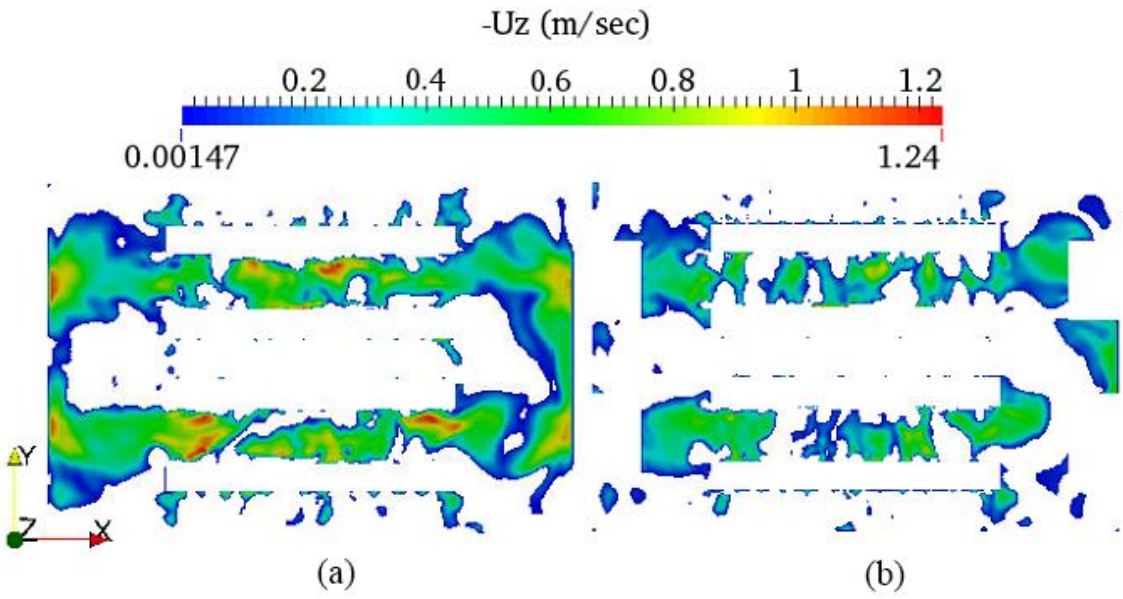

Figure 54: Hot air infiltration contour for configuration 6: (a) at height of $z = 1.84\ m$. (b) at height of $z = 1.41\ m$.

5.4.2. Thermal Performance

The thermal performance of the data centre configurations are initially considered qualitatively based on the rack inlet temperatures. To determine the rack inlet temperature for each configuration, the temperature contours for the same rows of racks are shown in Figure 55. The figure clearly illustrates the difference in rack inlet temperatures for each configuration. Configurations 1, 2 and 3 have similar thermal performance as in all these three configurations the blade servers were spread out across the rack. This may be because the return air temperature is similar when the discharged hot air from the 1U servers and blade servers was well mixed inside the hot aisle. Whereas, clustering the blade servers within the rack, configurations 4,5 and 6, gives different thermal performance, as clearly illustrated in the figure. Clustering the blade servers in the middle and bottom of the rack (configurations 4 and 6) gives the worst thermal conditions at the intake of the racks. On the other hand, clustering the blade servers at the top of the rack gives the best thermal conditions at the intake of the rack. This might be attributed to that the hot air recirculation into the cold aisle strongly depending on the hot air return temperature where when the return air temperature increases the hot air recirculation decreases.

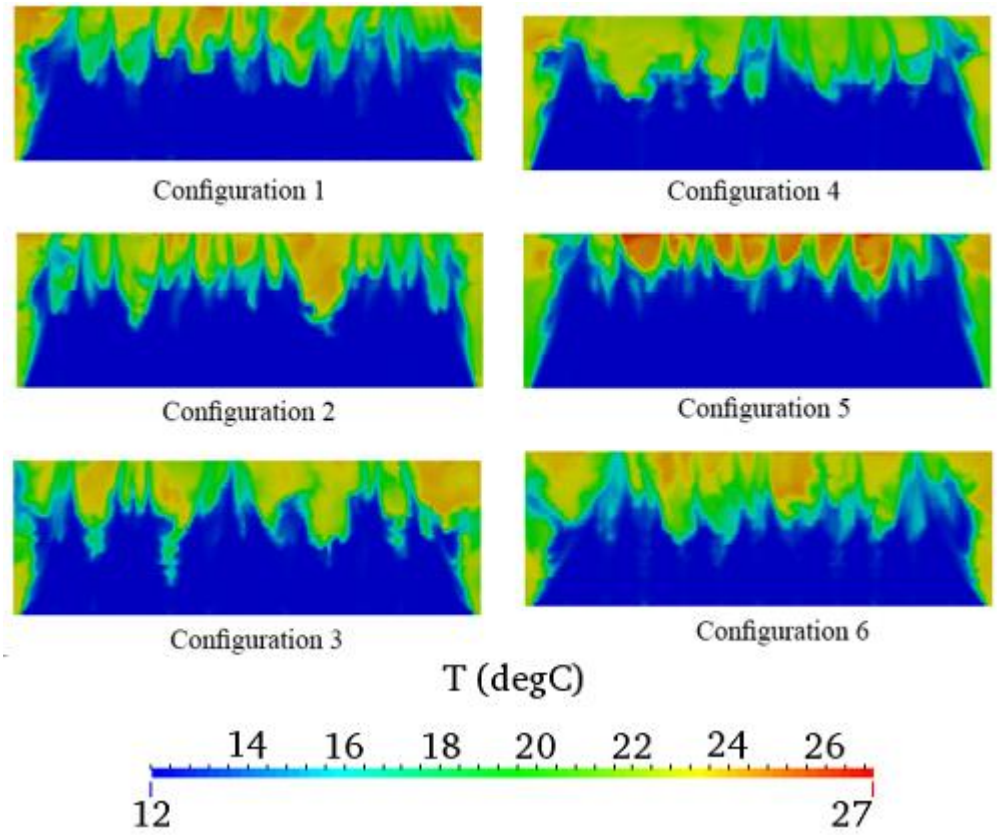

Figure 55: Instantaneous temperature values contours in front of the same row of racks for all configurations.

Quantitative analysis of the temperature at the intake of the rack allows the problematic servers for each configuration to be determined. The temperatures were taken for the middle eight racks excluding the racks located at the sides of the cold aisle (two racks from each side) to eliminate the influence of hot air infiltration directly adjacent to the rack sides. The temperature values were considered by monitoring a single point at the inlet of each individual server, then the average temperature of each row of servers was calculated for the servers labelled servers01 to servers13 in Figure 56. Based on these temperature values the Supply Heat Index (SHI) was calculated. It is defined as:

$$\text{SHI} = \frac{\text{The enthalpy rise in the cold aisle}}{\text{The total enthalpy rise at the rack exhaust}}$$

$$SHI = \frac{T_{in}^{r} - T_{ref}}{T_{out}^{r} - T_{ref}} \quad 5.4.1.$$

Table 18 and Table 19 summarise the temperature values and the SHI, respectively, at the intake of the servers for all configurations. The data shows that servers 01 to servers 07 are maintained in good thermal condition for all configurations as the temperature values are near the inlet air temperature with almost zero SHI. However, there is high temperature spike in front of servers08 for all configurations except for configuration 5. The highest temperature spike in front of servers08 was for configuration 6 with 18.75 ℃ and 33.76% SHI. Whereas, the lowest temperature spike in front of servers 08 was for configuration 5 with a temperature of 12.51 ℃ and 2.56% SHI. It is also noticed that by clustering the blade servers at the middle of the rack the thermal performance of the data centre is worse than spreading them throughout the rack. In general, the tables show that spreading out the blade servers either in the upper, lower or evenly throughout the rack gives similar thermal performance. Additionally, for the middle servers, clustering the blade servers in the lower part of the rack gives the worst thermal performance, while clustering them in the upper part of the rack gives the best thermal performance. However, the highest two rows of servers have similar inlet temperatures for all configurations. If this problem can be overcome, configuration 5 would be the best choice.

These results verify that the return air temperature has significant effect on the thermal conditions in front of the racks intake even though in this study the temperature differences are not very high. These findings match previous results suggested by [2, 5, 34, 43] where they found that the racks inlet thermal conditions are better with higher rack heat densities. In these studies, they compared the effect of different rack heat densities on the rack inlet temperature and the better thermal conditions at the intake of racks were attributed to the higher perforated tile flow rates. However, this chapter shows that buoyancy forces may play a significant role in enhancing the rack intake temperatures because the rack with high heat densities at the upper part have higher return air temperatures which resulted in better thermal conditions at the intake of the rack. This is due to buoyancy forces preventing some of the return air from infiltrating into the cold aisle even though the perforated tile flow rate was constant.

To further illustrate the effect of return air temperature on the hot air recirculation, a temperature slice was taken in front of rack 6 at x=5.4 m shown in Figure 57. It can be seen that the return air temperature strongly affects the hot air recirculation into the cold aisle. Where, as the hot air return temperatures increase the hot air recirculation decreases.

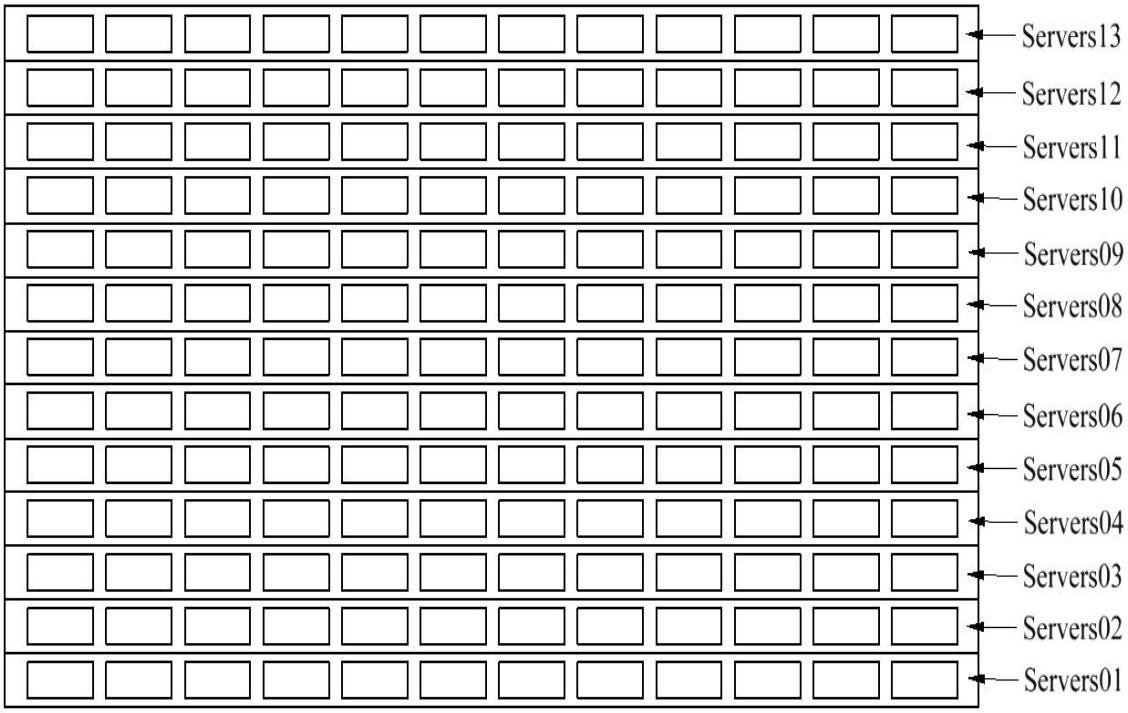

Figure 56: Servers arrangements for temperature monitoring.

Table 18: Temperature values at the intake of servers for all configurations.

	Config 1	**Config 2**	**Config 3**	**Config 4**	**Config 5**	**Config 6**
	$\mathbf{T_{in}}$(℃)	$\mathbf{T_{in}}$(℃)	$\mathbf{T_{in}}$(℃)	$\mathbf{T_{in}}$(℃)	$\mathbf{T_{in}}$(℃)	$\mathbf{T_{in}}$(℃)
Servers-13	27.2	26.1	25.1	24.38	26.52	27
Servers-12	25.54	25.34	23.7	23.76	25	26.22
Servers-11	23.21	23.1	22.02	23.2	20.99	24.03
Servers-10	19.71	20.8	19.59	21.68	17.76	22.97
Servers-09	17.29	17.55	17.65	20.1	14.79	21.85
Servers-08	14.39	14.63	15.07	17.5	12.51	18.75
Servers-07	12.27	12.1	12.22	12.3	12	12.68
Servers-06	12.12	12	12	12	12	12
Servers-05	12.1	12	12	12	12	12
Servers-04	12.02	12	12	12	12	12
Servers-03	12	12	12	12	12	12
Servers-02	12	12	12	12	12	12
Servers-01	12	12	12	12	12	12

Table 19: SHI at the intake of servers for all configurations.

	Config 1	**Config 2**	**Config 3**	**Config 4**	**Config 5**	**Config 6**
	SHI × 100	**SHI × 100**	**SHI × 100**	**SHI × 100**	**SHI × 100**	**SHI × 100**
Servers-13	0.7595	0.7034	0.6539	0.6189	0.7262	0.7481
Servers-12	0.6768	0.6668	0.5849	0.5879	0.6511	0.711
Servers-11	0.5603	0.5548	0.5010	0.559	0.4494	0.6014
Servers-10	0.3856	0.4398	0.3792	0.4838	0.2878	0.5481
Servers-09	0.2649	0.2773	0.2823	0.4022	0.1393	0.4924
Servers-08	0.1197	0.1316	0.1534	0.2745	0.02563	0.3376
Server-07	0.0134	0.0049	0.0109	0.0151	0	0.0337
Servers-06	0	0	0	0	0	0
Servers-05	0	0	0	0	0	0
Servers-04	0	0	0	0	0	0
Servers-03	0	0	0	0	0	0
Servers-02	0	0	0	0	0	0
Servers-01	0	0	0	0	0	0

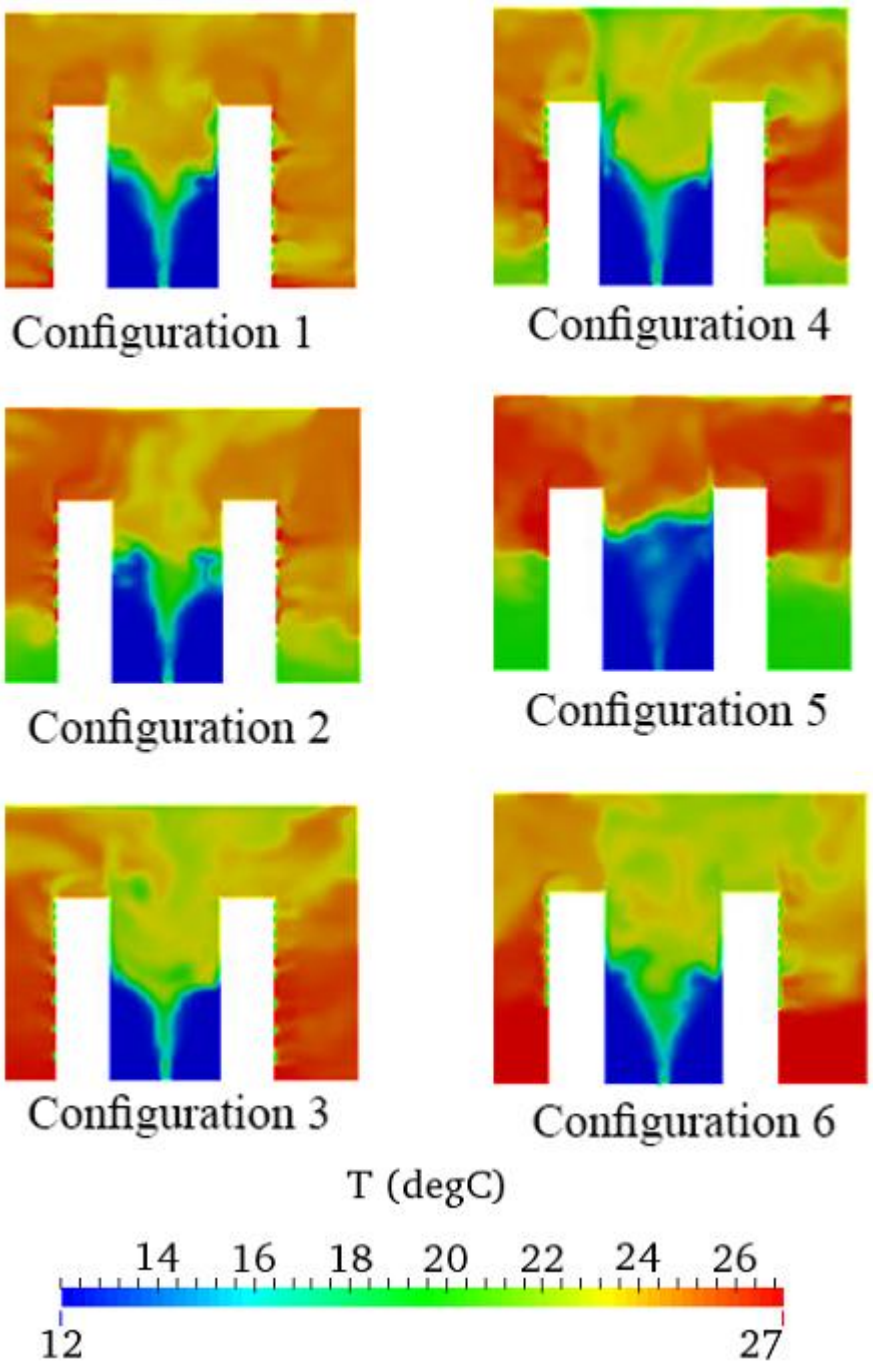

Figure 57: Instantaneous temperature values contours at the front of rack 6 ($x = 5.4m$).

To summarise this chapter, it was shown that the cooling effectiveness can be dramatically affected by the rack heat dissipation profile. For example, the thermal conditions at the intake of the servers are similar when the 1U servers are spread out across

the rack in any arrangement. In these configurations, the local hot spots at the exhaust of the racks are minimised which decreases the difference between the hot recirculated air and the cold air inside the cold aisle. This may reduce the benefit of the buoyancy forces which can prevent the hot air from being recirculated into the cold aisles. Whereas, the best cooling effectiveness was found when the blade servers are clustered at the top of rack. For this heat dissipation profile, the hot spots at the top of hot aisle are not affected by the 1U server exhaust air and hence the difference between the temperature of the recirculated air and the cold aisle is the same as the blade servers exhaust air temperature. The worst rack configuration scenarios were found to be when the blade servers are clustered at the middle and bottom of the rack as the recirculated air temperature is almost as same as the 1U servers exhaust air temperature with a slight advantage to clustering the blade servers at the middle.

As a point of reference, it is better to maximise the temperature difference between the hot aisle and the cold aisle to get better cooling effectiveness when considering any heat density profile at the exhaust of the rack cabinet. Although, in this case it should be noted that the upper part of the cold aisle servers would be subjected to high temperature because of the high return air temperature near these servers. Additionally, this study was conducted on the RF/RR-A configuration and other configurations would need to be studied separately to investigate their thermal performance.

5.5. Summary

Numerical simulations were carried out for different server arrangements to determine the best possible configuration with respect to the thermal performance of the data centre. Six different arrangements were considered by combining 1U servers and blade servers inside a single rack cabinet. These arrangements were aimed at investigating the best possible spacial profile of the rack heat dissipation inside the data centre room. The perforated tile flow rate was maintained constant for all rack cabinet arrangements. The hot air recirculation and thermal performance were analysed for each configuration. It was found both the hot air recirculation and temperature distribution within the data centre room rely heavily on the power profile across the rack. The best possible server

arrangement was found to be when the blade servers were clustered at the top of the rack cabinet. This resulted in the highest return air temperature. Whereas, the worst scenario was when the blade servers are clustered at the bottom of the rack cabinet, where the return temperature was found to be near the 1U server exhaust temperature. The rest of the scenarios were found to have similar thermal performance as all of these scenarios were found to have almost the same degree of mixing inside the hot aisles and consequently have similar return air temperatures. This showed that the return air temperature has a significant impact on the thermal conditions at the server intakes. These differences were attributed to the buoyancy forces in the flow since the perforated tile flow rate was constant for all configurations.

Chapter 6: Sub-Cooler for Rack Level Cooling

6.1. Introduction

Data centre cooling efficiency is a major concern for designers and operators as a large data centre may consume around 10-20 MW and the cooling process may consume half of this energy [9]. According to Cho and Kim [13] despite data centres having enough total cooling available, data centres may need further cooling in order to overcome local hot spots and requiring the installation of additional cooling equipment. This highlights the importance of designing an efficient cooling system and reduce the need to provide cooling rates exceeding the total server heat generation. In the literature, the rack level architecture and room layouts are found to have a large influence on the cooling efficiency of a data centre; however, rack level thermal analyses and their impact on data centre cooling efficiency have been discussed by few papers [11].

Hot air recirculation is the main source of the hot air infiltrating into the cold aisle, prior to be consumed by the servers. The matched air flow rate through the perforated tiles is not sufficient to eliminate hot air drawn into the upper and end racks [67, 69]. This suggests the need to modify current air cooling systems to overcome this problem. Therefore, it is proposed that a sub-cooler is installed at the top of each rack and integrated with the perforated tile supply system to overcome the hot air infiltration problem. In this design, the hot air drawn into these locations is directly cooled and leads to enhanced cooling efficiency and increased the server reliability. It also may lead to significant savings in the cooling power by reducing the total cold air quantity supplied to the data centre. This strategy has the advantage of being low cost and easy to implement through simple ducting connected through the ceiling.

Figure 17 shows the data centre which is the raised floor with flooded room return infrastructure (RR/RF-A). Figure 58 shows the proposed design where the hot air infiltration will be cooled by the cold air stream coming out of the sub-cooler at the top of the racks before entering the cold aisle. The main cooling air stream is supplied through the perforated tiles and the role of sub-cooler is to cool the hot return air. Gravity may

assist the cold air streams exiting the sub-coolers to not escape into the room space, instead it should be drawn down into the cold aisle. The cooling efficiency will be quantified while changing the cold air quantity supplied through the perforated tiles. The main objective of this chapter is to quantify any increase in cooling effectiveness due to the reduced cold air supply volume in this design.

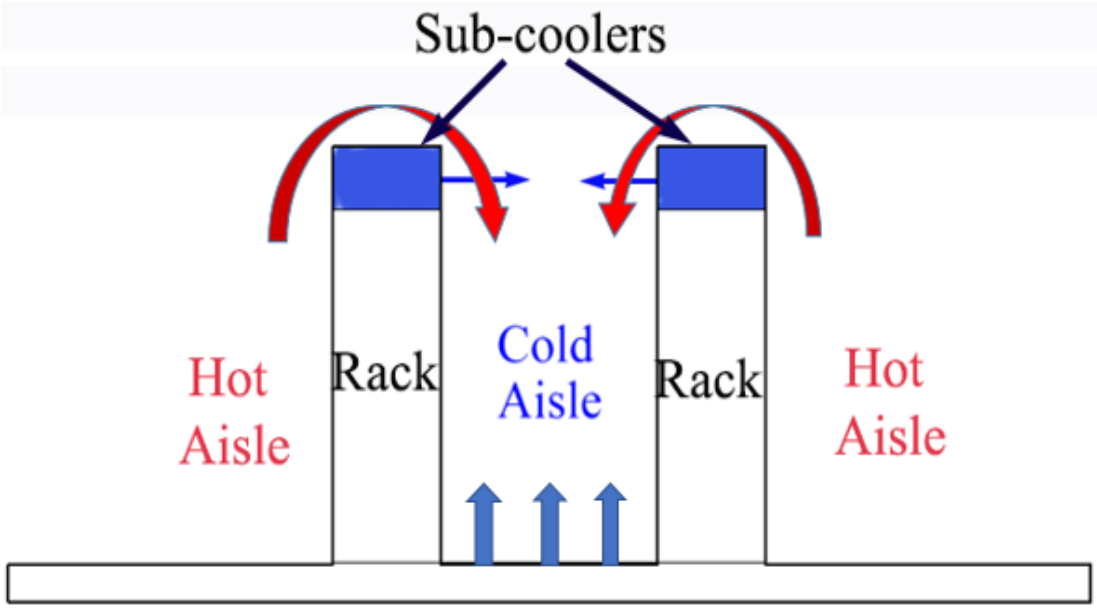

Figure 58: Schematic diagram of the proposed sub-cooler.

In the basic configuration of this design the cooling load needed by the data centre is supplied through the perforated tiles only. In the proposed design, the cooling load will be supplied through the perforated tiles and the sub-cooler. This will allow any enhancement in cooling effectiveness due to the presence of the sub-cooler to be measured.

The basic strategy is to use the same amount of energy more effectively. Therefore, with the help of the sub-cooler the perforated tiles cooling load will be decreased in three different scenarios, as shown in Table 20. In the first two scenarios, the data centre will be provided with a total cooling load equal to the heat generated by the servers. The main difference between these scenarios is that in scenario 2, part of the cooling load, 15% of

the total cooling load, will be provided by the sub-cooler and the rest of the cooling load will be provided by the perforated tiles, 85%. The aim of scenarios 3 & 4 is to demonstrate how energy could be saved by utilising the sub-cooler while at the same time keeping the cooling effectiveness in an acceptable range by maintaining the inlet temperature under a specified value to achieve reliable operation. The total cooling load will be decreased in scenarios 3 & 4 by an amount of 15% and 30%, respectively.

Table 20: Power optimisation scenarios.

	Perforated tile cooling load per rack	**Cooler cooling load per rack**	**Total cooling load per rack**	**Energy savings**
Scenario 1	7.8 kW (100%)	0 kW (0%)	7.8 kW (100%)	0%
Scenario 2	6.6 kW (84.6%)	1.2 kW (15.4%)	7.8 kW (100%)	0%
Scenario 3	5.43 kW (69.6%)	1.2 kW (15.4%)	6.63 kW (85%) (under provisioning)	15%
Scenario 4	4.26 kW (54.6%)	1.2 kW (15.4%)	5.46 kW (70%) (under provisioning)	30%

6.2. Numerical Modelling

In Chapter 4, the behaviour of the k-ε RANS model and k-ω SST SAS were evaluated and it was shown that the SAS model was more accurate for these simulations. Therefore, in this chapter the k-ω SST SAS turbulence model will be used in the numerical simulations. However, for this model there is an additional boundary condition imposed on the sub-cooler. This is represented as a constant velocity inlet to the domain with a temperature as given in Table 21. The table shows the velocity, temperature and pressure boundary conditions for the sub-cooler. The turbulence parameters boundary conditions are imposed as per that shown in Table 7.

Table 21: Sub-cooler velocity (U), temperature (T) and pressure (P) imposed boundary conditions.

Field	Mathematical formulation	OpenFOAM description
U	$U = U_{sub\text{-}cooler}$	`type surfaceNormalFixedValue; refValue uniform -0.82;`
T	$T = T_{sub\text{-}cooler}$	`type fixedValue; value uniform 285.15;`
P	$\nabla P.n = 0$	`type zeroGradient;`

6.3. Supply Heat Index (SHI)

The thermal performance of the proposed design will be measured using the Supply Heat Index (SHI). The SHI is the ratio of the heat gained by the cold air before entering the IT servers to the total heat gained by the air leaving the IT servers [13]. All data needed to evaluate the SHI can be computed from the CFD models. In an ideal situation, the rack inlet temperature is equal to the CRACs outlet temperature. However, because of hot air infiltration as well as hot air recirculation from the hot aisles to the cold aisles, the rack inlet temperature is, especially in the upper portion of the racks, usually higher than the CRACs outlet temperature.

To achieve an optimum cooling the SHI should tend to zero. Its maximum value is 100% in the case where the servers' inlet temperature is equals to the servers' outlet temperature though this cannot occur in practice as it implies zero heat output from the servers. Many researchers [4, 13, 29, 106, 107] argued that the SHI can give an efficient evaluation of the recirculation phenomena. The SHI can be defined as:

SHI= (The enthalpy rise in the cold aisle)/(The total enthalpy rise at the rack exhaust)

The enthalpy rise in the cold aisle can be computed by:

$$\delta Q = \sum_{j,i} m_{i,j}^{j} C_p [(T_{in}^{r})_{i,j} - T_{ref}] \quad 6.3.1.$$

The total enthalpy rise at the rack exhaust can be computed by:

$$Q = \sum_{j,i} m_{i,j}^{j} C_p [(T_{out}^{r})_{i,j} - (T_{in}^{r})_{i,j}] \quad 6.3.2.$$

Where $m_{i,j}^{j}$ is the mass air flow through i^{th} rack in the j^{th} row of racks, $(T_{out}^{r})_{i,j}$ and $(T_{in}^{r})_{i,j}$ average inlet and outlet temperature from i^{th} rack in the j^{th} row of racks, and T_{ref} is the vent tile supply air temperature. The equations and parameters' notations were adapted from [13].

The SHI is calculated by:

$$SHI = \frac{\delta Q}{Q + \delta Q} \quad 6.3.3.$$

Or

$$SHI = \frac{T_{in}^{r} - T_{ref}}{T_{out}^{r} - T_{ref}} \quad 6.3.4.$$

6.4. Cooling Effectiveness Enhancement and Energy Savings

The effect of the proposed design on the pressure, airflow and temperature distribution will be investigated especially within the cold aisle. It is anticipated that the cold air flow streams of the sub-cooler will cool the hot air infiltrating into the cold aisles and may allow decreasing the cooling energy supplied to data centre. In this section, these interactions will be investigated along with the viability of using the sub-cooler in the data centre cooling system.

6.4.1. Pressure Variations within the Data Centre Room

The main driving force of the fluid flow within the data centre room is the pressure. Therefore, the effect of the sub-cooler on the pressure distribution is shown in Figure 59. The figure shows four horizontal planes for the pressure distribution at a height of 1.8 m. These planes are located at the top part of the racks, which is considered as one of the most critical regions of the data centre room. The ratio between the pressure at the top of the cold aisles to the data centre room space plays a vital role in the amount of hot air infiltration into the cold aisles from the rest of the room. If the ratio drops significantly, more hot air finds its way to the servers' inlets.

In the basic configuration without the sub-cooler, scenario 1, the pressure at the upper part of the cold aisle is slightly lower than the data centre room pressure. Moreover, with the presence of the sub-cooler for scenarios 2-4, the pressure of the data centre room decreased dramatically. Also, it can be noted that the ratio between the pressure at the top of the cold aisle and the data centre room space pressure decreased for the configurations with the sub-cooler. This is because of the sub-cooler air streams, where the dynamic pressure increased in the expense of the static pressure. This can lead to more hot air infiltration into the cold aisle which could be considered as a drawback for the sub-cooler.

Additionally, a number of points in the room were sampled in order to know how the pressure changes within the cold aisles. 50 points were sampled over a line in the middle of each cold aisle from the floor up to the ceiling. As Figure 60 shows, the pressure variation is similar for all scenarios except that the lowest pressure for scenario 1 is at the top of the cold aisle. Whereas, for the other scenarios the lowest pressure is at a lower height, z=1.7m, which also may lead to more hot air infiltrating into the cold aisle from the data centre room. It is also noted that the pressure in the data centre room affected by the perforated tile flow rate where the pressure decreased with a decrease in the perforated tile flow rate, as evident by the figure.

The above analyses illustrate that the sub-cooler can have a significant negative impact on the pressure distribution within the data centre room. It could lead to more hot air infiltrating into the cold aisle which may cause the server's inlet temperature to be

increased as the relative pressure between the top of the cold aisle and the data centre room space dropped drop significantly.

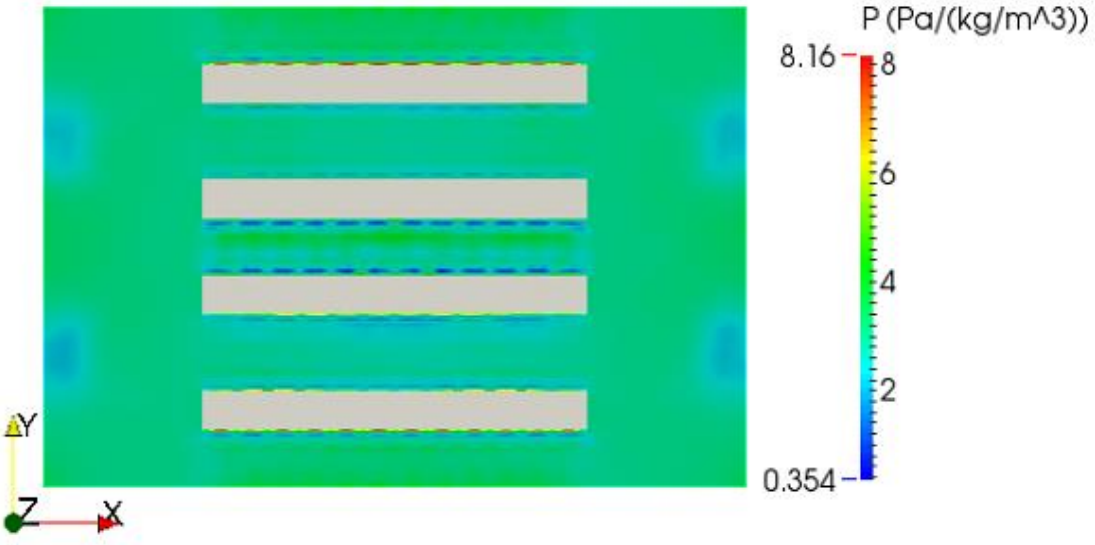

a- Scenario 1.

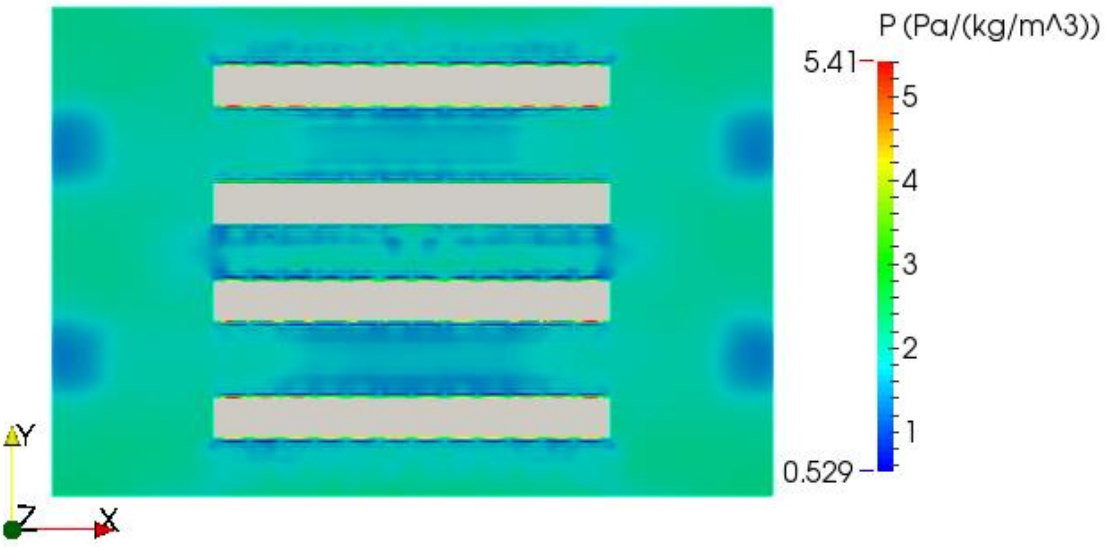

b- Scenario 2.

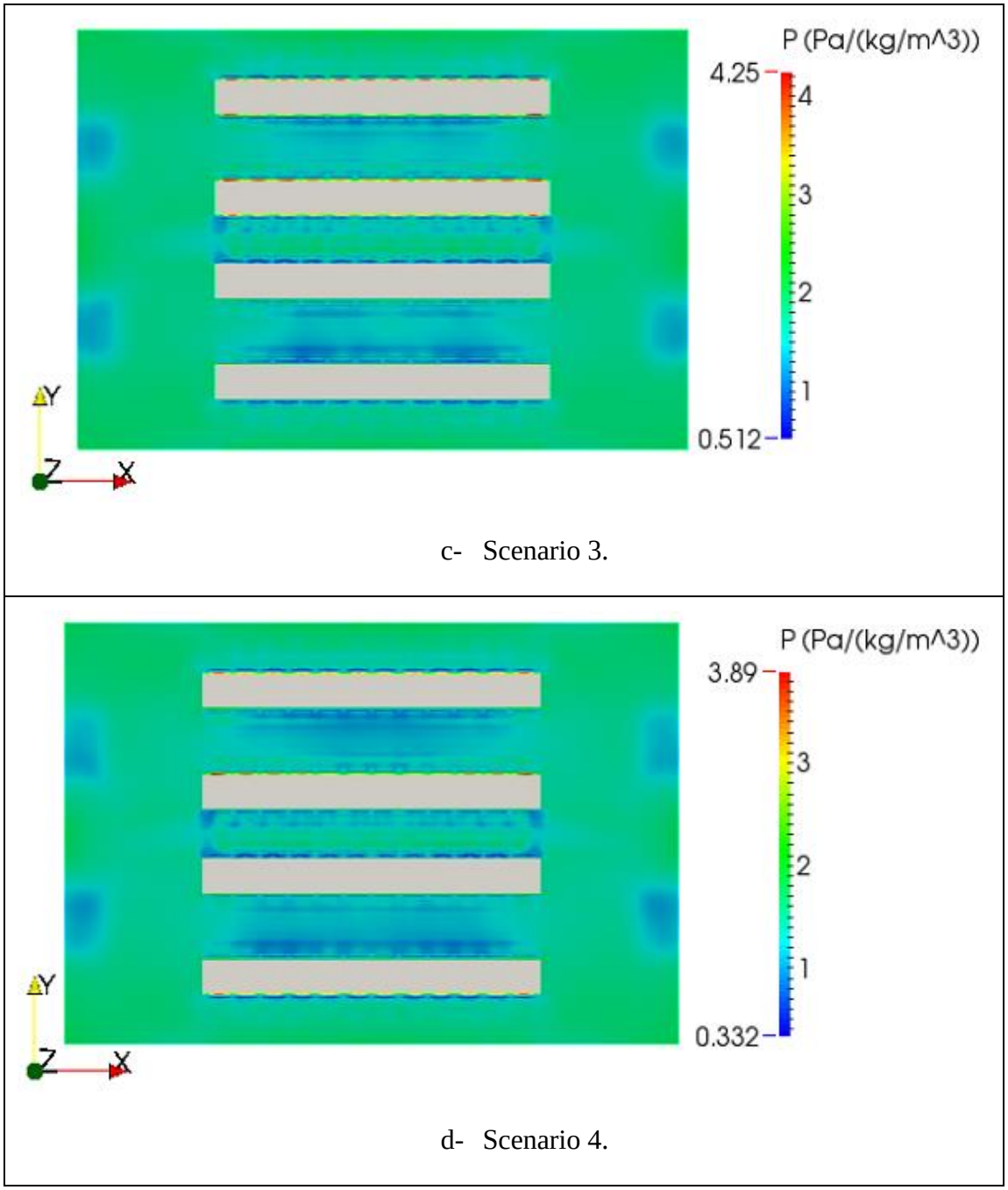

c- Scenario 3.

d- Scenario 4.

Figure 59: Instantaneous pressure distribution at the top of the racks for all scenarios, $z = 1.8\,m$.

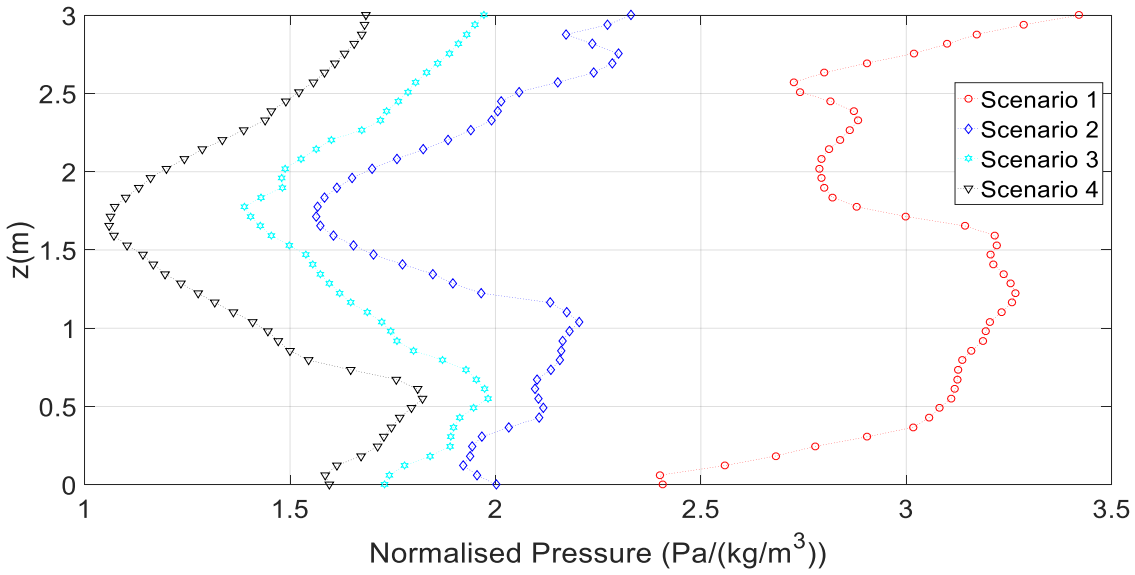

Figure 60: Time-averaged pressure distribution within the middle of the cold aisle from floor up to the ceiling.

6.4.2. Hot Air Infiltration

As illustrated in the last section the pressure of the data centre room is negatively affected by the sub-cooler. This in turn will affect the hot air recirculation into the cold aisle. Figure 61 shows the hot air recirculation contour for the suggested scenarios. The plane is located at the top of the racks to show the hot air recirculation into the cold aisles. From the figure it is clear that the velocity of the hot air at the top of the cold aisle is affected by both the sub-cooler and the perforated tile flow rate. For the configuration without the sub cooler, scenario 1, the hot air infiltration speed at the top of the cold aisle is about 0.7 m/s; whereas, for the rest of the scenarios, it increases into about 1 m/s. At the end racks, the hot air infiltration speed is similar except for scenario 4 where more air directly infiltrates into the racks. This can be attributed to the low velocity jets speed coming out of the perforated tiles. This can affect the intake temperature for the IT servers located in these regions. It is expected that with a lower cooling flow rate supplied to the cold aisles and higher hot air infiltration, the end rack server intake temperatures will increase.

It is expected that the hot air infiltration will be affected by the pressure distribution. Therefore, temperature profiles were taken in order to identify the hot air infiltration pattern for each scenario, where 50 points were sampled over a line in the middle of each aisle from the floor up to the ceiling. Figure 62 demonstrates the hot air infiltration, U_z (m/s). It is seen in the figure that the hot air infiltration is found for scenario1 to be an upwards velocity of U_z=0.3(m/s) in the middle of the cold aisle which means that no hot infiltration into the middle of the cold aisles in this scenario. While, for the rest of the scenarios the downwards velocity was U_z=0.4(m/s) in the middle of the cold aisle. Moreover, the patterns in scenarios 1 and 2 are similar because the air velocity from the perforated tiles is high which may resist the infiltration of hot air. For scenarios 3 and 4 the hot air infiltrates into the middle of the cold aisle with minimal resistance from the perforated tiles flow because of the lower speed which allows for the hot air to penetrate further into the middle of the cold aisle without any disturbance.

It is noted that the sub-cooler negatively affects the hot air infiltration due to its effect on the pressure distribution. The worst scenario was found to be for scenario 4, where hot air infiltrates not only into the middle of the cold aisles, but also the end racks are affected by hot air streams in contrast the rest of the scenarios. The main reason for that is the low flow rate from the perforated tiles. This will have a negative impact on the cooling effectiveness unless the hot air infiltration is cooled down by the sub-cooler prior entering the cold aisle. This will be investigated in the next section.

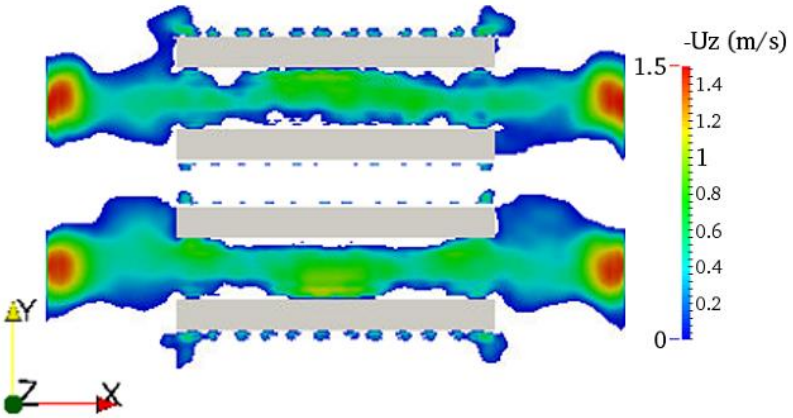

a- Scenario 1.

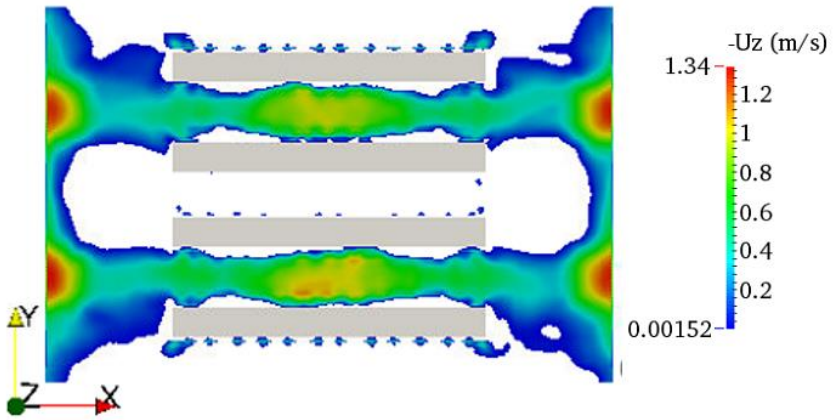

b- Scenario 2.

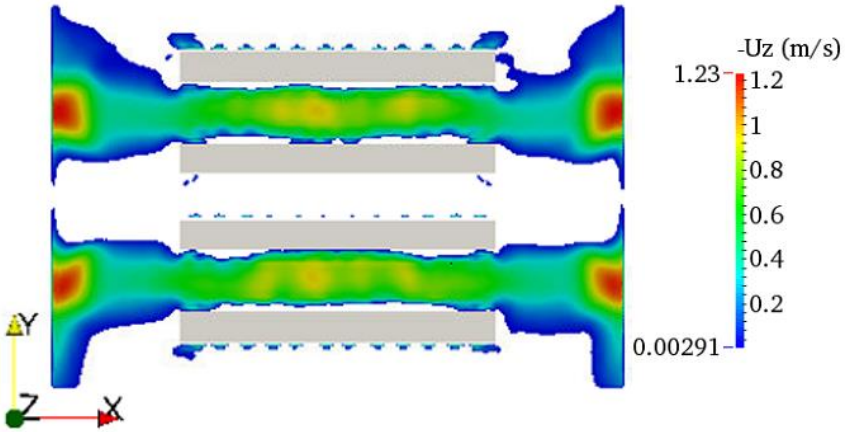

c- Scenario 3.

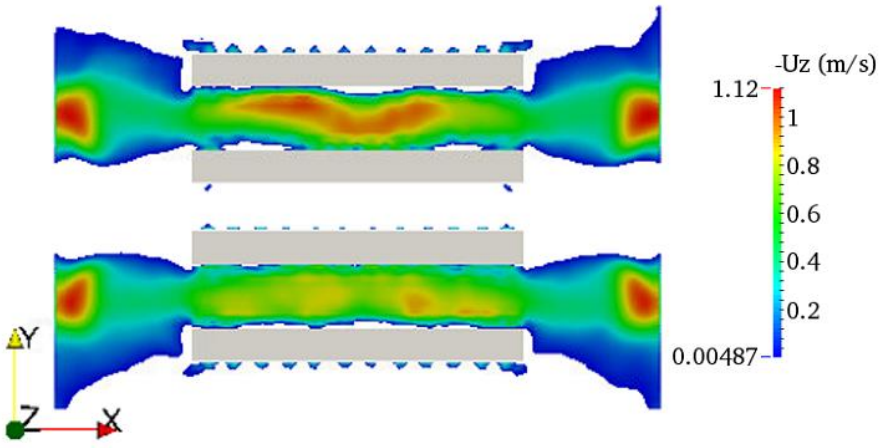

d- Scenario 4.

Figure 61: Hot air infiltration into the cold aisle at the top of the racks, $z = 1.8\,m$.

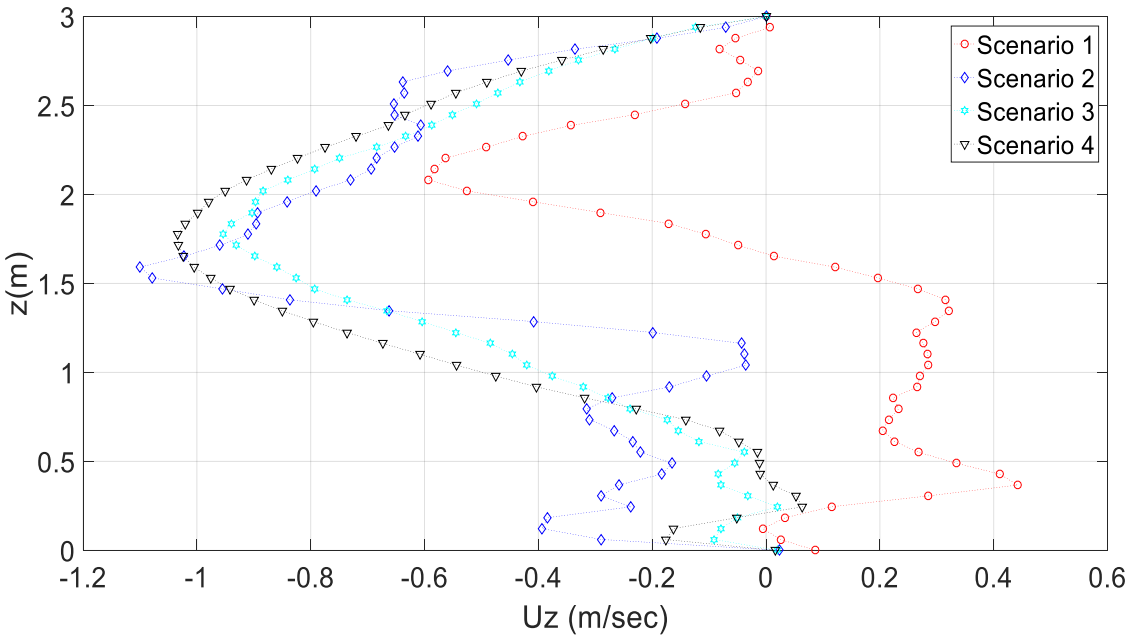

Figure 62: Hot air infiltration velocity vector (time-averaged), U_z (m/s), into the cold aisle at the middle of the cold aisle.

6.4.3. Thermal Performance

To assess the viability of using a sub-cooler in the data centre cooling system, the temperature distributions in the data centre room and in front of the IT server racks were explored. Four horizontal planes at the top of the racks are shown in Figure 63 for each

scenario. It can be seen in Figure 63 (a-d) that the presence of the sub-cooler enhances the thermal conditions dramatically at the top of the racks. For scenario 1, the temperature of the air at the top of the server racks is almost as same as the servers' outlet temperature. The air infiltrating into the cold aisle is highly influenced by the room environment temperature and in this case the IT servers would be excessively overheated especially those towards the top of the cold aisle. Whereas, for the rest of the scenarios, the sub-cooler greatly reduces the room temperature in this region as Figure 63 (b-d) illustrate. The under provisioning of cooling capacity has a noticeable effect on the room environment temperature which increases with the decrease in cooling capacity supplied through the perforated tiles. However, the room thermal conditions for the least under provisioned scenario, scenario 4, with 70% of the total needed energy, is much better than the room thermal conditions for scenario 1 where 100% of the total needed cooling energy was supplied.

Figure 64 (a-d) shows the temperature contour at the front of the same server racks with and without the sub-cooler. The figure shows the hot air infiltration patterns for the modelled scenarios. Figure 64 (a) shows that there is significant amount of hot air that infiltrates into the middle and end racks which will affect the reliability of the adjacent servers. Hence, it is important to overcome this issue by employing appropriate cooling solutions to keep the intake servers' temperature within acceptable limits. The suggested sub-cooler successfully mitigated the temperature at the intake of the severs as Figure 64 (b-d). Even though the hot air infiltration from the room environment has increased significantly because of the sub-cooler, it was cooled down to acceptable conditions before being drawn into the servers' inlets. Apart from some limited hot spots in the second scenario, the thermal conditions in the cold aisle have been greatly enhanced. For the third scenario, the hot spots increase noticeably due to the supply air under provisioning through the perforated tiles. It is also noted that in the fourth scenario, the hot spots increase dramatically for both the middle and end racks because of the further decrease in the cooling capacity supplied through the perforated tiles. This had a negative

impact on the supply air temperature which deteriorated the thermal conditions in the cold aisle.

It is clear that the thermal conditions in the data centre do not depend only on the cooling system total capacity, but also on the way that the cold air is supplied to the data centre. Scenarios 1 and 2 had the same cooling capacity; however, scenario 2 had much better thermal performance due to the presence of the sub-cooler since part of the cold air was supplied through the sub-cooler which cooled the hot air prior to entering the cold aisle, despite the fact that the hot air recirculation increases because of the sub-cooler as discussed in the previous section. Although, the cooling capacity was decreased by of 15% for scenario 3, its thermal performance was better than scenario 1 where the total cooling load was supplied. The thermal performance is comparable for scenarios 1 and 4. However, further analysis is required to identify which of these four scenarios has better cooling effectiveness. In the next section SHI will be determined to assess the cooling effectiveness.

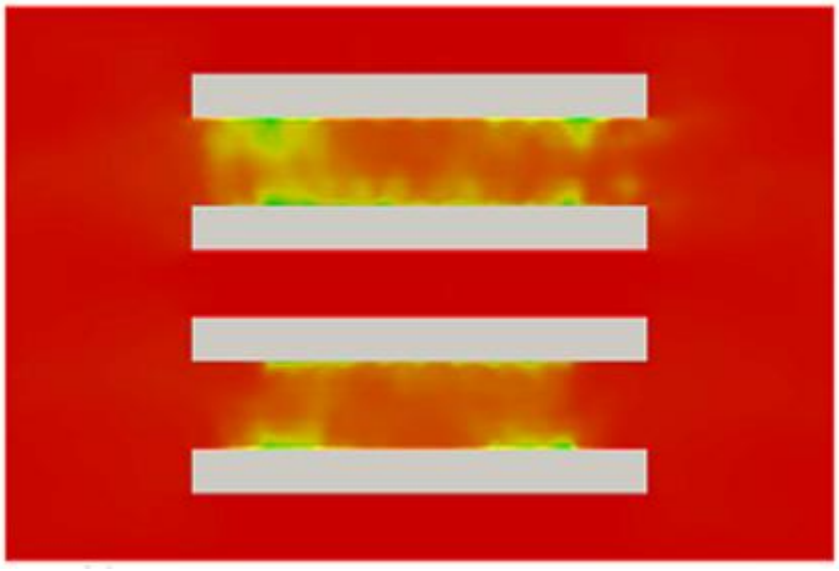

a- Scenario 1.

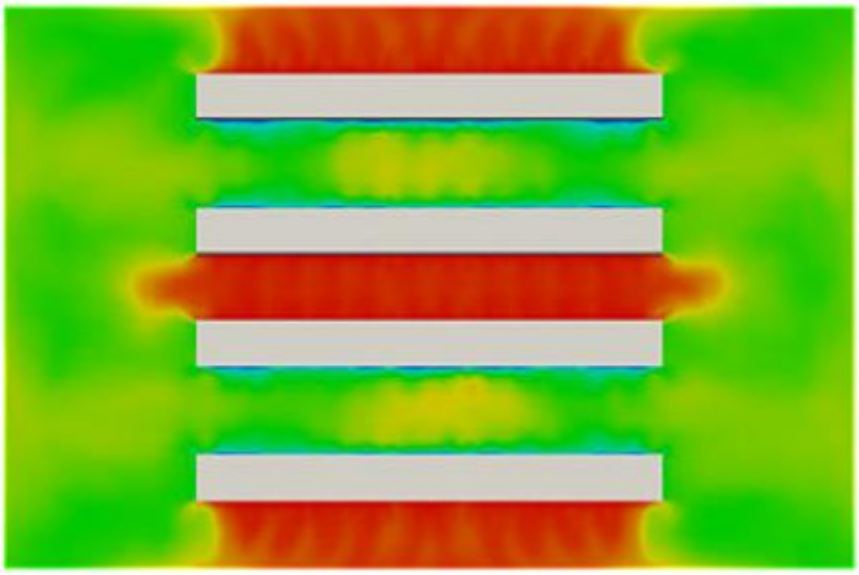

b- Scenario 2.

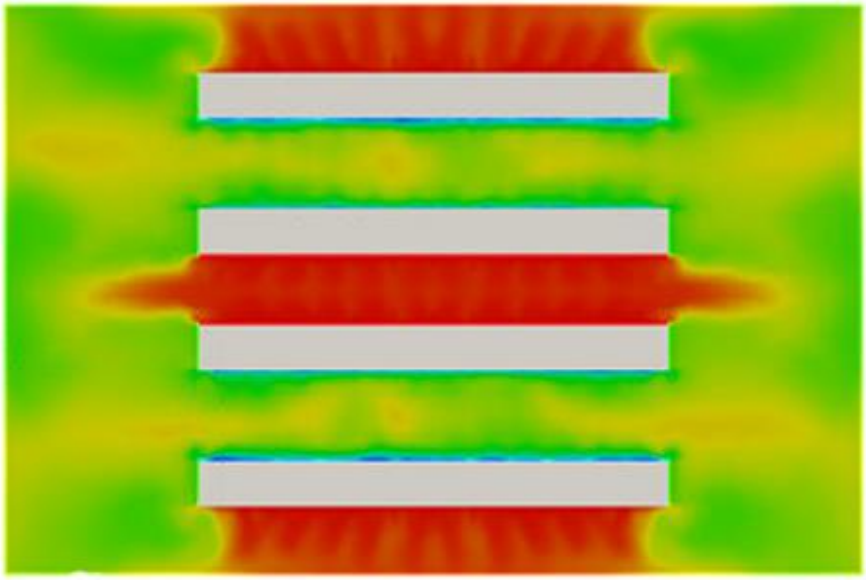

c- Scenario 3.

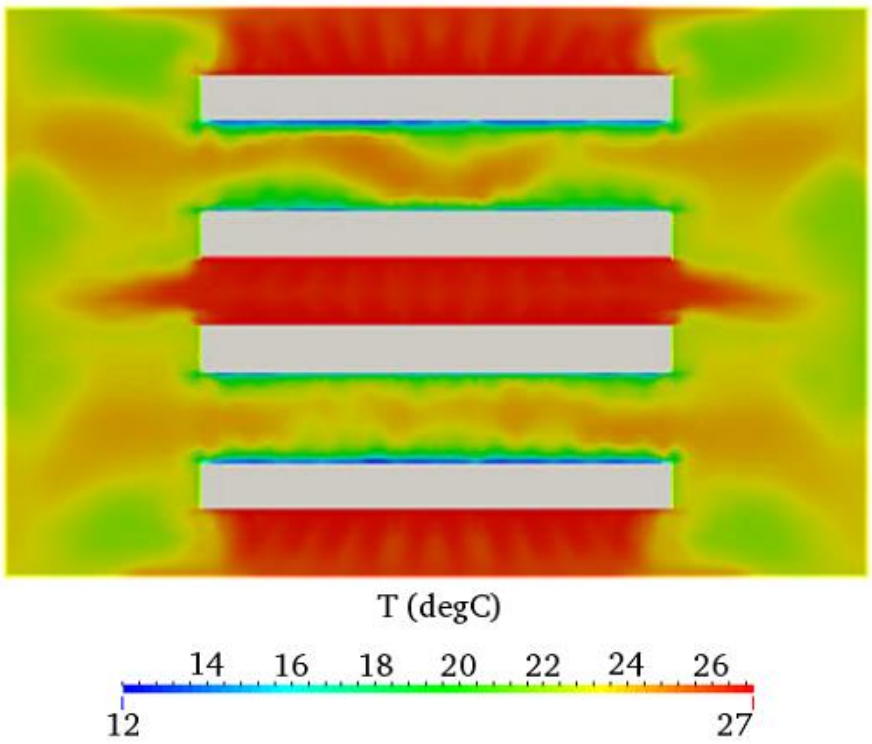

d- Scenario 4.

Figure 63: Instantaneous temperature distribution at the top of the cold aisles, $z = 1.8\ m$.

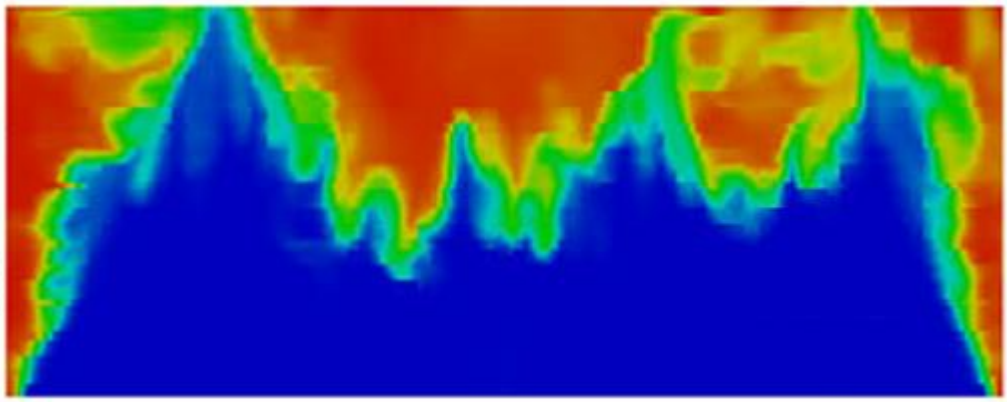

a- Scenario 1.

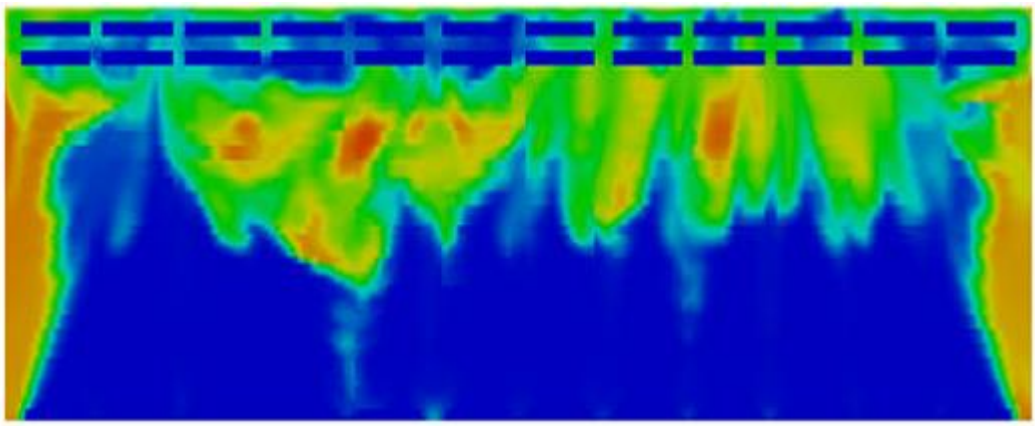

b- Scenario 2.

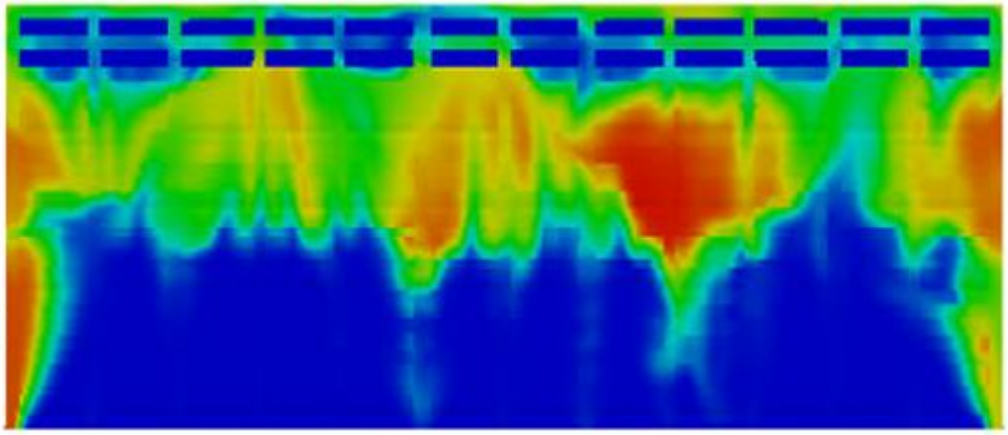

c- Scenario 3.

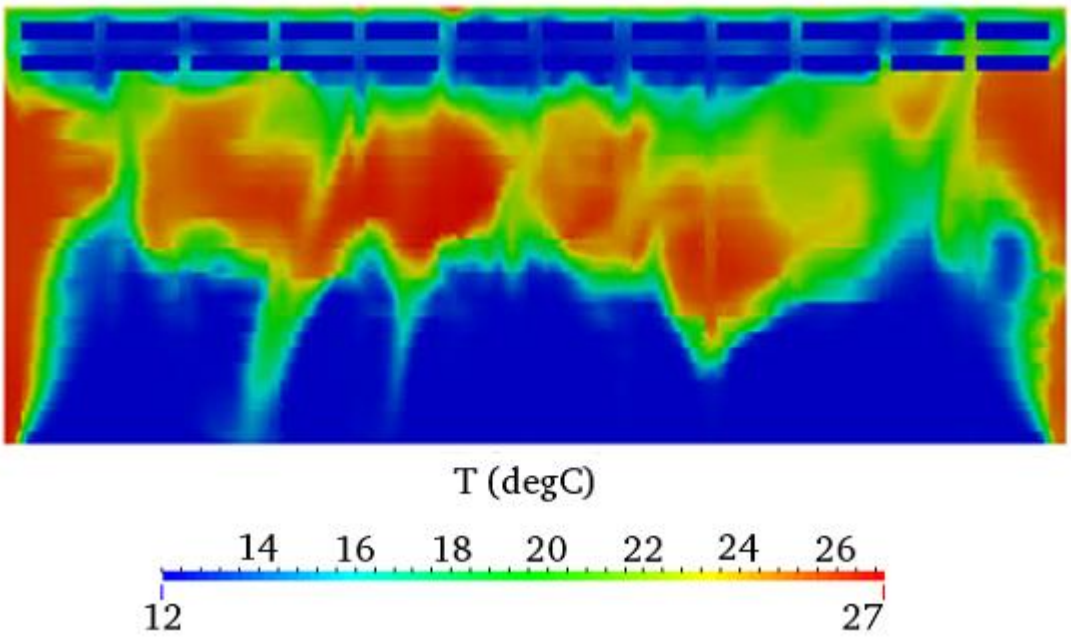

d- Scenario 4.

Figure 64: Instantaneous temperature values contours at the front side of the severs.

To understand the cooling effectiveness, the SHI will be used as a measure of the thermal performance of the modelled scenarios. Figure 65 shows the overall SHI for the basic and optimised configurations. It is clearly seen in the figure that the thermal performance for the basic configuration is unsatisfactory with the SHI about 32%; whereas, for scenario 2 it dropped significantly to 20% which is considered as an acceptable value. The total cooling capacity supplied into the data centre for these two scenarios is the same. Furthermore, due to the cold air under provisioning in scenarios 3 and 4, the SHI for increased compared to scenario 2. For scenario 3, the thermal performance is still better than the basic configuration with 26%. However, for scenario 4, the thermal performance is comparable to the basic configuration with an SHI of 34% due to the lack of the cold air supplied through the perforated tiles.

It has been found that for the RF/RR infrastructure, the hot air infiltration into the cold aisle is not uniform for all the racks. The middle racks and end racks will exhibit two different patterns of hot air infiltration. The SHI for the four middle racks is shown in

Figure 66. Surprisingly the best thermal performance is for the basic configuration without the sub-cooler. This can be attributed to the sub-cooler changing the pressure distribution and velocity in the middle of the cold aisle; therefore, less hot air will infiltrate into the middle of the cold aisle for this scenario. While, for the rest of the scenarios, the hot air will infiltrate into the lower portion of the cold aisle. Additionally, the SHI for the four middle racks for scenarios 2 and 3 is comparable, with a value about 28%. The worst thermal performance is for the scenario 4 where the SHI is noticeably higher than in the rest of the scenarios. The drawback with scenario 1, however, is that there will be problematic servers in the upper part of the cold aisle, where the intake temperature will exceed the acceptable limit due to the high return air temperature penetrated from the room unlike scenario 2 (as the temperature contour in the previous section showed). Figure 67 shows the SHI for the racks located at the end of the cold aisle. The sub-cooler enhanced the thermal conditions for these racks significantly where the SHI drops from about 69% for the scenario 1 to about 30% for the scenario 2. Also, the under provisioning of the cold air affected the SHI noticeably for scenarios 3 and 4. However, the SHI for scenario 4 is much better than SHI for the first scenario. This can be attributed to the room environment having better thermal conditions under the presence of the sub-cooler.

In general, the best cooling effectiveness among the scenarios was for scenario 2 while the worst thermal performance was for scenario 1 and 4. It is obvious that the sub-cooler enhanced the thermal conditions for the data centre dramatically. Moreover, scenario 3 also has good cooling effectives with a lower cooling capacity.

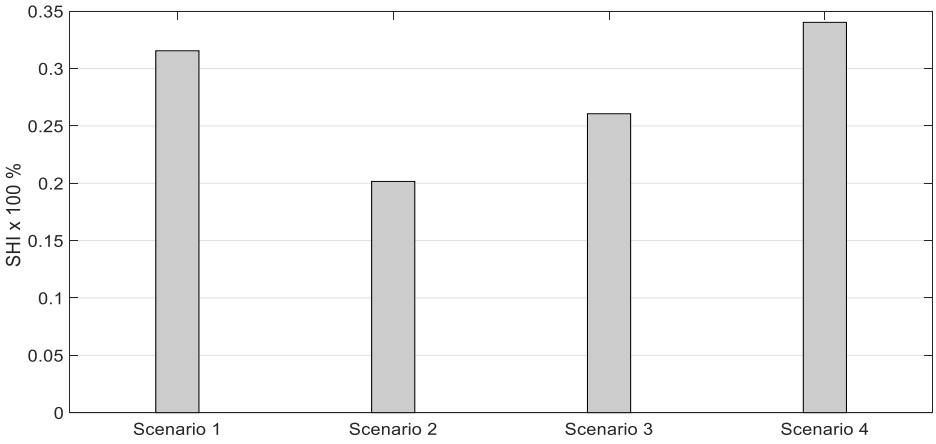

Figure 65: Overall SHI for the optimised configuration.

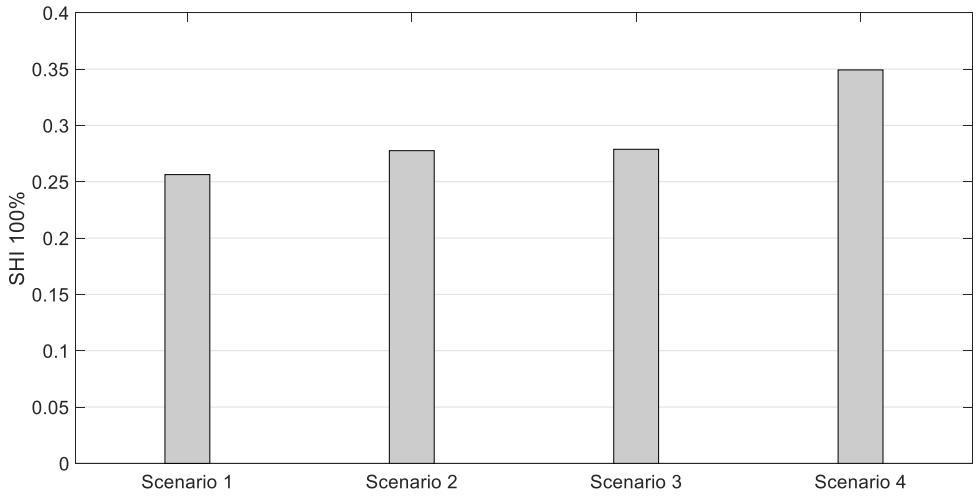

Figure 66: Middle racks SHI for the optimised configuration.

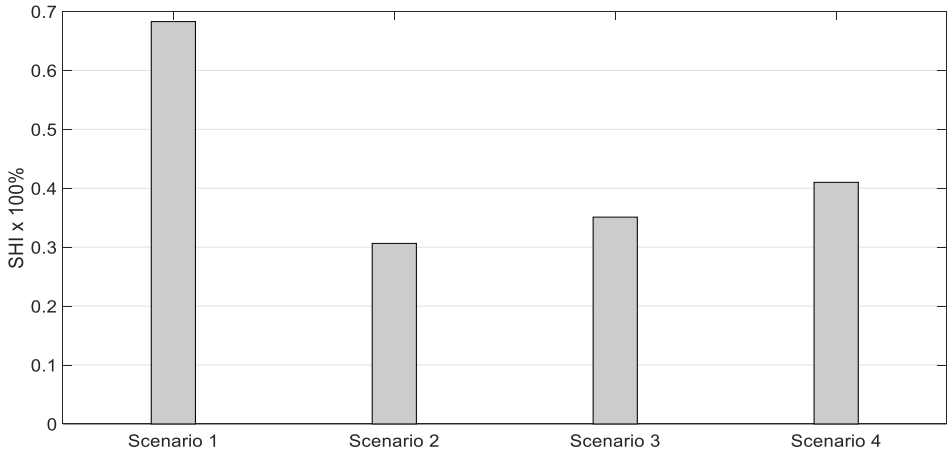

Figure 67: End-racks SHI for the optimised configuration.

6.5. Summary

In this chapter, analysis of a rack level sub-cooler to assist the perforated tile air flow rate has been conducted. In the design part of the CRAC cold air flow is supplied through the sub-cooler at the top of the cold aisle. It was found that this approach has a negative impact on the pressure and air flow distribution within the data centre room by increasing the hot air recirculation into the cold aisles. However, because the main source of the hot air recirculation is from the upper part of the cold aisles, the sub-cooler was able to cool down the hot air before it is drawn into the servers. Therefore, the servers' intake temperature was maintained within the manufacturer's specifications when supplying 100% and 85% of the total cooling capacity required by the data centre. Furthermore, when providing 70% of the total cooling capacity of the data centre, the thermal performance was not acceptable due to the lack of flow from the perforated tiles.

This chapter illustrates that wise use of the available cooling resources in data centre is essential. Also, it is not necessarily the case that supplying the full cooling capacity will guarantee acceptable thermal and energy performance. This was demonstrated in this chapter by the use of rack-level sub-cooler, where enhanced

effectiveness allowed acceptance performance to be achieved at with only 85% of the total cooling load provided to the data centre.

Chapter 7: Conclusion

7.1. General Discussion

Data centre power consumption is increasing dramatically due to a global increase in the demand for computational resources. Additionally, cooling of data processing equipment inside a data centre room can consume around 50% of the total power used by the data centre [10]. This highlights the importance of enhancing cooling effectiveness, not only to for operational reasons, but also to save energy. In this thesis an air-cooled data centre was considered due to its wide adoption in data centre designs. In an air-cooled data centre proper airflow management is critical to achieve satisfactory cooling of the equipment. However, the task of properly managing the airflow is difficult due to the complex interactions between different airflow paths within the data centre room.

To understand the characteristics of these flows, detailed measurement is required. As such detailed numerical simulations were conducted using computational fluid dynamics. The open source toolbox OpenFOAM was used to simulate the airflow and heat transfer inside the data centre room. Initially, validations were conducted for two candidate turbulence models. The first validation was made by comparing numerical results with vented enclosure experiments conducted by Tiong [100] at Curtin University. Good agreement was observed between the numerical simulation results and the experimental data for temperature, pressure and velocity for the available experiments conducted with the vented enclosure. Further validation was conducted for buoyancy driven flows against the benchmark numerical solution for natural convection of air in a square cavity carried out by De Vahl Davis [101] and again excellent agreement was observed. On this basis, the turbulence models and the selected boundary conditions were considered suitable for simulating the airflow and temperature variations in the full-scale data centre models.

A review of the literature revealed that the k-ε RANS (Reynolds Averaged Navier-Stokes) turbulence model has been used extensively (and almost exclusively) to explore the airflow and temperature distribution within data centres. It was found that simulations

using this model give reasonably accurate results for the average velocity, pressure and temperature in many industrial applications, especially for fully developed turbulent flows. While the k-ε model (and RANS models in general) have the benefit of being less computationally intensive compared to DES (Detached Eddy Simulation) models, they may behave poorly in cases of high streamline curvature, severe pressure gradients and flow separation. All of these features are potentially present in a data centre due to the complex interactions between different air streams. An aim of this thesis was to explore whether DES models provide additional insight into data centre flows. As such the majority of the work in this thesis used the k-ω SST SAS model to capture turbulence. To allow this a modified version of the buoyantBoussinesqPimpleFoam solver was developed during the first stages of the work to allow DES solutions to be performed. Apart from the comparisons in Chapter 4 all numerical simulations presented in this thesis were conducted by using the k-ω SST SAS turbulence model.

Chapter 4 presents the comparison of the two candidate turbulence models. In this chapter the k-ω SST SAS (Scale Adaptive Simulations) turbulence model was used, for the first time, to model the flows within a data centre. The k-ω SST SAS model is a hybrid model, using a RANS model near the wall and an LES approach away from the wall. Although this model was much more computationally intensive than the k-ε RANS model, it allowed large transient turbulent structures to be captured. Qualitative and quantitative comparisons with these results and those using the k-ε RANS model were carried out. Statistical analysis of the rack inlet temperatures showed that for the room return infrastructure configurations, the k-ω SST SAS model is better able to predict the hot air infiltration for the racks located in the sides of the cold aisle. For the ceiling return infrastructure configuration, the discrepancy was lower between the turbulence models and acceptable agreement was seen for all racks and k-ε RANS demonstrated good performance. However, in general using the k-ε RANS turbulence model for data centre numerical simulations can have significant shortcomings due to its inability to correctly predict air movement around rack corners which may result in misleading results.

Chapter 5 focussed on finding the optimal arrangement of 1U and blade servers stacked within a single data possessing cabinet. Six different server arrangements were

considered and the resulting room level thermal performance was investigated. To eliminate the effect of supply airflow on the results, the perforated tile flow rate was kept constant for all rack cabinet arrangements. This allowed the best possible spatial distribution of rack heat dissipation inside the data centre room to be identified. It was found that clustering blade servers at the top of the rack cabinet gave the best thermal performance. This was attributed to the return air temperature having a significant impact on the thermal conditions at the servers intake. Further, it was proposed that the chief reason for this was differences in the buoyancy forces. It was found that as the return air became hotter the thermal conditions at the intake of the servers was noticeably enhanced due to the high difference between the density of the hot return air and that of the air in the cold aisle. This prevented the hot air from being infiltrated into the cold aisles.

Chapter 6 proposed and investigated a method for increasing data centre thermal performance and energy savings through the installation of a sub-cooler at the top of the equipment racks. This is significant as most of the previous work on data centre cooling has focussed on airflow management considering only rack architecture and room layout, excluding rack level thermal analysis which might be harnessed to enhance the data centre cooling effectiveness. Four different scenarios were analysed to study the effect of the sub-cooler on the thermal performance and energy savings for the RF/RR configuration with perpendicular CRAC units. The reference configuration, scenario 1, was the default scenario without a sub cooler installed and the full cooling load capacity was supplied through the perforated tiles. For the other scenarios a part of the cooling load capacity was supplied by the sub-cooler while the rest was supplied through the perforated tiles. The total cooling load capacity supplied to the data centre for the first two scenarios were 100% and 85% of the servers' heat dissipation, respectively, while for scenarios 3 and 4 the cooling capacities were 85% and 70% of the total heating load of the servers. The results showed that the sub-cooler has significant positive effect on both the thermal performance and energy savings. Furthermore, it was clearly demonstrated that wise use of cooling resources can give good benefits, a point which should be taken into account data centres operators. It is accepted that supplying the full cooling capacity does not necessarily guarantee acceptable thermal and energy performance in a data centre. However, through the addition of a sub-cooler, the cooling effectiveness was shown to be

dramatically enhanced even at only 85% of the cooling capacity load required by the data centre.

In summary, this thesis presented a detailed analysis of air-cooled data centres using CFD. The k-w SAS turbulence model was evaluated and found to be an improvement on RANS based turbulence models, which have been used almost exclusively for these simulations in the past. Furthermore, the cooling effectiveness was increased for a data centre in two different ways. Firstly, careful clustering of servers in a single data processing equipment allowed increasing the heat generation rates for a given room size, and secondly, a novel sub cooler was proposed to be installed at the top of data processing equipment. This showed dramatic improvement in the thermal conditions at the intake of the servers as hot return air was cooled prior to intake. Applying the results of this work to new and existing data centre designs should allow increased operating efficiency in the future.

7.2. Future Work

This thesis allows an increased understanding of data centre flows and demonstrates that further improvement is not only important but possible. As a result of this work, and so that the benefits can be realised in practice some recommendations on future work are listed below:

- To improve the accuracy of data centre numerical simulations customised software for data centre design should adapt DES based turbulence models. This will allow detailed boundary conditions to be generated for CRAC units, servers and all other complex equipment, while also improving predictions.
- In this thesis the data centre cooling effectiveness was simulated for RF/RR data centre configurations. Alternative configurations should be studied separately to investigate their thermal performance as the observations made in this thesis may not be directly applicable due to changes in supply and return vents.

- While the integrated sub-cooler investigated in this thesis is novel only configurations where it was installed at the top of the rack were investigated. However, there is no obvious reason why it could not be installed at the rack sides or in-between racks. Examining the thermal performance in these different scenarios would be a useful undertaking.
- Similarly, the sub-cooler was investigated in a RF/RR configuration data centre, again it would be useful to explore the thermal performance of a data centre with sub-coolers installed on the ceiling, as this work has demonstrated that the return vent can noticeably impact the air movement in the data centre.

7.3. Summary of Thesis Contributions

This thesis added to the understanding of complex data centre airflow and heat transfer by conducting detailed CFD simulations on common, as well as new configurations. This thesis has contributed to the field by:

- Identifying limitations of the k-ε RANS turbulence model for data centre simulations and proposing the k-ω SST SAS turbulence model as a more suitable replacement, particularly for identifying hot-air infiltration into the cold aisles.
- Establishing that buoyancy forces are a key mechanism affecting the airflow, particularly infiltration, and the resulting thermal performance of a data centre. Understanding this mechanism allowed the volumetric heat generation rates for a given room size to be increased by careful clustering of servers with different heat generation rates to take advantage of buoyancy effect to minimise infiltration.
- Proposing a novel rack sub cooler to enhance thermal performance. The idea and final design was influenced by understanding the problem of infiltration, and that local cooling can reduce its effects to the extent that adequate thermal performance can be achieved even in under-provisioned data centres.

References

Every reasonable effort has been made to acknowledge the owners of copyright material. I would be pleased to hear from any copyright owner who has been omitted or indirectly acknowledged.

[1] A. Habibi Khalaj and S. K. Halgamuge, "A Review on efficient thermal management of air- and liquid-cooled data centers: From chip to the cooling system," *Applied Energy,* vol. 205, pp. 1165-1188, 2017.

[2] S. Ratnesh, B. Cullen, and P. Chandrakant, "Dimensionless Parameters for Evaluation of Thermal Design and Performance of Large-scale Data Centers," in *8th AIAA/ASME Joint Thermophysics and Heat Transfer Conference*(Fluid Dynamics and Co-located Conferences: American Institute of Aeronautics and Astronautics, 2002.

[3] J. Cho, T. Lim, and B. S. Kim, "Cooling Systems for IT Environment Heat Removal in (Internet) Data Centers," *Journal of Asian Architecture and Building Engineering,* vol. Vol. 7 (2008) No. 2 P 387-394, 2008.

[4] H. Bhagwat, A. Singh, A. Vasan, and A. Sivasubramaniam, "Faster exploration of data centre cooling using thermal influence indices," *Sustainable Computing: Informatics and Systems,* vol. 3, no. 3, pp. 120-131, 2013.

[5] M. K. Herrlin, "Rack Cooling Effectiveness in Data Centers and Telecom Central Offices: The Rack Cooling Index (RCI)," *ASHRAE Transactions,* vol. 111, pp. 725-731, 2005.

[6] R. R. Schmidt and M. Iyengar, "Best Practices for Data Center Thermal and Energy Management--Review of Literature," *ASHRAE Transactions,* vol. 113, no. 1, 2007.

[7] S. Nada, M. Said, and M. Rady, "CFD investigations of data centers' thermal performance for different configurations of CRACs units and aisles separation," *Alexandria Engineering Journal,* vol. 55, no. 2, pp. 959-971, 2016.

[8] B. Norouzi-Khangah, M. B. Mohammadsadeghi-Azad, S. M. Hoseyni, and S. M. Hoseyni, "Performance assessment of cooling systems in data centers; Methodology and application of a new thermal metric," *Case Studies in Thermal Engineering,* vol. 8, pp. 152-163, 2016.

[9] J. Cho, J. Yang, and W. Park, "Evaluation of air distribution system's airflow performance for cooling energy savings in high-density data centers," *Energy and Buildings,* vol. 68, pp. 270-279, 2014.

[10] M. Dayarathna, Y. Wen, and R. Fan, "Data Center Energy Consumption Modeling: A Survey," *IEEE Communications Surveys & Tutorials,* vol. 18, no. 1, pp. 732-794, 2016.

[11] B. Fakhim, N. Srinarayana, M. Behnia, and S. W. Armfield, "Thermal Performance of Data Centers-Rack Level Analysis," *IEEE Transactions on Components, Packaging and Manufacturing Technology,* vol. 3, no. 5, pp. 792-799, 2013.

[12] S. Sundaram and V. Ramalingam, "THERMAL MANAGEMENT OF ELECTRONICS: A REVIEW OF LITERATURE," *THERMAL SCIENCE,* vol. 12 (2008), no. UDC: 536.2:519.876.5:621.315.592, BIBLID: 0354-9836, 2008.

[13] J. Cho and B. S. Kim, "Evaluation of air management system's thermal performance for superior cooling efficiency in high-density data centers," *Energy and Buildings*, vol. 43, no. 9, pp. 2145-2155, 2011.

[14] N. M. S. Hassan, M. M. K. Khan, and M. G. Rasul, "Temperature Monitoring and CFD Analysis of Data Centre," *Procedia Engineering*, vol. 56, no. 0, pp. 551-559, 2013.

[15] J. Cho and Y. Kim, "Improving energy efficiency of dedicated cooling system and its contribution towards meeting an energy-optimized data center," *Applied Energy*, vol. 165, pp. 967-982, 2016.

[16] A. Almoli, A. Thompson, N. Kapur, J. Summers, H. Thompson, and G. Hannah, "Computational fluid dynamic investigation of liquid rack cooling in data centres," *Applied Energy*, vol. 89, no. 1, pp. 150-155, 2012.

[17] Z. Rongliang *et al.*, "A holistic and optimal approach for data center cooling management," in *American Control Conference (ACC), 2011*, 2011, pp. 1346-1351.

[18] M. S. L. Krug, and F. Saffre, "Understanding the environmental costs of fixed line networking," *in Proc. 5th Int. Conf. Future e-Energy Syst., 2014, pp. 87–95*, 2014.

[19] T. Christian *et al.*, "Automated synthesis of sustainable data centers," in *2009 IEEE International Symposium on Sustainable Systems and Technology*, pp. 1-6, 2009.

[20] O. VanGeet, "Best practices guide for energy-efficient data center design," EERE Publication and Product Library, 2010.

[21] M. K. Patterson, "The effect of data center temperature on energy efficiency," in *Thermal and Thermomechanical Phenomena in Electronic Systems, 2008. ITHERM 2008. 11th Intersociety Conference on*, 2008, pp. 1167-1174: IEEE.

[22] J. Siriwardana, S. Jayasekara, and S. K. Halgamuge, "Potential of air-side economizers for data center cooling: A case study for key Australian cities," *Applied Energy*, vol. 104, pp. 207-219, 2013.

[23] K.-P. Lee and H.-L. Chen, "Analysis of energy saving potential of air-side free cooling for data centers in worldwide climate zones," *Energy and Buildings*, vol. 64, pp. 103-112, 2013.

[24] K. Choo, R. M. Galante, and M. M. Ohadi, "Energy consumption analysis of a medium-size primary data center in an academic campus," *Energy and Buildings*, vol. 76, pp. 414-421, 2014.

[25] M. P. David *et al.*, "Experimental characterization of an energy efficient chiller-less data center test facility with warm water cooled servers," in *Semiconductor Thermal Measurement and Management Symposium (SEMI-THERM), 2012 28th Annual IEEE*, 2012, pp. 232-237: IEEE.

[26] T. Evans, "Humidification Strategies for Data Centers and Network Rooms," *White Paper*, 2004.

[27] A. T. 9.9, "2011 Thermal Guidelines for Data Processing Environments– Expanded Data Center Classes and Usage Guidance," *Whitepaper prepared by ASHRAE Technical Committee (TC) 9.9*, 2011.

[28] J. Cho, T. Lim, and B. S. Kim, "Measurements and predictions of the air distribution systems in high compute density (Internet) data centers," *Energy and Buildings*, vol. 41, no. 10, pp. 1107-1115, 2009.

[29] N. Srinarayana, B. Fakhim, M. Behnia, and S. W. Armfield, "Thermal Performance of an Air-Cooled Data Center With Raised-Floor and Non-Raised-Floor Configurations," *Heat Transfer Engineering,* vol. 35, no. 4, pp. 384-397, 2013.

[30] J. W. VanGilder and R. R. Schmidt, "Airflow Uniformity through perforated tiles in a raised-floor Data Center," in *ASME 2005 Pacific Rim Technical Conference and Exhibition on Integration and Packaging of MEMS, NEMS, and Electronic Systems collocated with the ASME 2005 Heat Transfer Summer Conference*, 2005, pp. 493-501: American Society of Mechanical Engineers.

[31] J. Rambo and Y. Joshi, "Convective Transport Processes in Data Centers," *Numerical Heat Transfer, Part A: Applications,* vol. 49, no. 10, pp. 923-945, 2006.

[32] S. Kang, R. R. Schmidt, K. M. Kelkar, A. Radmehr, and S. V. Patankar, "A methodology for the design of perforated tiles in raised floor data centers using computational flow analysis," *Components and Packaging Technologies, IEEE Transactions on,* vol. 24, no. 2, pp. 177-183, 2001.

[33] R. R. Schmidt, K. C. Karki, K. M. Kelkar, A. Radmehr, and S. V. Patankar, "Measurements and Predictions of The Flow Distribution Through Perforated Tiles In Raised Floor Data Centers," *The Pacific Rim/ASME International Electronic Packaging Technical Conference and Exhibition,* 8 July, 2001.

[34] E. C. Roger Schmidt, "Cluster of High-Powered Racks Within a Raised Floor-Computer Data Center: Effect of Perforated Tile Flow Distrbtion on Rack Inlet Air Temperatures," *ASME,* vol. 126, pp. 510-518, December, 2004.

[35] K. C. Karki and S. V. Patankar, "Airflow distribution through perforated tiles in raised-floor data centers," *Building and Environment,* vol. 41, no. 6, pp. 734-744, 2006.

[36] K. C. Karki, S. V. Patankar, and A. Radmehr, "TECHNIQUES FOR CONTROLLING AIRFLOW DISTRIBUTION IN RAISED-FLOOR DATA CENTERS," presented at the *The Pacific Rim/ASME International Electronic Packaging Technical Conference and Exhibition, Maui, Hawaii*, USA, July 6-11, 2003.

[37] S. Bhopte, D. Agonafer, R. Schmidt, and B. Sammakia, "Optimization of Data Center Room Layout to Minimize Rack Inlet Air Temperature," *Journal of Electronic Packaging,* vol. 128, no. 4, pp. 380-387, 2006.

[38] S. V. Patankar, "Airflow and Cooling in a Data Center," *Journal of Heat Transfer,* vol. 132, no. 7, 2010.

[39] R. Sullivan, "Alternating Cold and Hot Aisles Provides More Reliable Cooling for Server Farms," a White Paper From the Uptime Institute," *Incorporated, Santa Fe, NM,* 2002.

[40] C. D. Patel, R. Sharma, C. E. Bash, and A. Beitelmal, "Thermal considerations in cooling large scale high compute density data centers," in *Thermal and Thermomechanical Phenomena in Electronic Systems, 2002. ITHERM 2002. The Eighth Intersociety Conference on*, pp. 767-776, 2002.

[41] J. Rambo and Y. Joshi, "Thermal Performance Metrics for Arranging Forced Air Cooled Servers in a Data Processing Cabinet," *Journal of Electronic Packaging,* vol. 127, no. 4, pp. 452-459, 2005.

[42] B. Fakhim, N. Srinarayana, M. Behnia, and S. W. Armfield, "Thermal Performance of Data Centers-Rack Level Analysis," *Components, Packaging and Manufacturing Technology, IEEE Transactions on,* vol. 3, no. 5, pp. 792-799, 2013.

[43] R. Schmidt and E. Cruz, "Raised floor computer data center: effect on rack inlet temperatures of chilled air exiting both the hot and cold aisles," in *Thermal and Thermomechanical Phenomena in Electronic Systems, 2002. ITHERM 2002. The Eighth Intersociety Conference on,* pp. 580-594, 2002.

[44] R. R. Schmidt, K. C. Karki, K. M. Kelkar, A. Radmehr, and S. V. Patankar, "Measurements and Predictions of The Flow Distribution Through Perforated Tiles In Raised Floor Data Centers," *The Pacific Rim/ASME International Electronic Packaging Technical Conference and Exhibition,* 8 July, 2001.

[45] B. Fakhim, M. Behnia, S. W. Armfield, and N. Srinarayana, "Cooling solutions in an operational data centre: A case study," *Applied Thermal Engineering,* vol. 31, no. 14–15, pp. 2279-2291, 2011.

[46] K. K. a. S. Patankar, "Raised Floor Data Center: PerforatdTiles Flow Rates For Various Tile Layouts," presented at *the Inter Society Conference on Thermal phenomena*, Poughkeepsie, N. Y. 12601, USA, 2004.

[47] S. K. Shrivastava, M. Iyengar, B. G. Sammakia, R. Schmidt, and J. W. VanGilder, "Experimental-Numerical Comparison for a High-Density Data Center: Hot Spot Heat Fluxes in Excess of 500 W/ft," *Components and Packaging Technologies, IEEE Transactions on,* vol. 32, no. 1, pp. 166-172, 2009.

[48] H. Zhang, S. Shao, H. Xu, H. Zou, and C. Tian, "Free cooling of data centers: A review," *Renewable and Sustainable Energy Reviews,* vol. 35, pp. 171-182, 2014.

[49] Y. Ma, G. Ma, S. Zhang, and F. Zhou, "Cooling performance of a pump-driven two phase cooling system for free cooling in data centers," *Applied Thermal Engineering,* vol. 95, pp. 143-149, 2016.

[50] M. P. Tom Harvey, John Bean, "The Green Grid. UPDATED AIR-SIDE FREE COOLING MAPS: THE IMPACT OF ASHRAE 2011 ALLOWABLE RANGES," *White Paper 46,* 2012.

[51] A. Capozzoli and G. Primiceri, "Cooling Systems in Data Centers: State of Art and Emerging Technologies," *Energy Procedia,* vol. 83, pp. 484-493, 2015.

[52] T. Brunschwiler, B. Smith, E. Ruetsche, and B. Michel, "Toward zero-emission data centers through direct reuse of thermal energy," *IBM Journal of Research and Development,* vol. 53, no. 3, pp. 11:1-11:13, 2009.

[53] H. Rong, H. Zhang, S. Xiao, C. Li, and C. Hu, "Optimizing energy consumption for data centers," *Renewable and Sustainable Energy Reviews,* vol. 58, pp. 674-691, 2016.

[54] P. Centre. (2018). *GEOTHERMAL COOLING SYSTEM*. Available: https://www.pawsey.org.au/pawsey-centre/geothermal-cooling-system/

[55] S. A. Nada, M. A. Said, and M. A. Rady, "CFD investigations of data centers' thermal performance for different configurations of CRACs units and aisles separation," *Alexandria Engineering Journal,* vol. 55, no. 2, pp. 959-971, 2016.

[56] A. Capozzoli, G. Serale, L. Liuzzo, and M. Chinnici, "Thermal Metrics for Data Centers: A Critical Review," *Energy Procedia*, vol. 62, no. 0, pp. 391-400, 2014.

[57] Q. Tang, S. K. S. Gupta, and G. Varsamopoulos, "Thermal-aware task scheduling for data centers through minimizing heat recirculation," in *Cluster Computing, 2007 IEEE International Conference on*, 2007, pp. 129-138.

[58] J. Rambo and Y. Joshi, "Modeling of data center airflow and heat transfer: State of the art and future trends," *Distributed and Parallel Databases*, journal article vol. 21, no. 2, pp. 193-225, 2007.

[59] C. E. Bash, C. D. Patel, and R. K. Sharma, "Efficient Thermal Management of Data Centers-Immediate and Long-Term Research Needs," *HVAC&R Research*, vol. 9, no. 2, pp. 137-152, Apr 2003.

[60] R. R. Schmidt, M. Iyengar, and L. v. d. M. Pieter, "Best Practices for Data Center Thermal and Energy Management-Review of Literature/DISCUSSION," *ASHRAE Transactions*, vol. 113, pp. 206-218, 2007.

[61] X. Yuan, Y. Wang, J. Liu, X. Xu, and X. Yuan, "Experimental and numerical study of airflow distribution optimisation in high-density data centre with flexible baffles," *Building and Environment*, vol. 140, pp. 128-139, 2018.

[62] Z. Song, "Studying the fan-assisted cooling using the Taguchi approach in open and closed data centers," *International Journal of Heat and Mass Transfer*, vol. 111, pp. 593-601, 2017.

[63] J. Priyadumkol and C. Kittichaikarn, "Application of the combined air-conditioning systems for energy conservation in data center," *Energy and Buildings*, vol. 68, Part A, pp. 580-586, 2014.

[64] H. Bhagwat, A. Singh, A. Vasan, and S. Anand, "Thermal influence indices: Causality metrics for efficient exploration of data center cooling," in *Green Computing Conference (IGCC), 2012 International*, 2012, pp. 1-10.

[65] H. Fernando, J. Siriwardana, and S. Halgamuge, "Can a data center heat-flow model be scaled down?," in *2012 IEEE 6th International Conference on Information and Automation for Sustainability*, 2012, pp. 273-278.

[66] M. Ibrahim *et al.*, "Numerical modeling approach to dynamic data center cooling," in *Thermal and Thermomechanical Phenomena in Electronic Systems (ITherm), 2010 12th IEEE Intersociety Conference on*, 2010, pp. 1-7.

[67] M. K. Herrlin and C. Belady, "Gravity-assisted air mixing in data centers and how it affects the rack cooling effectiveness," in *Thermal and Thermomechanical Phenomena in Electronics Systems, 2006. ITHERM '06. The Tenth Intersociety Conference on*, 2006, pp. 5-438.

[68] Q. Tang, S. K. S. Gupta, D. Stanzione, and P. Cayton, "Thermal-Aware Task Scheduling to Minimize Energy Usage of Blade Server Based Datacenters," in *Dependable, Autonomic and Secure Computing, 2nd IEEE International Symposium on*, 2006, pp. 195-202.

[69] A. H. Beitelmal and C. D. Patel, "Thermo-Fluids Provisioning of a High Performance High Density Data Center," *Distributed and Parallel Databases*, journal article vol. 21, no. 2, pp. 227-238, 2007.

[70] A. Radmehr, R. Schmidt, K. C. Karki, and S. V. Patankar, "Distributed leakage flow in raised-floor data centers," *ASME Paper No. IPACK2005-73273*, 2005.

[71] K. C. Karki, A. Radmehr, and S. V. Patankar, "Use of Computational Fluid Dynamics for Calculating Flow Rates Through Perforated Tiles in Raised-Floor Data Centers," *HVAC&R Research*, vol. 9, no. 2, pp. 153-166, 2003.

[72] C. E. B. a. C. B. Chandrakant D. Patel, "Computational Fluid Dynamics Modeling of High Compute Density Data Centers to Assure System Inlet Air Specification," presented at the *The Pacific Rim/ASME International Electronic Packaging Technical Conference and Exhibition*, Kauai, Hawaii, USA, July 8-13, 2001.

[73] J. Summers, N. Kapur, and H. Thompson, "Design of data centre rack arrangements using open source software," in *Semiconductor Thermal Measurement and Management Symposium (SEMI-THERM), 2013 29th Annual IEEE*, 2013, pp. 45-51.

[74] Z. Rongliang, W. Zhikui, C. E. Bash, and A. McReynolds, "Data center cooling management and analysis - a model based approach," in *Semiconductor Thermal Measurement and Management Symposium (SEMI-THERM), 2012 28th Annual IEEE*, 2012, pp. 98-103.

[75] R. Schmidt, M. Ellsworth, M. Iyengar, and G. New, "IBM's power6 high performance water cooled cluster at NCAR: Infrastructure design," *In ASME 2009 InterPACK Conference collocated with the ASME 2009 Summer Heat Trasfer Conference and the ASME 2009 3rd Interntional Conference on Energy Sustainability (InterPACK2009)*, vol. San Francisco, California, USA, 2009.

[76] J. VanGilder, "Real-Time data center cooling analysis," *Electroics Cooling*, September, 2011.

[77] M. Seymour, C. Aldham, M. Warner, and H. Moezzi, "The increasing challenge of data center design and management: Is CFD a must?," *Electroics Cooling*, December, 2011.

[78] K. Khankari, "Thermal mass availability for cooling data centers during power shutdown," *ASHRAE Trasactions*, vol. 116(2):205-217, 2010.

[79] M. Kummert, W. Dempster, and K. McLean, "Thermal analysis of a data centre cooling system under fault conditions," *In 11 th Interntional Building Peiformance Simulation Association Conference and Exhibition, Building Simulation 2009, Glasgow, Scotland*, 2009.

[80] S. K. Shrivastava, B. Sammakia, R. Schmidt, M. Iyengar, and J. W. Van Gilder, "Experimental-Numerical Comparison for a High-Density Data Center: Hot Spot Heat Fluxes in Excess of 500 W/ft2," in *Thermal and Thermomechanical Phenomena in Electronics Systems, 2006. ITHERM'06. The Tenth Intersociety Conference on*, 2006, pp. 402-411: IEEE.

[81] Y. Fulpagare and A. Bhargav, "Advances in data center thermal management," *Renewable and Sustainable Energy Reviews*, vol. 43, pp. 981-996, 2015.

[82] H. K. Versteeg and W. Malalasekera, *An Introduction to Computational Fluid Dynamics: The Finite Volume Method*. Pearson Education Limited, 2007.

[83] W. Frei, "Which Turbulence Model Should I Choose for My CFD Application?," *COSMOL BLOG*, September 16, 2013.

[84] A. Travin, M. Shur, M. Strelets, and P. Spalart, "Detached-Eddy Simulations Past a Circular Cylinder," (in English), *Flow, Turbulence and Combustion,* vol. 63, no. 1-4, pp. 293-313, 2000.

[85] B. E. Launder, and D. Spalding,, "The numerical computation of turbulent flows. Computer methods in applied mechanics and engineering," 1974.

[86] F. R. Menter, "Two-equation eddy-viscosity turbulence models for engineering applications," *AIAA journal,* vol. 32, no. 8, pp. 1598-1605, 1994.

[87] B. Šekutkovski, I. Kostić, A. Simonović, P. Cardiff, and V. Jazarević, "Three-dimensional fluid–structure interaction simulation with a hybrid RANS–LES turbulence model for applications in transonic flow domain," *Aerospace Science and Technology,* vol. 49, pp. 1-16, 2016.

[88] C. D. Argyropoulos and N. C. Markatos, "Recent advances on the numerical modelling of turbulent flows," *Applied Mathematical Modelling,* vol. 39, no. 2, pp. 693-732, 1/15/ 2015.

[89] F. Menter, M. Kuntz, and R. Bender, "A Scale-Adaptive Simulation Model for Turbulent Flow Predictions," in *41st Aerospace Sciences Meeting and Exhibit*, Aerospace Sciences Meetings: American Institute of Aeronautics and Astronautics, 2003.

[90] L. Davidson, "Evaluation of the SST-SAS model: channel flow, asymmetric diffuser and axi-symmetric hill," in *ECCOMAS CFD 2006: Proceedings of the European Conference on Computational Fluid Dynamics, Egmond aan Zee, The Netherlands, September 5-8, 2006*, 2006: Delft University of Technology; European Community on Computational Methods in Applied Sciences (ECCOMAS).

[91] W. Haase, M. Braza, and A. Revell, *DESider–A European Effort on Hybrid RANS-LES Modelling: Results of the European-Union Funded Project, 2004-2007*. Springer Science & Business Media, 2009.

[92] F. Menter and Y. Egorov, "A Scale Adaptive Simulation Model using Two-Equation Models," in *43rd AIAA Aerospace Sciences Meeting and Exhibit*(Aerospace Sciences Meetings: American Institute of Aeronautics and Astronautics, 2005.

[93] OpenFOAM, "The open source CFD toolbox," 2004-2017.

[94] OpenFOAM, "OpenFOAM User Guide," 2015.

[95] V. K. Arghode and Y. Joshi, "Rapid modeling of air flow through perforated tiles in a raised floor data center," in *Fourteenth Intersociety Conference on Thermal and Thermomechanical Phenomena in Electronic Systems (ITherm)*, 2014, pp. 1354-1365.

[96] V. K. Arghode and Y. Joshi, "Modeling Strategies for Air Flow Through Perforated Tiles in a Data Center," *IEEE Transactions on Components, Packaging and Manufacturing Technology,* vol. 3, no. 5, pp. 800-810, 2013.

[97] O. M. D. Kuzmin, S. Turek, "On the implementation of the k − ε turbulence model in incompressible flow solvers based on a finite element discretization," *International Journal of Computing Science .and Mathematics 1 (2): p. 193-206,* 2007.

[98] I. B. Celik, Z. N. Cehreli, and I. Yavuz, "Index of Resolution Quality for Large Eddy Simulations," *Journal of Fluids Engineering,* vol. 127, no. 5, pp. 949-958, 2005.

[99] S. B. Pope, "Turbulent Flows," *CAMBRIDGE UNIVERSITY PRESS,* 2000.

[100] I. K. Tiong, "Experimental study on the effect of a heated plume within vented enclosures," Master of Philosophy, School of Civil and Mechanical Engineering, Curtin University, 2011.

[101] G. De Vahl Davis, "Natural convection of air in a square cavity: A bench mark numerical solution," *International Journal for Numerical Methods in Fluids,* vol. 3, no. 3, pp. 249-264, 1983.

[102] A. H. Almaneea, "Thermal analysis of liquid immersed electronics for data centres," PhD, School of Mechanical Engineering, The University of Leeds, 2014.

[103] V. Sundaralingam, V. K. Arghode, and Y. Joshi, "Experimental characterization of cold aisle containment for data centers," in *Semiconductor Thermal Measurement and Management Symposium (SEMI-THERM), 2013 29th Annual IEEE*, 2013, pp. 223-230.

[104] V. K. Arghode, V. Sundaralingam, Y. Joshi, and W. Phelps, "Thermal Characteristics of Open and Contained Data Center Cold Aisle," *Journal of Heat Transfer,* vol. 135, no. 6, 2013.

[105] C. D. Patel, C. E. Bash, C. Belady, L. Stahl, and D. Sullivan, "Computational fluid dynamics modeling of high compute density data centers to assure system inlet air specifications," in *Proceedings of IPACK*, 2001, vol. 1, pp. 8-13.

[106] R. R. Schmidt, E. E. Cruz, and M. Iyengar, "Challenges of data center thermal management," *IBM Journal of Research and Development,* vol. 49, no. 4.5, pp. 709-723, 2005.

[107] Q. Tang, T. Mukherjee, S. K. S. Gupta, and P. Cayton, "Sensor-Based Fast Thermal Evaluation Model For Energy Efficient High-Performance Datacenters," in *Intelligent Sensing and Information Processing, 2006. ICISIP 2006. Fourth International Conference on*, 2006, pp. 203-208.

[108] OpenFOAM, "Compiling applications & libraries," 02/03/2015 2015.

Appendices

Appendix A

Implementation of SAS Simulation in OpenFOAM

The solver that used in this thesis is `buoyantBoussinesqPimpleFoam` as it is the most appropriate solver that describes the physics of the data centres. However, standard solver does not have the ability to call the LES class turbulence models. Therefore, some modifications were implemented to this solver to call the k-ω SST SAS since it is part of the LES class turbulence models. The place of the files and declaration of k-ω SST SAS in OpenFOAM is shown in Figure 68. Though, with the k-ε RANS model the `buoyantBoussinesqPimpleFoam` solver will be used as this model is part of the RANS class turbulence models as illustrated by Figure 69.

```
$FOAM_SRC/turbulenceModels/incompressible/LES/kOmegaSSTSAS/
```

Figure 68: k-ω SST SAS LES model declaration files path.

```
$FOAM_SRC/turbulenceModels/incompressible/RAS/kEpsilon/
```

Figure 69: k – ε RANS model declaration files path.

`buoyantBoussinesqPimpleFoam`

`buoyantBoussinesqPimpleFoam` is transient solver for buoyant, incompressible turbulent flow. It is part of the heat transfer solvers as shown in Figure 70; thus, it is suitable choice to be used in data centre numerical simulations.

```
$FOAM_SOLVERS/heatTransfer/buoyantBoussinesqPimpleFoam/
```

Figure 70: `buoyantBoussinesqPimpleFoam` solver path.

Before the solution loop starts, the createFields.H header file, which is a part of the solver folder as illustrated in Figure 71, is called. The createFields.H file contains all the variables that the solver will solve including the turbulence model initialisation. Figure 72 shows the part that initialises the turbulence model in the createFields.H. The header file initialises the RANS class turbulence models only, thus a new solver was compiled to overcome this shortcoming.

```
buoyantBoussinesqPimpleFoam/
├── buoyantBoussinesqPimpleFoam.C
├── createFields.H
├── Make
│   ├── files
│   └── options
├── pEqn.H
├── TEqn.H
└── UEqn.H
```

Figure 71: Header files of the `buoyantBoussinesqPimpleFoam` solver.

```
#include "createPhi.H"

#include "readTransportProperties.H"

Info<< "Creating turbulence model\n" << endl;
autoPtr<incompressible::RASModel> turbulence
(
    incompressible::RASModel::New(U, phi, laminarTransport)
);
```

Figure 72: The part that initialises the turbulence model in the createFields.H for the standard solver.

my_ buoyantBoussinesqPimpleFoam

OpenFOAM is an open source tool which enables users to get access into the source codes and solvers and can create their own custom solvers, turbulence models or boundary conditions. In this thesis, a new solver will be customised by copying and compiling an existing solver. The solver that will be compiled is `buoyantBoussinesqPimpleFoam`. First step is to create a folder for the compiled the new solver in the user directory. Then, `buoyantBoussinesqPimpleFoam` is copied and renamed into the new solver folder. The necessary changes are added into the new solver before the compilation process.

In the majority of OpenFOAM applications createFields.H contains the field input data and the codes of creating fields. For example, in the modified createFields.H file, the LES class turbulence models and their relevant functions for the incompressible flows were added to the solver by changing the RANSModel field in the basic solver into turbulence field as illustrated by Figure 73. The solver directory structure is shown in Figure 74. The Make folder must be included in the main directory of the solver which contains two important files, files and options. The options file is used by the compiler to include the header files that specified by the -I option in the wmake. The compiler also

links the shared object library files that specified with -l option in wmake. The details of the options file for the compiled solver is shown in Figure 75.

```
#include "createPhi.H"

#include "readTransportProperties.H"

Info<< "Creating turbulence model\n" << endl;
autoPtr<incompressible::turbulenceModel> turbulence
(
    incompressible::turbulenceModel::New(U, phi, laminarTransport)
);
```

Figure 73: The modified part of the createFields.H.

Figure 74: Solver directory structure [108].

```
EXE_INC = \
    -I../my_buoyantBoussinesqSimpleFoam \
    -I$(LIB_SRC)/sampling/lnInclude \
    -I$(LIB_SRC)/meshTools/lnInclude \
    -I$(LIB_SRC)/fvOptions/lnInclude \
    -I$(LIB_SRC)/finiteVolume/lnInclude \
    -I$(LIB_SRC)/turbulenceModels \
    -I$(LIB_SRC)/turbulenceModels/incompressible/turbulenceModel \
    -I$(LIB_SRC)/transportModels \
    -I$(LIB_SRC)/transportModels/incompressible/singlePhaseTransportModel \
    -I$(LIB_SRC)/thermophysicalModels/radiationModels/lnInclude

EXE_LIBS = \
    -lfiniteVolume \
    -lfvOptions \
    -lsampling \
    -lmeshTools \
    -lincompressibleTurbulenceModel \
    -lincompressibleRASModels \
    -lincompressibleLESModels \
    -lincompressibleTransportModels \
    -lradiationModels
```

Figure 75: The make/options file of the compiled solver.

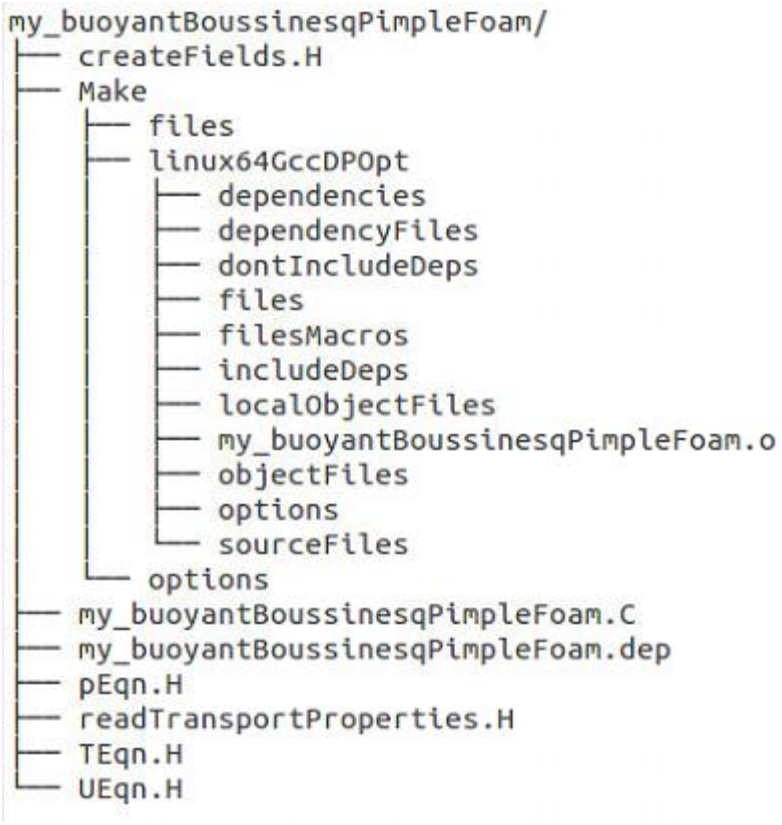

Figure 76: Header files of the compiled solver.

Appendix B

Mesh Generation by Using `snappyHexMesh`

OpenFOAM does not have built in CAD tool, thus Autodesk Inventor 3D CAD has been used to generate 3D models of the details of data centres. The 3D models then converted into STL files to be exported to OpenFOAM in order to generate the final mesh. The mesh generation dictionary (`snappyHexMesh`) is an automatic and parallel mesh generation in which the mesh will be exported as STL files to be converted to OpenFOAM format by using mesh conversion. `SnappyHexMesh` generates hexahedral unstructured mesh by building the mesh by sculpting upon the STL surfaces.

The first stage of using the `snappyHexMesh` is by defining hexahedral background mesh by using `blockMesh` dictionary. `SnappyHexMesh` dictionary consists of three main steps, `castellstedMesh`, snap and `addLayers` as shown in Figure 77. The `castellstedMesh` has three functions, to define the flow region by defining the cells inside the STL surfaces, to perform the refinement process for the defined regions, and to remove the cells that outside the STL surfaces and inside the `blockMesh` domain. The snap control moves the jagged castellated cells onto the STL surfaces to remove the cell vertices that outside the flow domain. The `addLayers` process is to refine the mesh near the walls.

```
// Which of the steps to run
castellatedMesh true;
snap            true;
addLayers       false;
```

Figure 77: The main steps to control the mesh in the `snappyHexMesh` dictionary.

The data centre has complex geometry; therefore, the patches of the data centres have been exported separately for each defined patch. For instance; the IT servers, racks, CRAC units and the walls have been exported separately to easily define the patches and the walls of the mesh. Figure 78 and Figure 79 show surface mesh and cross sectional for the internal mesh, respectively.

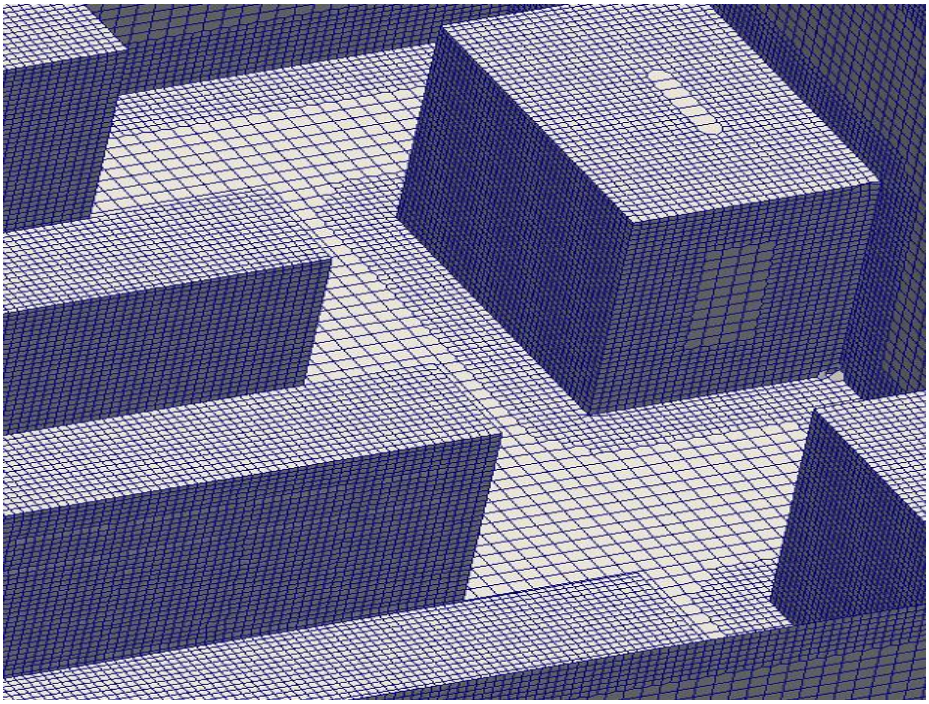

Figure 78: `SnappyHexMesh` surface mesh illustrating refinement level.

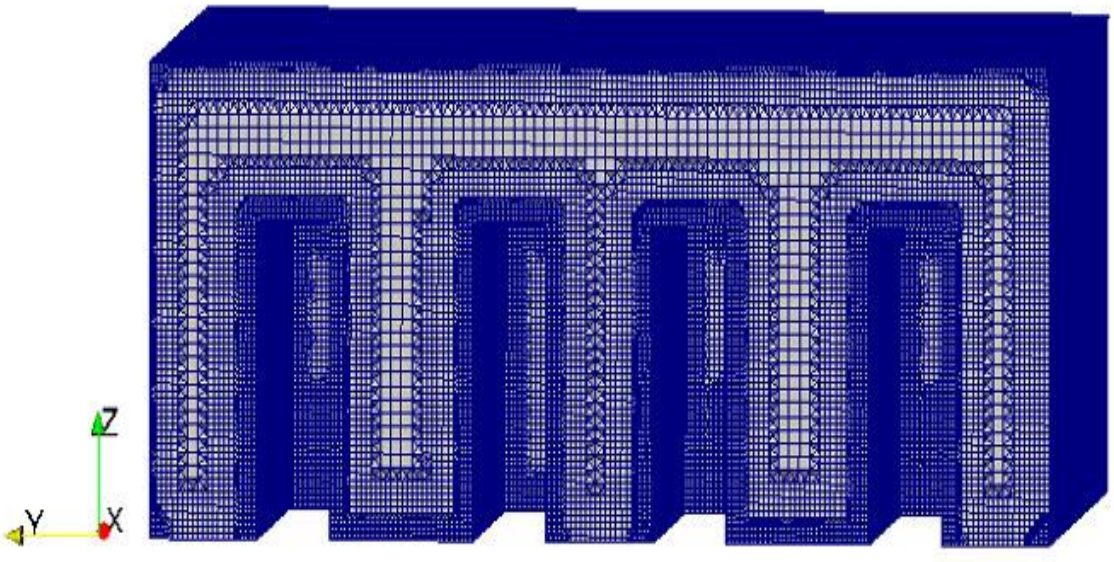

Figure 79: A cross sectional for the internal mesh.